ornl

OAK RIDGE NATIONAL LABORATORY

LOCKHEED MARTIN

ORNL/GWPO-023

Simulation of a Field Scale Tritium Tracer Experiment in a Fractured, Weathered Shale Using Discrete-Fracture/Matrix-Diffusion and Equivalent Porous Medium Models

A Thesis
Presented for the
Master of Science Degree
The University of Tennessee, Knoxville

Paige L. Stafford
May 1996

MANAGED BY
LOCKHEED MARTIN ENERGY SYSTEMS, INC.
FOR THE UNITED STATES
DEPARTMENT OF ENERGY

UCN-13673 (36 6-95)

ORNL/GWPO-023

Simulation of a Field Scale Tritium Tracer Experiment in a Fractured, Weathered Shale Using Discrete-Fracture/Matrix-Diffusion and Equivalent Porous Medium Models

P. L. Stafford
Department of Geological Sciences
The University of Tennessee

May 1996

Prepared by
Environmental Sciences Division
Oak Ridge National Laboratory

Prepared for the
U.S. Department of Energy
Office of Environmental Restoration and Waste Management
under budget and reporting code EW 20 10 30 2

OAK RIDGE NATIONAL LABORATORY
Oak Ridge, Tennessee 37831-6285
managed by
LOCKHEED MARTIN ENERGY RESEARCH CORP.
For the
U.S. DEPARTMENT OF ENERGY
under contract DE-AC05-96OR22464

ACKNOWLEDGMENTS

The people that made this thesis possible include Tom LaLoggia, who believed in me when it counted most, Wendy Roberg for setting an example, and Keith Stafford who led me to the University of Tennessee. People who provided moral and financial support include Karen (Mom) & Jim Kinsman, and Richard (Dad) & Stephanie Brathovde.

I would like to give special thanks to Larry McKay and Laura Toran who spent many hours and considerable mental anguish advising and assisting me, and to David Webster for allowing me to use the results of his experiment.

I would also like to thank the following organizations for providing special funding:

- Oak Ridge National Laboratory, managed by Lockheed Martin Energy Research Corporation for the United States Department of Energy under contract number DE-AC05-96OR22464.
- University of Tennessee, Knoxville, Department of Geological Sciences who provided funding through Graduate Teaching Assistantships.

ABSTRACT

Simulations of a tritium tracer experiment in fractured shale saprolite, conducted at the Oak Ridge National Laboratory, were performed using 1D and 2D equivalent porous medium (EPM) and discrete-fracture/matrix-diffusion (DFMD) models. The models successfully reproduced the general shape of the breakthrough curves in down-gradient monitoring wells which are characterized by rapid first arrival, a slow-moving center of mass, and a persistent "tail" of low concentration. In plan view, the plume shows a large degree of transverse spreading with the width almost as great as the length. EPM models were sensitive to dispersivity coefficient values which had to be large (relative to the 3.7m distance between the injection and monitoring wells) to fit the tail and transverse spreading. For example, to fit the tail a longitudinal dispersivity coefficient, α_L, of 0.8 meters for the 2D simulations was used. To fit the transverse spreading, a transverse dispersivity coefficient, α_T, of 0.8 to 0.08 meters was used indicating an α_L/α_T ratio between 10 and 1. Transverse spreading trends were also simulated using a 2D DFMD model using a few larger aperture fractures superimposed onto an EPM. Of the fracture networks studied, only those with truncated fractures caused transverse spreading. Simulated tritium levels in all of the cases were larger than observed values by a factor of approximately 100. Although this is partly due to input of too much

tritium mass by the models it appears that dilution in the wells, which were not purged prior to sampling, is also a significant factor. The 1D and 2D EPM models were fitted to monitoring data from the first five years of the experiment and then used to predict future tritium concentrations. The predicted concentrations are similar (after accounting for the input and dilution factors) to a recent value measured 16 years after the start of the experiment. The experiment and simulations confirm that tritium contamination in this type of fractured porous material can persist for many tens of years due to "storage" in the relatively immobile groundwater between fractures.

TABLE OF CONTENTS

LIST OF TABLES

LIST OF FIGURES

Figure *page*

LIST OF SYMBOLS AND ABBREVIATIONS

2b	fracture aperture
2B	fracture spacing
α_L	longitudinal dispersivity coefficient
α_f	transverse dispersivity coefficient
c	concentration
c'	concentration in the fracture
D	hydrodynamic dispersion
D^o	free water diffusion coefficient
D*	effective diffusion coefficient
g	acceleration due to gravity
i	hydraulic gradient
K_b	bulk hydraulic conductivity
K_m	matrix hydraulic conducitivity
K_f	fracture hydraulic conductivity
K_d	distribution coefficient
K_{df}	distribution coefficient in fracture
l	rate coefficient
n_e	effective porosity
n_f	fracture porosity
n_m	matrix porosity
n_t	total porosity
q	Darcy flux
q_f	discharge per unit length of a smooth walled fracture
q_s	solute flux
R	retardation
R_f	retardation in the fracture
ρ	density of water
ρ_b	soil bulk density
m	viscosity of water
v	groundwater velocity
v_f	groundwater velocity in the fracture
ω	tortuosity
Ω	advective-dispersive loss or gain across fracture
Ψ	pressure head
z	elevation head

1D	one dimensional
2D	two dimensional
3D	three dimensional
BG4	burial ground 4
BG6	burial ground 6
BPF	bedding plane fractures
BTC	breakthrough curve
COM	center of mass
EF	extension fracture
EPM	equivalent porous media
DF	discrete fracture
DFMD	discrete fracture/matrix diffusion
ORNL	Oak Ridge National Laboratory
ORR	Oak Ridge Reservation
REV	representative elemental volume
USGS	United State Geological Survey
WBCV	West Bear Creek Valley

CHAPTER 1

INTRODUCTION

Shales at the Oak Ridge Reservation (ORR) were, until recently, considered adequate barriers against migration of contaminants. However, the upper portion of these deposits (usually above 10 meter depth) are highly weathered and fractured, which substantially increases the hydraulic conductivity and potential for contaminant migration (Solomon et al., 1992). For example, tritium migration from shallow low-level radioactive waste trenches within the weathered shales has been observed at a number of sites on the ORR (Solomon et al., 1992; Moore and Toran, 1992). Recent field and lab investigations in the weathered shales at ORR (Shevenell et al., 1994; Sanford and Solomon, 1995; Olsen et al., 1983; Wickliff et al., 1989) and in fractured clay-rich glacial deposits, which are similar to the weathered shales (Keller et al., 1986; D'Astous et al., 1989; Thompson, 1990; Balfour, 1991, Ruland et al., 1991; McKay et al., 1993a) have also shown that contaminant migration can occur at environmentally significant rates.

Two groundwater tracer experiments (Webster, in press) were conducted by D.A. Webster of the United States Geological Survey in fractured weathered shale at the Oak Ridge National Laboratory (ORNL), Oak Ridge, Tennessee,

near burial grounds 4 (BG4), and 6 (BG6) (Figure 1*). The experiments were designed to investigate fracture-controlled migration of solutes in groundwater. The experiments are unique because of the high levels of tritium used (50 curies at BG4 and 100 curies at BG6) and the long duration of monitoring (1977 to present). Furthermore, these experiments are two of the few controlled field-scale tracer experiments in a fractured media containing significant matrix porosity ($\leq 40\%$) and permeability ($\sim 10^{-2}$ m/d). The experiments were performed in an uncontaminated area adjacent to low level radioactive waste disposal sites on the ORR, and hence should be relevant to assessing contaminant migration and behavior at this and other waste sites in the same geologic deposits. The results of the tracer experiments have never been quantitatively evaluated using groundwater flow and contaminant transport computer models. This thesis will quantitatively assess, using numerical models, the results of the tracer experiment at BG4 to investigate contaminant transport through the weathered shales. The tritium plumes at the two sites have similar characteristics and because the BG4 site is smaller and has a better resolution of the plume, it was chosen for modeling in this thesis.

---

* Tables and Figures are located in Appendix A

Numerical modeling for research or applied purposes of groundwater flow and solute migration in the weathered and fractured shale poses special challenges because it is not clear whether the material can be considered as a continuum (continuum approach or equivalent porous media (EPM) approach), or whether it must be approached on the scale of individual fractures (discrete fracture approach). Long and others (1982) determined which characteristics of a fractured system increase the likelihood of the EPM approach being appropriate. Some of these characteristics are:

1. high fracture density, which creates connected fractures and therefore connected flow paths;
2. constant fracture aperture to prevent only a few fractures from contributing most of the flow;
3. random orientation of fractures so that flow is not unidirectional;
4. a representative elemental volume (REV) where heterogeneity is negligible;
5. the size of the REV is large relative to the fracture lengths to represent complete flow paths;
6. the REV must be small compared to the system being modelled;

The EPM approach defines a fractured system as a single continuum, or series of continuums, where groundwater flow and advection-dispersion equations describe contaminant transport. The advantage of this approach is that just a few

parameters, such as hydraulic conductivity, hydraulic gradient, effective porosity and dispersivity, are necessary. They are either measured in the field or laboratory, or are obtained from "fitting" simulations to data from tracer experiments. This approach can still have a high degree of uncertainty because of problems with "fitting" parameters, such as dispersivity and effective porosity, that may vary with time and scale. Many studies exist that examine the applicability of EPM (or continuum) models to idealised fractured systems (e.g., Long et al., 1982; Berkowitz et al., 1988; Maloszewski and Zuber, 1993). However, very little research has been conducted pertaining to actual field-scale systems (e.g. Bibby, 1981; Pankow et al. 1986; and McKay et al. ,1993a and b).

A discrete fracture approach requires information about both the fractures and the blocks of soil or rock between fractures. Some of these parameters, particularly fracture aperture and degree of fracture interconnection, are difficult to measure and may contain a high degree of uncertainty (Table 1). Discrete fracture models typically require considerably more computer memory than an EPM model, which is often a limitation on how large, or in how much detail, a region can be modelled.

Studies of discrete fracture models conducted in the 1980's (Endo et al., 1984, Schwartz et al., 1983, Long et al., 1982; and Long and Witherspoon, 1985) described the importance of effective porosity (which they define as the porosity

contributed by fractures) and fracture orientation, but matrix transport parameters were considered insignificant and were not included in their models. On the other hand, other studies (Foster, 1975; Day 1977; Sudicky and Frind, 1982; Malowszewski and Zuber, 1985 and 1993; Harrison et al., 1992; Sudicky and McLaren, 1992) established the importance of matrix diffusion in fractured, high porosity materials by indicating its effect on delaying solute breakthrough. Sudicky and Frind (1982), in simulating solute migration (tritium) in a fractured porous material, showed that matrix diffusion acts as a dynamic storage mechanism. The process was sufficient to retard the overall migration rate of the plume by several orders of magnitude, as compared to advective transport rates in fractures alone, where no diffusion is assumed.

Based on the probable small fracture spacing (cm's to 10's of cm's) at the BG4 experiment site and the expected high matrix porosity, it is hypothesized that both EPM and discrete-fracture/matrix-diffusion (DFMD) models are appropriate for simulating solute transport at this site. The objectives of this thesis are to:

1. determine whether both of the modeling approaches can simulate the observed tritium migration, using reasonable parameter values in a steady-state flow field;

2. determine whether the models using parameters "fitted" to data from the initial five years of the experiment can "predict" present concentrations of tritium (16 years after start of experiment);
3. to assess the sensitivity of the models to factors, such as the presence of a few larger aperture fractures.

CHAPTER 2

USGS/ORNL TRITIUM TRACER EXPERIMENT

Geologic and Hydrogeologic Setting of BG4 Site

The experiment site adjacent to BG4 is located near the base of Haw Ridge (Figure 1). The ridge is underlain by the resistant Cambrian Rome formation, which is in the hanging wall of the Copper Creek thrust fault (McMaster, 1963, Webster and Bradley, 1988 and Solomon, et al., 1992). The site is underlain by Pumpkin Valley Shale of the Conasauga Group (Table 2). The upper unit of the Pumpkin Valley Shale is a mudstone and shale inter-bedded with siltstone. The lower unit is a siltstone inter-bedded with mudstone. The saprolite, or highly weathered portion, is approximately nine meters thick (Webster, in press), retains primary bedrock textures and structural features, including fractures, and has greater porosity than the unweathered bedrock (Solomon et al., 1992). Gravimetric measurements of porosity of saprolite from similar type material in the Nolichucky Shale, from one to two meter depth are approximately 0.40 (Wilson, et al., 1992). The bedrock has porosity values between 0.08 to 0.12, based on measurements obtained from depths below 90 meters, and by helium porosimetry and water immersion (J. Dorsch, in preparation). No measurements of porosity were taken from the experiment site near BG4. However, it is expected that the porosity of the material in which the wells are located

decreases from 0.40 near ground surface to approximately 0.10 at the saprolite/bedrock interface. The hydraulic conductivity of the underlying bedrock is often up to four orders of magnitude lower than the saprolite, 10^{-6} m/d compared to 10^{-2} m/d (Moore and Toran, 1992).

The water table in the vicinity of BG4 varies seasonally due to seasonal variations in precipitation and evapotranspiration. The vegetation at the BG4 experimental site consists of a mixture of deciduous and coniferous trees. The soils derived from Pumpkin Valley Shale are acidic, contain little carbonate and have low natural fertility, which strongly influences the type of vegetation (Hatcher et al., 1992). The trees at the experiment site were removed before the start of the experiment in 1977 (Webster, in press). The climate of East Tennessee is warm, and humid with a mean annual air temperature at the Oak Ridge Reservation (ORR) (1945 to 1964) of 14.5°C, and mean annual precipitation (1954 to 1983) of 133 cm (52 in) as shown in Figure 2 (Air Resources Atmospheric Turbulence and Diffusion Laboratory, in Webster et al., 1982; Webster and Bradley, 1988).

Rainfall infiltration through soils derived from Pumpkin Valley Shale is poor due to the presence of a clay-plugged upper saprolite horizon which causes runoff, perched water tables and near-surface lateral flow (Hatcher et al., 1992). The location of the water table within ORR is typically at or a few meters above the

regolith/bedrock interface and tends to follow the topographic slope (Solomon et al., 1992). The dip of bedding in the upper bedrock and the saprolite commonly ranges from 30° to 45° to the southeast and a strike of N56°E in the vicinity of BG4 (Webster, in press).

No fracture parameters are available from the BG4 experiment site. The expected fracture characteristics are estimated, based on information obtained from research conducted elsewhere on the ORR. The only detailed field investigation of geologic structure in the saprolite was conducted by Dreier et al. (1987). They examined 1.2 m deep trenches in the Conasauga near BG6, about one kilometer southwest of the BG4 site. The fractures appear to represent relict structural fabrics due to local folding events. There are two distinct northeast and northwest fracture sets, but fracture orientation varied with local bedding attitude. As shown in Figure 3, there is generally one set of bedding-plane parallel fractures (BPFs), two sets of extension fractures (EFs) and a less abundant set of shear fractures (SFs). The BPFs and the EFs form an orthogonal system with a brickwork-type geometry. Fracture spacing in the top 1.2 m of the regolith is approximately 0.5 cm, but it is likely that spacing increases with depth because of the greater confining pressure and lesser influence of biological factors, such as tree roots.

According to Lemiszki and Hatcher (in Hatcher et al., 1992), there are few documented investigations of fractures in the unweathered bedrock of the Conasauga Group (Sledz and Huff, 1981; Davis et al., 1987; Dreier and Toran, 1989; and Foreman and Dunne, 1991). Lemiszki and Hatcher (in Hatcher et al., 1992) concluded that fractures in the Conasauga Group in the hanging wall of the Copper Creek thrust are related to: (1) development of symmetrical occurring hybrid and shear fracture sets about the extension fractures; (2) variations in bedding plane dip; and (3) local fracture set development. The fracture orientations, or architectures, that have been identified on the ORR are presented in Figure 4 (Hatcher et al., 1992).

Overview of Well Set-up, Injection and Monitoring for BG4 Site

Seven monitoring wells were constructed in a semi-circle down-slope from the injection well (Figure 5). From the injection well, each monitoring well is 3.7 meters away and separated by approximately 30°. Each well was augured with an 20.3 cm diameter auger to approximately 1.5 m depth, then cased with 16.5 cm outside diameter PVC pipe which was grouted in place and equipped with a PVC cap. Wells were deepened with a 12.7 cm diameter auger, and left open from the bottom of the casing to the bottom of the well. The depth of the monitoring wells ranges from 8.3 m to 9.4 m, and the depth of the injection well is 6.3 m. Well 7 was the only well augured down to refusal (about 3 cm into hard

rock). Well 7 has a completed depth of 8.3 meters, and assuming it reached the underlying unweathered bedrock, penetrates the full extent of the saprolite (Webster, in press).

Slug tests were carried out in each well at the experiment site to determine bulk hydraulic conductivity, K_b. The K_b values range from $1.2x10^{-2}$ to $3.0x10^{-3}$ m/d and average $6.8x10^{-3}$ m/d (Table 3). However, because the wells were augured, smearing may have occurred, which can cause significantly lower measured K_b values, especially where open fractures are present (D'Astous et al., 1989). Measured K_b values may also be sensitive to water table elevation at the time of testing, because K_b often decreases with depth in shallow weathered and fractured materials.

Water table elevations were measured manually with a water level tape in all wells at least monthly from July 1977 until May 1982 (Webster, in press). The elevations vary seasonally in response to rainfall as shown in Figure 6, and correspond to a seasonal variation in the thickness of the vadose zone. The gradient and direction of maximum slope of the water table also varies seasonally (Figure 7). The range in water table gradient from the injection well to monitoring well 7 is 0.09 to 0.22 over a period of 12 months, and averages 0.15. During the first 80 days of the experiment, the water table elevation dropped

nearly 3 meters in the injection well (Figure 6). A maximum variation of 5.5 m was observed in the injection well during the first five years of the experiment.

Tritium, or more accurately, tritiated water, was used as the tracer (Webster, in press). It is expected to be relatively unaffected by chemical reaction or sorption in the subsurface, and is affected only by radioactive decay (Ames and Rai, 1978). Tritium was chosen as the tracer partly because tritium and other radionuclide materials were buried in shallow unlined pits at the burial grounds of ORR and hence there is a great deal of interest in the transport of tritium in the weathered shales.

At the start of the experiment, a small glass ampoule containing 50 curies of tritiated water was introduced into the approximately six meter deep injection well. The ampoule was crushed to release the tritium and the well was mechanically agitated to ensure even mixing of the tracer (Webster, in press). Water samples were collected in the monitoring wells daily to bi-weekly for the first two years, and then once a year until 1982 to determine tritium concentrations. The injection well was sampled less frequently, with the first sample taken immediately after injection, and no further sampling until 85 days later. The sampling procedure involved using a constricted neck funnel which was lowered through the water column and required several seconds to fill,

thereby obtaining a sample from most, if not all of the water column. The wells were not purged prior to sampling. All the wells (except the injection well and well 6, which were dry) were sampled again in October 1993, approximately 16 years after the tritium injection (McKay, personal communication).

The samples were then analyzed by the Analytical Chemistry Division, at ORNL. Tritium concentrations were measured by mixing 1.0 ml of sample with 15 ml of a scintillation cocktail and then direct counting of decay rates. Tritium counting was calibrated using standards obtained from the National Bureau of Standards. For questionable sample results, a new sample was prepared and analyzed, and quality control was maintained by preparing duplicate samples and submitting them with later samples. Using these methods, the detection limit for tritium was approximately 1 decay per minute per milliliter (1 dpm/ml). Background tritium levels in the injection well and monitoring wells prior to the experiment were below the detection limit (Webster, in press).

Experiment Results and Discussion

The initial tritium concentration in the injection well after addition of the glass ampoule and mixing was 2×10^{10} dpm/ml. Tritium concentrations declined rapidly in the injection well (two orders of magnitude in 85 days) shortly after the start of the experiment (Figure 8). The rate of concentration decline then slowed with a

decrease of three orders of magnitude over the next 2.5 years, after which the concentration remained relatively stable. Calculations of water flux through the injection well based on the dimensions of the water column at the start of the injection indicate a 111 day period for one well bore volume to be flushed through the injection well (Appendix B). This flux is consistent with the observed rapid decline of tritium concentration in the injection well during the first 85 days. However, after this period, tritium levels in the injection well persisted at lower, but still significant levels (~ 10^6 dpm/ml) for the entire 5 years of monitoring. This persistence can be explained by "storage" of tritium in the material surrounding the injection well. The material surrounding the injection well is highly fractured, and although most of the flow occurs through fractures, the groundwater in the matrix becomes contaminated by diffusion from the tritiated groundwater in the fracture. Subsequently, clean water moving towards the well through fractures becomes contaminated by diffusion of tritium from the groundwater in the matrix back into the "clean" groundwater in the fracture. As well, while the water table declined during the first 80 days, tritium was left trapped in the matrix pores above the water table. Later, when water levels returned to higher levels, the tritium stored in the vadose zone was remobilized, and could again diffuse back into the injection well.

Removal of the tritium from the injection well was attempted at 250 days by flushing out the contaminated water and replacing it with clean water (Figure 8). Within a few days after flushing, tritium in the injection well returned to pre-flushing levels. The flushing apparently removed only the tritium stored in the fractures, not in the surrounding blocks of matrix. Shortly after the flushing, concentrations increased in the well because of tritium "stored" in the matrix. This interpretation implies that once the "matrix" between the fractures is contaminated, solute removal by pumping can be extremely slow.

Contamination during handling of samples from the surrounding monitoring wells was a problem for the first 16 days, probably because of atmospheric release of tritium from the injection well into collected water samples of other wells (Webster, in press). Following changes in the sample collection and handling procedures, it was evident that by 19 days, the tritium tracer had appeared in the well directly down-slope from the injection well (well 7). The tritium plume is shown in map view (Figure 9) at times ranging from 21 to 5851 days after the start of injection.

The breakthrough curve (BTC), which is a plot of tracer concentration at a single monitoring point versus elapsed time since the start of the experiment, for well 7 is shown on Figure 10. On Figure 10A, tritium is plotted on a log scale which is needed to show the lower concentration values, particularly for the rapid (relative

to the slower moving center of mass (COM)) first arrival of tritium (by 19 days) and the long "tail" of very slowly declining concentrations. An 11 year gap exists between the last two data points. The small difference in concentration between these two data points (at 5 years $8.5x10^4$ dpm/ml, and at 16 years $3.5x10^4$ dpm/ml) further illustrates the relatively gentle slope of the "tail" (relative to the first five years) of slowly declining concentrations. On Figure 10B, tritium is plotted on an arithmetic scale which more clearly shows the arrival of the main pulse of tritium and the location of the COM. According to this plot, the COM reached well 7 by approximately 400 days, indicating a velocity of 0.009 m/d.

The migration of the COM is much slower than the first arrival, which is interpreted to result from the diffusive exchange between the fast moving water in the fractures and the relatively immobile water in the blocks of saprolite (or matrix) between fractures. Diffusive exchange also explains the very long "tail" because it can take a very long time for the tritium to diffuse back out of the matrix to the fractures.

CHAPTER 3

MODEL DESCRIPTION

Three different types of software were used to analyze the tritium experiment. They include CXTFIT (based on Parker and van Genuchten, 1984), which was used for one-dimensional equivalent porous medium simulations, CRAFLUSH (based on Sudicky and Frind, 1982), which was used for one dimensional discrete-fracture/matrix-diffusion simulations, and FRAC3DVS (based on Therrien and Sudicky, in press) which was used for both two-dimensional EPM and DFMD simulations. Both of the one-dimensional codes are in FORTRAN, and operate under DOS. FRAC3DVS is also in FORTRAN and was run under UNIX workstations to take advantage of its higher memory compared to personal computers.

One dimensional models were used to obtain preliminary results. Two dimensional plan view models, instead of three dimensional models, were used because:

1. the amount of required computer memory was reduced, especially for simulating fracture flow and transport
2. the system is bounded vertically by the relatively impermeable underlying bedrock, and

3. the sampling technique resulted in mixing of waters from different depths, so no concentration versus depth data in the saprolite is available.

CXTFIT

The model CXTFIT (Parker and van Genuchten, 1984) was used for the one-dimensional EPM simulations. The assumptions of the model are that the system is one-dimensional, homogeneous, isotropic, and fully saturated.

Solute transport is governed by the advection-dispersion equation:

$$R\frac{\delta c}{\delta t} = D\frac{\delta^2 c}{\delta x^2} - v\frac{\delta c}{\delta x} - R\lambda c \qquad (1)$$

where c is solute concentration (ML^{-3}), t is time (T), x is the distance along the flow path (L), and R is the retardation factor (dimensionless), defined as

$$R = 1 + \frac{\rho_b}{n_t} K_d \qquad (2)$$

where ρ_b is the bulk density, K_d is the distribution coefficient, and n_t is the total porosity. The longitudinal dispersion, D (L^2T^{-1}), is defined as

$$D = \alpha_L v + D^* \qquad (3)$$

where α_L is the coefficient of longitudinal dispersivity (L), and D^* is the diffusion coefficient of the solute in the porous material (L^2T^{-1}), defined as

$$D^* = D^\circ \omega \quad (4)$$

where ω is the tortuosity factor (dimensionless) of the porous material and D° is the free water diffusion coefficient (L^2T^{-1}). The rate coefficient, λ (T^{-1}), is defined as

$$\lambda = \frac{\ln 2}{t_{1/2}} \quad (5)$$

where $t_{1/2}$ is the half-life (T) of the radioactive contaminant. The average groundwater velocity, v (LT^{-1}) can be calculated using

$$v = K_b \frac{i}{n_e} \quad (6)$$

where K_b is the bulk hydraulic conductivity (L/T), i is the hydraulic gradient (dimensionless), and n_e is the effective porosity (dimensionless).

Although CXTFIT has a curve-fitting procedure to determine parameters from observed data, it was not used. CXTFIT is used to create BTCs from assumed parameters that were visually fitted to the tracer experiment BTC, which was necessary because of differences in simulated and observed concentrations.

CRAFLUSH

Figure 11 is a graphical representation of the system used for CRAFLUSH one-dimensional DFMD simulations (Sudicky and Frind, 1982) which was modified to

incorporate the cubic law to calculate flow velocities. Solute transport is governed by two equations, one for advective transport in the fractures, and the other for diffusive exchange between the fracture and the surrounding matrix. The two equations are interrelated due to the continuity of concentration along the matrix/fracture interface.

The distribution of a given solute within a fracture is described by (Tang et al., 1981)

$$\frac{\delta c}{\delta t}+\frac{v}{R_f}\frac{\delta c}{\delta z}-\frac{D_f}{R_f}\frac{\delta^2 c}{\delta z^2}+\lambda c+\frac{q}{R_f b}=0 \qquad 0\le z\le\infty \tag{7}$$

The concentration of a solute in solution, c (M/L^3), is defined as c=c(z,t), where z is the distance along the fracture (L), and t is time (T). Longitudinal dispersion, D_f (L) in the fracture , is defined as

$$D_f=\alpha_f v_f+D^o, \tag{8}$$

where α_f is the longitudinal dispersivity in the fracture. The retardation in the fracture, R_f (dimensionless), is defined as

$$R_f=1+\frac{K_{df}}{b}, \tag{9}$$

where K_{df} is the fracture distribution coefficient (L) and b is half the fracture aperture. The diffusive loss from the fracture to the matrix, is described by the solute flux term, q_s ($M/L^2/T$) which is defined as

$$q_x = -nD^* \frac{\delta c'}{\delta x}\bigg|_{x=b} \quad (10)$$

where c' is the concentration (ML^{-3}) within the porous matrix with c'=c'(x,z,t).

The equation describing the diffusive transport perpendicular to the fracture is

$$\frac{\delta c'}{\delta t} - \frac{D}{R}\frac{\delta^2 c'}{\delta x^2} + \lambda c' = 0 \quad (11)$$

where R is the matrix retardation which represents the adsorptive loss in the matrix and is defined in (2).

The CRAFLUSH program was modified to calculate the fracture aperture, 2b (L), and the velocity in the fracture, v_f (LT^{-1}), for a system of evenly-spaced parallel fractures using measured or estimated values of bulk hydraulic conductivity, K_b, matrix hydraulic conductivity, K_m, and fracture spacing, 2B (L). The equations are outlined in McKay et al. (1993a) and are based on the "cubic law" (Snow, 1968, 1969), which states that discharge per unit length of a smooth-walled fracture, q_f (LT^{-1}) is related to the cube of the aperture of the fracture, 2b:

$$q_f = (2b)^3 \frac{\rho g}{12\mu} i \quad (12)$$

where μ ($ML^{-3}T^{-2}$) is the viscosity of water, ρ (ML^{-3}) is the density of water, g

(LT^{-2}) is the acceleration due to gravity constant, and i is the hydraulic gradient along the fracture. Based on this relationship and Darcy's Law, Snow (1968, 69) defined the hydraulic conductivity of the fracture, K_f, as

$$K_f = (2b)^2 \frac{\rho g}{12\mu} . \tag{13}$$

Assuming a system of evenly-spaced, parallel fractures, all with the same aperture, in a porous matrix, the bulk hydraulic conductivity, K_b, in the direction of the fractures is

$$K_b = \frac{2b}{2B} K_f + K_m \tag{14}$$

where K_m is the hydraulic conductivity of the blocks of porous matrix between fractures. Equations (13) and (14) are combined to solve for the aperture of the fractures in the system

$$2b = \left[\frac{(K_b - K_m)(2B)12\mu}{\rho g} \right]^{1/3} . \tag{15}$$

The flow velocity within the fracture is determined using the calculated value of aperture, 2b, and the measured hydraulic gradient, i

$$v_f = \frac{(2b)^2 \rho g}{12\mu} i . \tag{16}$$

The fracture flow velocity, v_f, and the fracture aperture, 2b, are then used in solving the solute transport problem as described by Tang et al. (1981), and Sudicky and Frind (1982).

FRAC3DVS

FRAC3DVS is a discrete fracture numerical model where advective transport and diffusion are accounted for in the matrix (Therrien and Sudicky, in press). Although the system used for this thesis was a 2D system, Figure 12 is a graphical representation of a typical 3D system used for FRAC3DVS. The matrix is represented in three dimensions, and fractures are represented by two-dimensional planes. It is also possible to operate FRAC3DVS with no fractures, thereby having an EPM model.

The model employs a time marching Galerkin finite element technique which is used to discretize the solute transport equation with either finite element or by mimicking a finite difference discretization. For this thesis, the model was set up with finite difference discretization, the system fully saturated, and operating under steady-state flow conditions. Other boundary conditions for flow and transport are further explained in Chapter 4 under FRAC3DVS simulations.

The governing equation for solute transport in the matrix is

$$R\frac{\delta c}{\delta t} = \frac{\delta}{\delta x_i}(D_{ij}\frac{\delta c}{\delta x_j}) - v_i\frac{\delta c}{\delta x_i} - R\lambda c \qquad \text{i,j=1,2} \qquad (17)$$

where D_{ij} (L^2T^{-1}) is dispersion defined as

$$D_{ij} = (\alpha_L - \alpha_T)\frac{q_1 q_2}{|q|} + \alpha_T|q|\delta_{ij} + D^*\delta_{ij} \qquad \text{i,j=1,2} \qquad (18)$$

where α_L (L) is the longitudinal dispersivity, α_T (L) is the transverse dispersivity, |q| is the magnitude of the Darcy flux, defined as

$$q = \frac{\delta}{\delta x_i}(K_{ij}\frac{\delta(\psi + z)}{\delta x_j}) \qquad \text{i,j=1,2} \qquad (19)$$

where ψ (L) is the pressure head, z (L) is the elevation head.

For transport in the fracture, the governing equation is

$$0 = 2b\left[R_f\frac{\delta c_f}{\delta t} - \frac{\delta}{\delta x_i}\left(D_{fij}\frac{\delta c_f}{\delta x_j}\right) + q_f\frac{\delta c_f}{\delta x_i} + R_f\lambda c_f\right] - \Omega_n|I^- + \Omega|I^+ \qquad \text{i,j=1,2} \qquad (20)$$

where the terms Ω_n represents the advective-dispersive loss or gain of solute mass across the fracture-matrix interfaces I^- and I^+ due to fluid leakage and hydrodynamic dispersion. The Darcy flux in the fracture is

$$q_f = \frac{\delta}{\delta x_i}(2b)K_f\frac{\delta(\psi_f + z_f)}{\delta x_j} \qquad \text{i,j=1,2} \qquad (21)$$

where ψ_f (L) is the pressure head in the fracture, z_f (L) is the elevation head in the fracture, and q_f is the fluid flux in the fracture (L/T). The fracture dispersivity is

defined in the same way as matrix dispersivity where dispersivity coefficients and fluxes correspond to the fracture.

Flow in the matrix and fractures is solved by using the standard Galerkin technique (see e.g. Huyakorn and Pinder, 1983) which is used to discretize the transport equation over the domain of interest. The solution for the flow equation is solved by the control volume finite element approach (Kropinski, 1990) and a preconditioned ORTHOMIN solver. The fracture elements are common to nodes comprising the porous matrix elements which ensures the continuity of hydraulic head at the fracture-matrix interface.

CHAPTER 4

RESULTS AND DISCUSSION

One Dimensional Modeling

One-dimensional models were used to determine whether or not the general characteristics of the solute BTCs observed in a down-gradient well (well 7) at the BG4 tracer experiment site could be reproduced using both an equivalent porous media and a discrete-fracture/matrix-diffusion approach. As well, the one-dimensional modeling was performed to estimate preliminary values for parameters such as fracture aperture and effective porosity, and to determine the sensitivity to variations in these values for use in the two-dimensional models.

The tritium breakthrough observed in down-gradient wells has three distinct characteristics: (1) the rapid early breakthrough; (2) the period of relatively high concentration, including the arrival of the center of mass (COM); and (3) the long tail of slowly declining concentration. Matching the simulations to the data involves trying to reproduce all three characteristics of the BTC with a single simulation. The high degree of lateral spreading is also an important characteristic of the solute plume, but it could not be addressed in the 1D modeling.

The one-dimensional models assume an infinitely extensive line source of tracer, similar to a long trench filled with tracer solution, rather than the injection well, which behaves more like a point source. As a result, the one-dimensional models do not simulate transverse spreading of the solute, and hence over-estimate concentrations. However, the shape of the simulated BTC will be similar to that expected for a point source and can be compared to the shape of the observed BTC. This procedure was used to determine a preliminary estimate of the physical parameters needed to match the observed data.

The source term used for all the one-dimensional simulations was a step function with an immediate rise at zero days to a relative concentration of 1.0, followed by a step decrease to zero at 40 days. This source term was chosen based on the curve of tritium concentration vs. time as observed in the injection well over the first 80 days (Figure 8). The 40 day step function has approximately the same area under the concentration vs. time curve as the tritium in the injection well and was expected to represent injection of approximately the same mass of tritium (50 curies). Other values used for the one-dimensional simulations are shown in Table 4, and a detailed discussion of some of the critical parameters follows.

The hydraulic gradient value used for all simulations was 0.15 and was calculated based on the water table elevation values measured in the injection well and monitoring well 7. Water table elevations were measured over a period of 12 months, and calculated gradients range from 0.09 to 0.22. An effective diffusion coefficient for tritium of 5.18×10^{-5} m^2/d was used for the DFMD simulations and was chosen based on comparison with values for $^{18}0$, ^{2}H, and ^{3}H measured in laboratory columns of undisturbed fractured clay till (McKay et al., 1993b). The porosity of the till (0.32) is within the range of values expected for the saprolite (0.1 to 0.4) and the effective diffusion coefficient for tritium in the fractured clay till was expected to be similar to that of tritium in the fractured shale saprolite. The tritium half-life used in all the simulations was 4.53×10^{3} d (12.3 years).

CXTFIT Simulations

Velocity, v, and dispersivity, α, were the only parameters varied for the 1D-EPM simulations. The simulations were visually fitted to the data from well 7 by first varying velocity until the position of the simulated peak, or center of mass (COM) of the pulse, matches the data. For these simulations (Figure 13A), the dispersivity was held constant at a value of 0.4 m (which is approximately 10% of the length of the flow path). After determining a "best-fit" velocity, the

dispersivity, α, was then varied to fit the rapid initial breakthrough and the long "tail" (Figure 13B).

The simulated concentrations were all several orders of magnitude higher than the observed concentrations. Some differences between simulated and observed concentrations were expected because the model assumes a line source rather than a point source, but the large difference (100 times) indicates that the 40 day step-source may allow too much tritium to enter the flow system. Possible causes of the difference are discussed in a later section.

It was possible to provide a match to the shape of the tritium BTC using values of v=0.009 m/d, and α=2.0 m (Figure 13). The fitted velocity of 0.009 m/d, which represents the simulated average velocity of groundwater flow, matches the observed velocity of the COM, v=0.009 m/d, which is calculated by dividing the distance of well 7 from the injection well (3.7 m), by the 400 days required for the COM to reach the well. The effective porosity, n_e, for the simulation was 0.15 and was calculated from the simulated velocity, v (0.009 m/d), the measured bulk hydraulic conductivity, K_b (0.009 m/d), and the hydraulic gradient, i (0.15), in the simulations using

$$n_e = \frac{K_b i}{v} \tag{22}$$

This effective porosity value of 0.15, is between the value of total porosity expected for the upper 1 to 2 meters of soil (0.4) and for the unweathered bedrock (0.1). These expected values are based on measurements in similar shales on the Oak Ridge Reservation (ORR) (Wilson, 1992; Dorsch, in preparation). The total porosity of the saprolite or underlying bedrock at the tracer test site was not measured. Because the water table was usually at a depth of 3 to 5 meters below the highly weathered soil zone, it is likely that total porosity in the region of the plume is closer to 0.1 than to 0.4, in which case the effective porosity would be nearly equal to the total porosity. If this is true, and if the porosity is homogeneous, then the tritium did not follow a preferential flow path, and was spread evenly throughout the fractures and in the matrix. The effective porosity described above is the porosity through which solutes migrate, namely the fractures (through advective transport governed by the cubic law) and the matrix (through diffusion). Some researchers (e.g. Endo et al., 1984) describe effective porosity as equal to only the porosity contributed by fractures (this would be correct if there was no solute migration into the matrix).

CRAFLUSH Simulations

Simulations generated using a modified version of the CRAFLUSH code were initially "fitted" in the same way CXTFIT simulated curves were visually fitted to the BTCs for well 7. Simulations using CRAFLUSH were accomplished by varying two

parameters: fracture spacing, 2B, and fracture dispersivity, α_f. Values of the other parameters used in the simulations are shown on Table 4 and are summarized as follows. Bulk hydraulic conductivity was fixed at 0.009 m/d which corresponds to the average value obtained from slug tests. The matrix porosity, n_m, was set at 0.15, which is the same as the value of effective porosity, n_e, determined from the CXTFIT simulations and it is expected to be near the value of total porosity at the depth of the tritium plume. Another important parameter, effective diffusion coefficient, D*, for tritium was set at 5.18×10^{-5} m^2/d. As discussed previously, this value was chosen based on measured values in a clay till (McKay et al., 1993b). The input source was the same type of 40 day duration step-function used for the CXTFIT simulations.

The simulations were fit to the data (Figure 14A) first by varying 2B with α_f=0.10 m (α_f based on tracer experiment in fractured clay till by McKay et al., 1993b). As was the case with the EPM simulations, the DFMD simulated values were several orders of magnitude higher than the measured values, but the shape of the BTC could easily be fitted to the observed BTC. Varying 2B strongly influences the position of the COM and the best fit was achieved at a fracture spacing of approximately 0.1 m. With fracture spacing less than 0.1 m, there was no real difference in the shape or position of the BTC. This is because the solute was already evenly spread through the fractures and the surrounding blocks of matrix,

in which case flow velocity in the individual fractures (which is calculated from K_b and 2b) no longer has a strong influence on transport.

The fracture dispersivity, α_f, was then varied (Figure 14B) using fixed values of K_b=0.009 m/d and 2B=0.1 m. Varying α_f has much less influence on the COM than varying K_b but does influence the early and late time behavior. Although the shape of the curve could not be fit perfectly, reasonable fits were achieved using values of α_f of 0.5 or 1.0 meters.

Sensitivity analyses (Figure 15) were then carried out using the "fitted" values of 2B=0.1 m and α_f=0.5 m to test the influence of the following key parameters: bulk hydraulic conductivity, K_b, matrix porosity, n_m, and effective diffusion coefficient, D* (Figure 15). Each parameter was varied over the range of values expected in the field. Figure 15A shows a high degree of sensitivity to K_b which was varied by almost two orders of magnitude (K_b values for fractured materials can vary greatly and are sensitive to the method and scale of measurement.). The simulations are much less sensitive (Figure 15B) to the expected range of variations in n_t (0.10 to 0.25) and D* (2.6 to 7.8x10^{-5} m^2/day), both of which typically show much less variability than hydraulic conductivity values.

By comparing the concentrations in the matrix midway between fractures and the fracture for the best matching simulation, it is possible to make preliminary assessment concerning the applicability of modeling the system as an EPM. If concentrations in the middle of the matrix block are similar to those in the fractures, then the effective porosity, n_e, which is a crucial fitting parameter for the EPM modeling, is essentially equal to the total porosity, n_t. Because total porosity is easily measured, this greatly reduces the uncertainty in modeling the system using an EPM approach. As shown on Figure 16, simulations were repeated at several different fracture spacings, 2B, to determine the concentration in the matrix midway between fractures, and compare it to concentrations in the fracture. The difference between the concentrations for a fracture spacing of 0.1 meters or less is very small. At this point, the system is behaving as an EPM (or continuum) such that Darcy's equations can be used, and is appropriate for EPM modeling, using effective porosity, n_e, equal to total porosity, n_t.

In summary, both the 1D-EPM (or continuum) and 1D-DFMD models are equally capable of reproducing the tritium breakthrough characteristics in well 7, although both over-predict the concentration. With the EPM model, an effective porosity value of 15% was calculated. With the 1D-DFMD model, it was determined that for the measured hydraulic conductivity value of 0.009 m/d, a fracture spacing of 0.10 meters or less, is required for the simulations to fit the data.

Two-dimensional Modeling

Two-dimensional models were used to:

1. determine if the observed rapid early breakthrough, the slow moving center of mass, the long tail of slowly declining concentration and large degree of transverse spreading of the tritium plume can be simulated using both EPM and DF modeling approaches under 2D steady-state flow conditions;
2. investigate possible causes of transverse spreading of plumes in fractured systems;
3. determine if either of the models can simulate the magnitude of the observed tritium concentrations rather than just the shape of the plume or the BTC;
4. compare the operational advantages or disadvantages of DF and EPM options when applied to field-scale problems.

All of the two-dimensional modeling was performed with the FRAC3DVS code for a 10 m x 10 m plan view region as shown in Figure 17. The flow system was assumed to be at steady-state and fully saturated, with the medium (before addition of fractures) homogeneous and isotropic. A uniform, constant head along the top and bottom of the grid was used to establish an overall hydraulic gradient of 0.15. The bulk hydraulic conductivity for the medium was assumed to

be isotropic, even though it may be anisotropic at the field site, because of fractures parallel to bedding strike. The anisotropy, if present, should not influence the steady-state simulations because the hydraulic gradient was aligned with one of the expected principal directions of the hydraulic conductivity ellipse (Figure 5, 17). The source term used was the same as for the one-dimensional simulations, which was a step-function with a relative concentration of 1.0 for 40 days. Other parameters used for the two-dimensional simulations are shown on Table 5.

Two-dimensional EPM Simulations

For the two-dimensional EPM simulations, the parameters used to visually "fit" the simulations to the BTC data from monitoring well 7 were average groundwater velocity, v, longitudinal dispersivity, α_L, and transverse dispersivity, α_T. The simulations were fitted to the position of the center of mass, COM, of the plume by varying v, while using fixed values of α_L =0.2 m, and α_T=0.02 m (Figure 18A). As in the case of the 1D simulations, the simulated concentrations were several orders of magnitude higher than the observed values, but the position of the COM of the plume could be fit with a velocity of 0.01 m/d. Possible causes of the difference between simulated and observed concentrations are discussed in a later section.

The longitudinal dispersivity, α_L, was then varied using the "best-fit" velocity (0.01 m/d) and transverse dispersivity (0.02 m) (Figure 18B). Using a value of α_L =0.8 m, the rapid initial breakthrough and the long tail in well 7 were reproduced, without changing the position of the COM. Again, simulated concentrations were several orders of magnitude higher than observed values. Because transverse dispersivity influences tritium spreading in a transverse direction, it was expected that increasing transverse dispersivity, α_T, would reduce tritium levels in simulated breakthrough in well 7. Typically, transverse dispersivity values are much less than longitudinal values. However, because of the large degree of observed transverse spreading of the actual tracer test plume, a large transverse dispersivity was expected. For the simulations, transverse dispersivity, α_T, was varied from 0.08 to 2 meters (Figure 18C). With increasing transverse dispersivity, simulated tritium levels in well 7 were slightly lower than measured, but the change was small relative to the difference between simulated and observed values. Because concentrations in the well directly down-gradient are relatively insensitive to varying α_T, data from other wells must be included to "fit" α_T.

BTCs for four other wells on either side of well 7 were generated using the two-dimensional simulation that matched the breakthrough in well 7, and are presented in Figure 19. Although the simulations were not fitted individually to

these wells (by varying v and α_L), the shape of the individual BTCs could be reproduced using values of α_T ranging from 0.08 to 0.8 meters. The simulated plume is also presented in plan view (Figure 20) at 85 and 360 days after the start of the injection using values of α_T ranging from 0.0 to 0.8 meters. Because of the difference in magnitude of simulated and measured concentrations, comparison with the data is accomplished by comparing COM locations, and the shape of the plume. Based on the plan view plume simulations, it is clear that the transverse spreading can be simulated using an α_T value between 0.08 and 0.8m.

In summary, the two-dimensional EPM steady-state simulations were able to reproduce the shape of the BTCs in the individual wells and to reproduce the overall shape of the plume in plan view. The overall approximate best-fit to the data was obtained using the following values: v=0.01 m/d, α_L=0.8 m and α_T of 0.08 to 0.8 m. However, in all cases simulated concentrations were several orders of magnitude higher than measured values. Possible causes of this excess concentration are discussed in a later section.

Two-dimensional Discrete Fracture-EPM (DF-EPM) Simulations

Representation of the entire 10 m x 10 m system with a network of discrete fractures at the scale observed in the field was initially considered. This would

require a system with approximately 10^4 to 10^6 fractures, based on estimates of fracture spacing from test pits and outcrops of similar material on the ORR and from estimates of fracture spacing obtained from the 1D DFMD modeling. This proposed model would have been computationally very difficult and it would not have been feasible to expand such a model to larger areas, say to represent tritium migration from burial pits in BG4. Lack of computer memory is a common problem when trying to apply discrete fracture modeling methods to highly fractured systems.

In this study, the discrete fracture approach was combined with the EPM approach (DF-EPM) to investigate the influence of a few widely-spaced larger-aperture fractures in a highly fractured mass. These widely-spaced fractures, if present, could have a large influence on transverse spreading of a plume. The fracture networks chosen are hypothetical and may not be the cause of transverse spreading at the experimental site. Other factors, such as seasonal variations in the elevation and direction of slope of the water table are expected to be significant at the site, but could not be incorporated in the 2D steady-state approach.

The highly fractured network was assumed to act as an EPM and was represented by taking the best fit two-dimensional EPM simulation and reducing the transverse dispersivity to zero. Different scenarios were then run with a few widely-spaced fractures superimposed on the EPM to see if transverse spreading can be reproduced by these fractures. Fracture aperture values for the widely-spaced fractures were set at 150 or 250 μm, and are much larger than those calculated with one-dimensional discrete-fracture/matrix diffusion simulations (26 μm assuming a fracture spacing of 0.1 meters). Other parameters used in the simulations are listed in Table 5. Isolated fractures which did not penetrate a boundary or another fracture were not considered because they are expected to have less influence than interconnected fractures.

Initially, simulations were carried out with very simple networks with one to four fractures. For each of the simulated fracture orientations, the resulting head distribution, assuming a fracture aperture of 250 μm, is displayed in Figure 21. The head distribution and the results of the solute transport simulations for each of the simple networks are presented in Figures 22-28, and are described below.

A. A single fracture which fully penetrated the system and was perpendicular to flow direction had no effect on the head distribution (Figure 21A), and no

effect on transport (Figure 22). The simulated plume in Figure 22 was identical to the plume generated for the case with no fractures.

B. A single fracture which fully penetrated the system and was aligned parallel to the direction of flow (Figure 21B) had no influence on hydraulic head and relatively little influence on transverse spreading (Figure 23). However, the fracture, which intersected the source well, caused longitudinal transport rates to increase.

C. Two orthogonal fractures which fully penetrate the system and intersect down-gradient of the source well had no effect on head distribution (Figure 21C), and had the same effects on transport (Figure 24) as described in B above.

D. A single fracture parallel to the direction of flow which penetrated the up-gradient constant head boundary and did not reach the other end of the system, influenced the hydraulic head distribution, indicating radial flow away from the terminus of the fracture (Figure 21D) and caused solute spreading in the transverse direction (Figure 25).

E. Two fractures, one perpendicular to the direction of flow and the second parallel to flow but terminating at the intersection with the other fracture, disrupted the head distribution (Figure 21E) and increased the amount of transverse spreading (Figure 26).

F. When the fracture orientation described in E was repeated such that there was a regular brickwork of fractures, hydraulic heads were disrupted (Figure 21F) and a large degree of transverse spreading of the plume occurred (Figure 27). In this case, there was now a continuous network of fractures in the direction of flow and the rate of longitudinal migration of the plume increased substantially.

Of the fracture orientations studied, those discussed in D, E, and F (Figures 25, 26 and 27) all strongly influence transverse spreading. The degree of spreading is also influenced by the size of the fracture aperture, which is shown in Figure 28 (case E) where simulations are shown for aperture values of 150 and 250 μm. By decreasing the aperture to 150 μm, the head disruption and transverse spreading of the plume were reduced. Increasing fracture density for the brickwork pattern (case E), also increased the rate of longitudinal transport, and the amount of transverse spreading (Figure 29).

Another simulation was performed to establish the influence of fracture placement relative to the source. Figure 30 represents the same fracture orientation and aperture as in case D (Figure 25), but the fracture was placed 0.4 meters to the left of the source well. Both cases show disruption of the hydraulic head and transverse spreading of the plume. The plume for the case with the fracture offset from the well by 0.4 m was slightly non-symmetric and showed slightly less up-gradient spreading.

In summary, the 2D discrete-fracture/EPM modeling shows that a few larger aperture fractures can strongly influence the shape of the plume. Truncated fractures more effectively cause transverse spreading and the degree of transverse spreading is sensitive to fracture aperture and fracture placement. It is clear that these and probably other fracture arrangements could cause the observed degree of transverse spreading in a steady-state flow field. The simulations have not been "fit" to the actual plume, but it is likely that by varying the EPM parameters (v, α_L and α_T) and by varying aperture values, that all the characteristics of the plume (shape, position of the center of mass, rapidly moving leading edge, slow moving tail) could be reproduced for several different fracture arrangements. It is not possible to arrive at a unique "fit" for the plume using the DF-EPM approach, but a possible scenario (transverse spreading due

to a few larger aperture truncated fractures) has been identified. This could in the future be compared to fracture geometry at the site and to other possible scenarios, such as transverse spreading due to seasonal variations of the water table.

Possible Causes of the Difference in Simulated and Observed Concentrations

In all simulations, 1D and 2D, EPM, DFMD or DF-EPM, the simulated concentration were substantially greater (up to 100 times) than observed values. Possible causes of this difference include: 1) addition of too much simulated tritium by the 40-day step-function input; 2) dilution in the monitoring wells; 3) losses of tritium to the vadose zone caused by the fluctuating water table; 4) losses of tritium by flow into the underlying bedrock. Each of these possible causes are discussed, as follows.

1. Input function. The mass of tritium added to the system was calculated for the best-fit 2D EPM simulation (v=0.01 m/d, α_L=0.8 m and α_T= 0.08 m) at 40 days, which is the end of the step-function input. This was done by measuring the areas enclosed by the concentration contours of the plume and multiplying by the average concentration of each zone (see Appendix B).

This approach gives a tritium mass of 201 Ci per unit thickness of the saturated zone. Based on a saturated zone thickness of approximately 2.7 m, the simulated tritium input is 543 Ci, a factor of 11 more than the actual 50 Ci which was added to the source well. It is clear, at least for the 2D-EPM case, and likely for the other cases as well, that input of too much tritium in the simulations is an important cause of the difference between observed and simulated (or expected) concentration values in the monitoring wells.

2. Dilution in the monitoring wells. The 12.7 cm (5 inch) diameter wells were not purged prior to sampling. As a result, the measured concentration values always reflect a mixture of new and older groundwater, which may not be representative of the tritium plume. The wells were uncased for the most of their length and hence would be very susceptible to periodic dilution by influx of uncontaminated water from the shallow stormflow zone. Since the calculated flow of contaminated groundwater into each well is small (0.0003 m^3/d per m^2 of saprolite) relative to the storage volume of the wells (up to 0.034 m^3), the effects of monitoring well dilution could be very substantial, and could be an important cause of the difference between observed and simulated tritium concentrations.

3. Losses to the vadose zone. The principal cause of loss to the vadose zone is expected to be due to infiltration and diffusion into the matrix during periods of high water table elevation. Much of this mass is not really "lost" because it becomes mobile again due to exchange with infiltrating groundwater or during subsequent periods of high water table and ultimately passes through, or by, the monitoring wells. Its main effect is to increase dispersion of the plume. Some losses of tritium may also occur due to exchange with soil vapor, but since the tritium was in the form of tritiated water, rather than dissolved tritium gas, this is expected to be relatively small. Losses to the vadose zone are not a likely cause of the large difference between observed and simulated (or expected) concentrations.

4. Losses to the bedrock. Some losses may occur due to flow into the underlying bedrock, but this effect is difficult to quantify because of the absence of monitoring wells in the bedrock. For the bedrock to have caused even a one order of magnitude difference between observed and simulated concentrations, approximately 90% of the mass of the tritium would have to enter the bedrock before reaching the monitoring wells. Because measured hydraulic conductivity values in shale bedrock at other sites on the ORR are typically lower than in the saprolite, this scenario is not very likely.

Model Prediction

An important goal of many contaminant transport modeling exercises is to predict concentrations a few years, or tens of years, into the future. These predictions often carry a high degree of uncertainty but few studies have tested their accuracy.

A comparison of model-predicted and measured concentrations can be carried out for the USGS tritium plume because of the long duration of monitoring. The main period of monitoring lasted for five years after the injection of tritium, and was the data constraint used for fitting the models. An additional sample was taken from each of the wells (except the injection well and well 6 which were dry) in 1993, 16 years after the tritium injection. It showed that tritium levels had changed only slightly over the past 11 years. Tritium levels in wells 5, 7, 8 and 10 declined less than an order of magnitude, and tritium levels in wells 4 and 9 actually increased slightly in concentration (less than a factor of 2).

The best-fit simulations for each of the three model types (1D-EPM, 1D-DFMD, and 2D-EPM) to the data from well 7, were extended to 16 years and compared to the measured value at that time (Figure 31). The 2D-DF-EPM was not evaluated because it was used to model transverse spreading trends and was not fit to the well 7 BTC. As shown on Figure 31, the predicted value from the 2D-EPM simulation closely parallels the measured trend. The predicted values from the 1D

simulations do not follow the trend as closely, although both follow the observed trend of a very long low concentration "tail." The predicted values are influenced by the initial visual fitting procedure, which involved only one iteration of varying the fitting parameters. It is likely that the 1D predictions could be improved by more rigorous fitting of the models to data from the first five years. As well, the measured concentration is expected to show some seasonal variations and further monitoring is recommended to better determine present concentrations. Given these factors, it is clear that all three "fitted" models can predict the general long-term trend of concentrations in this experiment.

Comparison with West Bear Creek Valley Tracer Experiment

A rhodamine dye tracer experiment (Lee et al., 1989; Lee et al., 1992; Sanford and Solomon, 1995) was conducted at a site in West Bear Creek Valley (WBCV) on the ORR. The geologic material at this site is Nolichucky Shale saprolite of the Conasauga Group and is similar to that at the USGS site (at BG4) in terms of porosity, low hydraulic conductivity, and fracture spacing and orientation. However, the shape of the plume that developed from the WBCV tracer experiment was very narrow (Figure 32) as compared to the wide shape of the USGS plume (Figure 9).

The major difference between the two sites which may have contributed to the difference in plume shape, is that the average water table gradient direction at the WBCV site is parallel to strike of the bedding plane, and that at the USGS site it is perpendicular to strike. This is particularly significant because of the expected higher hydraulic conductivity in the direction of strike at both locations due to bedding plane partings (or fractures). With this in mind, transverse spreading at the WBCV site would not be strongly influenced by fluctuating water table direction because of the lower hydraulic conductivity in the transverse direction. Conversely, at the USGS site, where the average hydraulic gradient is in the direction of the lower hydraulic conductivity (perpendicular to strike) fluctuating water table direction is expected to have more of an influence on transverse spreading than that at the WBCV site.

Two dimensional EPM modeling results for the WBCV tracer plume, assuming a non-isotropic system, required a transverse dispersivity more than 100 times smaller than the longitudinal (Lee et al., 1989), whereas the USGS tracer plume only required a transverse dispersivity from 1-10 times smaller. Other modeling research conducted for the WBCV site using noble gas tracers, indicated that transverse spreading at the WBCV site may be governed principally by diffusion (Sanford and Solomon, 1995), hence transverse dispersivity values of zero can be used to model the plume.

The tracer experiments at the USGS site and the WBCV site show great differences in plume shape, and may represent the two end-members of plumes in this setting. It is likely that at other locations where water table slope is neither parallel or perpendicular to bedding strike, that the shape of the plumes would be intermediate between these two extremes.

Implications for Remediation

Tritium migration through the fractured porous material at the experiment site is strongly influenced by matrix diffusion. If this was not so, tritium would have rapidly flushed out through the fractures under natural gradient conditions, rather than persisting for at least 16 years, as was observed. It is likely that tritium removal by pump-and-treat or drainage methods would be a very slow process due to "storage" effects created by matrix diffusion. It is clearly demonstrated by the "remediation" effort described previously which involved flushing contaminated groundwater out of the injection well 250 days after the start of the experiment. Within a month of flushing, concentrations in the injection well had risen nearly to pre-flush levels, apparently due to diffusion from the matrix pore water around the well.

The EPM modeling results presented above successfully predicted tritium migration through time. However, if flow rates are increased by lowering the water

table, such as could occur for remediation purposes, it is not clear whether the fitted values of the parameters (n_e, α_L, and α_T) would be appropriate. This would effect predictions of the effectiveness and required duration of remediation. Modeling using DFMD methods could have similar problems because, although a variety of fracture networks could reproduce the present plume, they may behave very differently when simulated remediation efforts, such as pumping from wells, are added to the system.

Future Work

The 2D-EPM model used to fit the tritium tracer plume migration is adequate for describing the general behavior of the plume. However, the fitted parameters can be refined, especially the source term, in order to more accurately predict future tritium concentrations. The system could also be simulated in 3D using the variable saturation mode to determine if the observed seasonal variations in the water table (particularly the changes in the direction of the slope of the water table) could have caused the large degree of transverse spreading observed.

Further field investigations could help improve the understanding of the transport processes. Additional long term monitoring of the existing tracer experiment at the USGS BG4 site is recommended. This data would be valuable for further refining the models and evaluating the ability to predict future concentrations in the plume.

construction and monitoring of additional down-gradient and up-gradient wells at this site would also aid in evaluation of the plume. More extensive field investigations could include mapping and sampling in boreholes or excavations to examine fracture orientation, spacing, and matrix porosity in the saprolite, particularly near the bedrock-saprolite contact. This could be carried out at the BG4 site or at a site in a similar, but uncontaminated setting. The distribution of hydraulic conductivity in the saprolite is also a source of uncertainty. Field investigations using hydraulic tests and/or tracer tests could be carried out to determine the distribution of hydraulic conductivity with depth and determine the degree of anisotropy. This type of information is needed to predict long term behavior of contaminants in these deposits.

CHAPTER 5

CONCLUSIONS

The tritium plume in the fractured saprolite material at the tracer test site can be simulated using either an equivalent porous medium (or continuum), a discretely-fractured material with matrix diffusion or a combination of discrete fractures, superimposed on an equivalent porous medium. All of the different approaches can reproduce the general characteristics of the BTCs in the monitoring wells, which include the rapid initial arrival, the slow moving center of mass, and the long tail of slowly declining concentrations through time. The simulated tritium concentrations were consistently two orders of magnitude larger than the observed values. The most probable causes of this discrepancy are the input of too much mass by the source term and dilution in the large diameter (12.7 cm) monitoring wells which were not purged prior to sampling. Less important contributors could include tritium losses in the vadose zone, and tritium transport into the underlying bedrock. The influence of the input mass could be assessed in future studies by using tritium mass as a fitting parameter and varying duration or concentration of the input. The other factors are more difficult to quantitatively assess and would require additional data, such as concentrations at different depths, which were not monitoring during the USGS experiment.

The "best-fit" 2D-EPM simulation (Figure 31) which was fitted based on the initial 5 years of monitoring data, came close to predicting the measured concentration in well 7 at 16 years, provided that the two orders of magnitude over-estimation is taken into account. The 1D models did not come as close to predicting the measured value, but still indicated that the low concentration "tail" would persist. The transverse spreading could readily be reproduced using the 2D-EPM approach, or the DF-EPM approach using a few larger aperture (150-250 μm) truncated fractures superimposed on an EPM. This does not imply that truncated fractures are responsible for the spreading, but merely identifies them as a possible cause.

The study suggests that relatively simple EPM models can be effective in predicting the general behavior of a plume in the fractured weathered shales, provided that there is sufficient existing plume data to which they can be fitted. The predicted concentration at 16 years would have probably been very inaccurate without the earlier data (especially from 2 to 5 years after the start) which indicated the approximate values of longitudinal and transverse dispersivity required to fit the plume. The combined discrete-fracture/equivalent porous media (DF-EPM) approach is useful for looking at possible causes of features such as the observed transverse spreading, but in the absence of detailed data on the fracture network, it is likely that it would be no more effective than the EPM approach in predicting

future behavior of the plume. It is not clear whether the fitted parameters, particularly n_e, α_L and α_T, for the 2D EPM model would be appropriate under different flow conditions, such as might occur during pump and treat remediation. This could also be a problem for discrete fracture modeling approaches because a variety of fracture networks could result in similar plumes under a given set of hydraulic boundary conditions, but might behave different from one another when these conditions are changed.

The modeling approaches presented in this thesis provide several reasonable alternative for interpreting the available data and indicate directions for future research.

REFERENCES

Ames, L.L., and Dhanpat Rai. 1978. Radionuclide interactions with soil and rock media, Vol. 1: U.S. Environmental Protection Agency, EPA 520/6-78-007.

Balfour, D.J. 1991. Evaluation of lateral solute migration in surficial weathered clayey till, M.Sc. thesis, Univ. of Waterloo, Waterloo, Ont., Canada.

Berkowitz, B., J. Bear, and C. Braester. 1988. Continuum models for contaminant transport in fractured porous formations. *Water Resources Research*, Vol. 24., no. 8, pp. 1225-1236.

Bibby, R. 1981. Mass transport of solutes in dual-porosity media, *Water Resources Research*, Vol. 17, no. 4, pp. 1075-1081.

D'Astous, A. Y., W. W. Ruland, J. R. G. Bruce, J. A. Cherry, and R. W. Gillham. 1989. Fracture effects in the shallow groundwater zone in weathered Sarnia-area clay, *Canadian Geotechnical Journal*, Vol. 26, 43-56.

Davis, E. C., D. K. Solomon, R. B. Clapp, S. Y. Lee, P.M. Craig, A. D. Kelmers, and D. A. Lietzke. 1987. Summary of environmental characterization activities at the Oak Ridge National Laboratory Solid Waste Storage Area Six, FY 1986 through 1987. ORNL/RAP/LTR-87/68. Oak Ridge National Laboratory.

Day, J. J. 1977. Analysis of movement and hydrochemistry of goundwater in the fractured clay and till deposits of the Winnipeg area, Manitoba, M. Sc. thesis. Dep. of Earth Sci., Univ. of Waterloo, Waterloo, Ont., Canada.

Dorsch, J., Katsube, T. J., Sanford, W.E., Dugan, B.E., and Tourkow, A. (in preparation). Effective porosity and pore-throat sizes of Conasauga Group mudrocks: Application, test and evaluation of petrophysical techniques. ORNL/GWPO-021, xxx p.

Dreier, R., D.K. Solomon, C.M. Beaudoin. 1987. Fracture characterization in the unsaturated zone of a shallow Land burial facility. Flow and Transport through Unsaturated Fractured Rock; Edited by D.D. Evans and T.J. Nicholson, *Geophysical Monograph* 42, pp. 51-59.

Endo, H. K., J.C.S. Long, C.R. Wilson, and P.A. Witherspoon. 1984. A model for investigating mechanical transport in fracture networks. *Water Resources Research*, Vol. 20, no 10., pp. 1390-1400.

Foreman, J. L., and W. M. Dunne. 1991. Conditions of vein formation in the southern Appalachian foreland: constraints from vein geometries and fluid inclusions. *Journal of Structural Geology*, Vol. 13, pp. 1173-83.

Foster, S. S. D. 1975. The chalk groundwater tritium anomaly - a possible explanation. *Journal of Hydrology,* Vol. 25, 159-165.

Harrison, B., E. A. Sudicky, and J. A. Cherry. 1992. Numerical analysis of solute migration through fractured clayey deposits into underlying aquifers. *Water Resources Research*, Vol. 28, no. 2, pp. 515-526.

Hatcher, R. D., P. J. Lemiszki, R. B. Dreier, R. H. Ketelle, R. R. Lee, D. A. Leitzke, W. M. McMaster, J. L. Foreman, and S. Y. Lee. 1992. Status report on the geology of the Oak Ridge Reservation. ORNL/TN 12074. Oak Ridge National Laboratory.

Huyakorn, P. S. and G. F. Pinder. 1983. Computational Methods in Subsurface Flow, Academic Press, New York.

Keller, C.K., G. van der Kamp, and J.A. Cherry. 1986. Fracture permeability and groundwater flow in clayey till near Saskatoon, Saskatchewan, Can *Geotechnical Journal,* Vol. 23, pp. 229-240.

Kropinski, M. C. A. 1990. Numerical techniques for saturated-unsaturated groundwater flow, M. Sc. thesis, Dep. of Earth Sci., Univ. of Waterloo, Waterloo, Ont., Canada.

Lee, R. R., R. H. Ketelle, J. M. Bownds, T. A. Rizk. 1989. Calibration of a groundwater flow and contaminant transport computer model: progress toward model validation. ORNL/TM-11294. Oak Ridge National Laboratory.

Lee, R. R., R. H. Ketelle, J. M. Bownds, and T. A. Rizk. 1992. Aquifer analysis and modeling in a fractured, heterogeneous medium. *Ground Water*, Vol. 30, no. 4, pp. 589-597.

Long, J.C.S., J.S. Remer, C.R. Wilson, and P.A. Witherspoon. 1982. Porous media equivalents for network of discontinuous fractures. *Water Resources Research*, Vol. 18, no. 3, pp. 645-658.

Long, J. C. S. and P. A. Witherspoon. 1985. The relationship of the degree of interconnection to permeability in fracture networks. *Journal of Geophysical Research*, Vol. 90, no B4, pp. 3087-3098.

McKay, L. D., J.A. Cherry, and R.W. Gillham. 1993a. Field experiments in a fractured clay till 1. Hydraulic conductivity and fracture aperture, *Water Resources Research*, Vol. 29, no 4, pp. 1149-1162.

McKay, L. D., R. W. Gillham, and J. A. Cherry. 1993b. Field Experiments in fractured clay till 2. Solute and colloid transport. *Water Resources Research*, Vol. 29, no. 12, pp. 3879-3890.

McMaster, W.M. 1963. [Report on] geologic map of the Oak Ridge Reservation, TN. ORNL/TM-713. Oak Ridge National Laboratory.

Maloszewski, P. and A. Zuber. 1985. On the theory of tracer experiments in fissured rocks with a porous matrix, *Journal of Hydrology*, Vol. 79, pp. 333-358.

Maloszewski, P., and A. Zuber. 1993. Tracer experiments in fractured rocks: matrix diffusion and the validity of models. *Water Resources Research*, Vol. 29, no. 8, pp. 2723-2735.

Moore, G. K., and L. E. Toran. 1992. Supplement to a hydrologic framework for the Oak Ridge Reservation, Oak Ridge, Tennessee. ORNL/TM-12191. Oak Ridge national Laboratory.

Olsen, C. R., P. D., Lowry, S. Y. Lee, I. L. Larsen, and N. H. Cutshall. 1983. Chemical, geological and hydrological factors governing radionuclide migration from a formerly used seepage trench: A field Study. ORNL/TM-8839. Oak Ridge National Laboratory.

Pankow, J. F., R. L. Johnson, J. P. Hewetson, and J. A. Cherry. 1986. An evaluation of contaminant migration patterns at two waste disposal sites on fractured porous media in terms of the equivalent porous medium (EPM) model. *Journal of Contaminant Hydrology*, Vol. 1, pp. 65-76.

Parker, J.C., and M. Th. van Genuchten. 1984. Determining transport parameters from laboratory and field tracer experiments. *Virginia Agricultural Experiment Station Bulletin* 84-3.

Ruland, W.W., J.A. Cherry, and S. Feenstra. 1991. The depth of active groundwater flow in a clayey till plain in southwestern Ontario, *Groundwater*, Vol. 29, no. 3, pp. 405-417.

Sanford, W. E., and D. K. Solomon. 1995. Noble gas solute tracer experiment in a fractured, weathered shale near Oak Ridge, TN. Presented at the *International Association of Hydrogeologists Congress*, Edmonton, Alberta, Canada, June 5-10.

Schwartz, F.W., L. Smith, and A. S. Crowe. 1983. A stochastic analysis of macroscopic dispersion in fractured media. *Water Resources Research*, Vol. 19, no. 5, pp. 1253-1265.

Shevenell, L. A., G. K. Moore, and R. B. Dreier. 1994. Contaminant Spread and flushing in fractured rocks near Oak Ridge, Tennessee. *Groundwater Monitoring Review*, Vol. 14, no. 2, pp. 120-129.

Sledz, J.J., and D.D. Huff. 1981. Computer model for determining fracture porosity and permeability in the Conasauga Group. ORNL/TM-9314. Oak Ridge National Laboratory.

Solomon, D., G. K. Moore, L. E. Toran, R. B. Dreier, and W. M. McMaster. 1991. Status report: a hydrologic framework for the Oak Ridge Reservation. ORNL/TM-12026. Oak Ridge National Laboratory.

Snow, D. T. 1968. Rock fracture spacings, openings and porosities, *Journal of Soil Mechanics Foundation, Division of American Society of Civil Engineering*, Vol. 94 (SM1), pp. 73-91.

Snow, D. T. 1969. Anisotropic permeability of fractured media, *Water Resources Research*, Vol. 5, no. 6, pp. 1273-1289.

Sudicky, E. A. and E. O. Frind. 1982. Contaminant transport in fractured porous media: Analytical solutions for a system of parallel fractures, *Water Resources Research*, Vol. 18, no. 6, pp. 1634-1642.

Sudicky, E. A. and R. G. McLaren. 1992. The Laplace Transform Galerkin technique for large-scale simulation of mass transport in discretely fractured porous formations, *Water Resources Research*, Vol. 28, no. 2.

Tang, D. H., E. O. Frind, and E. A. Sudicky. 1981. Contaminant transport in fractured porous media: analytical solution for a single fracture, *Water Resources Research*, Vol. 17, no. 3, pp. 555-564.

Therrien, R. and E.A. Sudicky. In press. Three-dimensional analysis of variably-saturated flow and Solute transport in discretely-fractured porous media.

Submitted for publication to *Journal of Contaminant Hydrology*, September, 1994.

Thompson, D. 1990. Hydraulic evidence of Wisconsinan-aged open fractures in a deep clayey till, M.Sc. thesis, University of Waterloo, Waterloo, Ont., Canada.

Webster, D. A.. In press. Results of ground-water tracer tests using tritiated water, at Oak Ridge Laboratory, Tennessee. U.S. Geological Survey Water-Resources Investigations Report.

Webster, D.A., J. S. Beatty, P.M. Benjamin, and W.M. Tranum. 1982. Precipitation data for burial grounds 5 and 6, Oak Ridge National Laboratory, Tennessee, 1976-1980. *USGS Open-File Report* 82-254, 15p.

Webster, D.A., and M.W. Bradley. 1988. Hydrology of the Melton Valley radioactive-waste burial grounds at Oak Ridge National Laboratory, Tennessee, *USGS Open-File Report* 87-686, 115p.

Wickliff, D. S., S. M. Gregory, I. L. Larsen, and R. B. Clapp. 1989. Contaminant transport during storms near solid waste storage areas 4 and 5. ORNL/RAP/LTR-89/20. Oak Ridge National Laboratory.

Wilson, G. V., P.M. Jardine, and J.P. Gwo. 1992. Modeling the hydraulic properties of a multiregion soil. *Soil Science Society of America Journal*, Vol. 56, pp. 4731-1737.

APPENDICES

Appendix A

Tables and Figures

Table 1. Parameters required for Discrete-Fracture/Matrix-Diffusion modeling and the methods and problems for obtaining them for non-reactive solute tracers.

Parameter	Method of Obtaining Parameter(s)	Comments
Fracture aperture	Indirectly obtained from hydraulic response tests using the cubic law.	Sensitive to assumed fracture network. Usually assume that all fractures have same aperture (which is a major source of uncertainty)
Fracture spacing, orientation and degree of inter-connection	Directly obtained from outcrops or core samples, and through down-hole geophysical methods and flow meter testing.	Outcrops or core samples influenced by stress-relief. Zones where secondary minerals form due to weathering do not necessarily indicate currently hydraulically active fractures, and fracture spacing may not be consistent throughout a given material. Even if the fractures are all hydraulically active, a few large aperture fractures can dominate fluid flow.
Fracture dispersivity	calculated by fitting tracer test break-through curves with discrete fracture model	Can often get non-unique solutions (i.e., different combinations of dispersivity and flow velocity).
Total porosity, n_T	usually calculated from saturated moisture content using gravimetry or porosimetry	assumes total porosity is accessible to solute
Effective diffusion coefficient	measured using diffusion tests or estimated from free-water diffusion coefficient and estimate of matrix tortuosity	expensive to measure, and few published values available

Table 2. Description of Geology from Solomon et al., 1992.

Unit	Age	Thickness (in meters)	Lithology
Rockwood Formation	Silurian	120	Sandstone
Sequatchie Formation	Upper Ordovician	60	Argillaceous Limestone
Reedsville Shale	Upper Ordovician	60	Calcareous shale
Chickamauga Group	Middle Ordovician	400-700	Limestone, argillaceous limestone, shale, siltstone
Knox Group			
Mascot Dolomite		75-120	Massive dolomite,
Kingsport Formation	Lower Ordovician,	90-150	siliceous dolomite,
Longview Dolomite	Upper Cambrian	40-60	bedded chert,
Chepultepec Dolomite		150-215	limestone,
Copper Ridge Dolomite		245-335	some clastics
Conasauga Group			
Maynardville Limestone		125-145	Dolomitic limestone,
Nolichucky Shale		100-150	limestone
Dismal Gap Formation	Middle,	95-120	
(Formerly Maryville Ls)	Upper Cambrian		
Rogersville Shale		20-35	Shale,
Rutledge Limestone		30-40	siltstone and shale,
Pumpkin Valley Shale*		90-100	shaly simestone, limestone
Rome Formation	Lower Cambrian	90-125	Shale, siltstone, sandstone, local dolomite lenses

* The Experiment at BG4 is within the Pumpkin Valley Shale.

Table 3. Slug test data for wells completed in the regolith at the tracer test site near BG4 (Revised from Webster and Bradley, 1988)

Well Number	Apparent Transmissivity		Apparent Hydraulic Conductivity	
	(ft^2/d)	(m^2/d)	(ft/d)	(m/d)
4	0.23	0.021	0.012	0.0037
5	0.36	0.033	0.020	0.0061
6	0.45	0.042	0.023	0.0070
7	0.57	0.053	0.034	0.0100
8	0.25	0.023	0.010	0.0030
9	0.52	0.048	0.025	0.0076
10	0.74	0.069	0.040	0.0120
11	0.14	0.013	0.016	0.0048

Table 4. Parameters used for 1D CXTFIT and CRAFLUSH simulations.

Parameters Used	Symbol	Values (CXTFIT)	Values (CRAFLUSH)
Bulk Hydraulic Conductivity	K_b	0.009 m/d	0.009 m/d
Flow Velocity	v	***varied***	calculated[2]
Hydraulic Gradient	i	0.15	0.15
Matrix Porosity	n	N/A	0.15
Effective Porosity	n_e	calculated[1]	N/A
Matrix Tortuosity	ω	N/A	1.0
Dispersivity	α	***varied***	N/A
Diffusion Coefficient	D*	5.18×10^{-5} m^2/d	5.18×10^{-5} m^2/d
Retardation	R	1.0	1.0
Solute Half-Life	λ	4.53×10^3 d	4.53×10^3 d
Source Concentration	C	1.0	1.0
Duration of Source	T	40.0 days	40.0 days
Fracture Dispersivity	α_f	N/A	***varied***
Fracture Spacing	2B	N/A	***varied***
Fracture Aperture	2b	N/A	calculated[2]
Fracture Retardation	R_f	N/A	1.0

[1] Effective porosity, n_e, was calculated from measured bulk hydraulic conductivity, K_b, hydraulic gradient, i, and simulated groundwater flow velocity, v. See equation (22).

[2] Fracture aperture, 2b, and fracture flow velocity, v, are calculated based on K_b and 2B. See equations (15) and (16).

Table 5. Parameters used for FRAC3DVS simulations.

Parameters Used	Symbol	Values (EPM)	Values (DF-EPM)
Bulk Hydraulic Conductivity,	K_b	0.009 m/d	ND[2]
Flow Velocity	v	***varied***	0.01 m/d
Hydraulic Gradient	i	0.15	0.15
Matrix Porosity	n	0.40	0.40
Effective porosity	n_e	calculated[1]	0.15
Matrix Tortuosity	ω	1.0	1.0
Longitudinal Dispersivity	α_L	***varied***	0.8m
Transverse Dispersivity	α_T	***varied***	0
Diffusion Coefficient	D*	5.18×10^{-5} m^2/d	5.18×10^{-5} m^2/d
Retardation	R	1.0	1.0
Solute Half-Life	λ	$4.53 \times 10^{3} d^{-1}$	4.53×10^{3} d^{-1}
Source Concentration	C	1.0	1.0
Duration of Source	T	40.0 days	40.0 days
Longitudinal Fracture Dispersivity	$\alpha_{f,L}$	N/A	0.10
Transverse Fracture Dispersivity	$\alpha_{f,T}$	N/A	0
Fracture Aperture	2b	N/A	150, 250μm
Fracture Retardation	R_f	N/A	1.0

[1] same as note on Table 4

[2] Not determined. Assumed a background hydraulic conductivity of 0.009 m/d, but the total bulk hydraulic conductivity will be greater because of the presence of the superimposed larger aperture fractures.

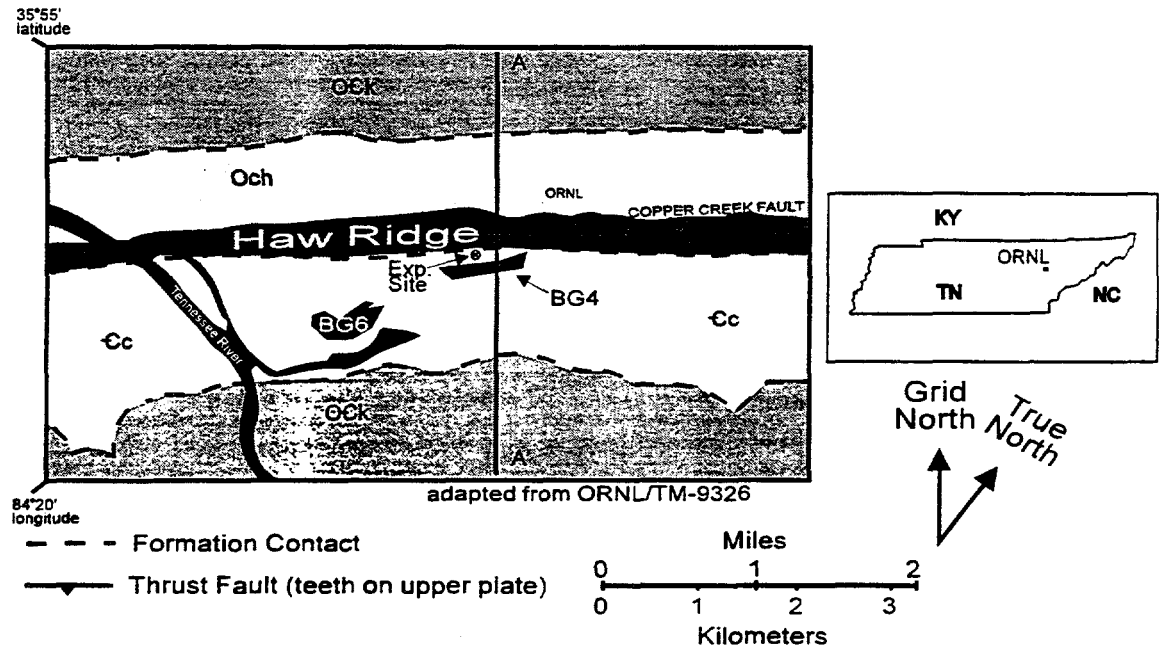

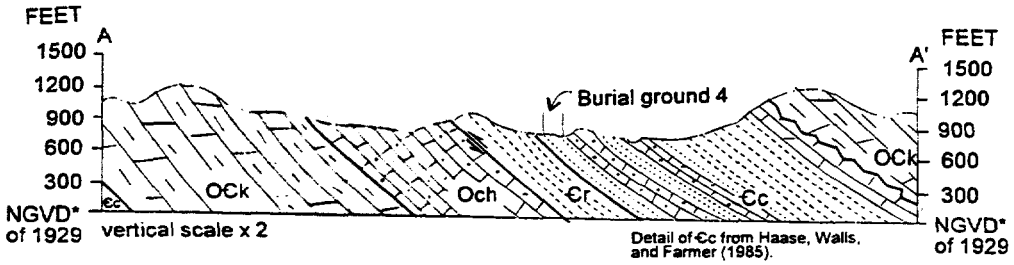

Och Chickamauga Group
OCk Knox Group
Cc Conasauga Group
Cr Rome Formation

* National Geodetic Vertical Datum of 1929

Figure 1. Geologic map showing the location of Oak Ridge National Lab and Burial Grounds 4 (BG4) and 6 (BG6).

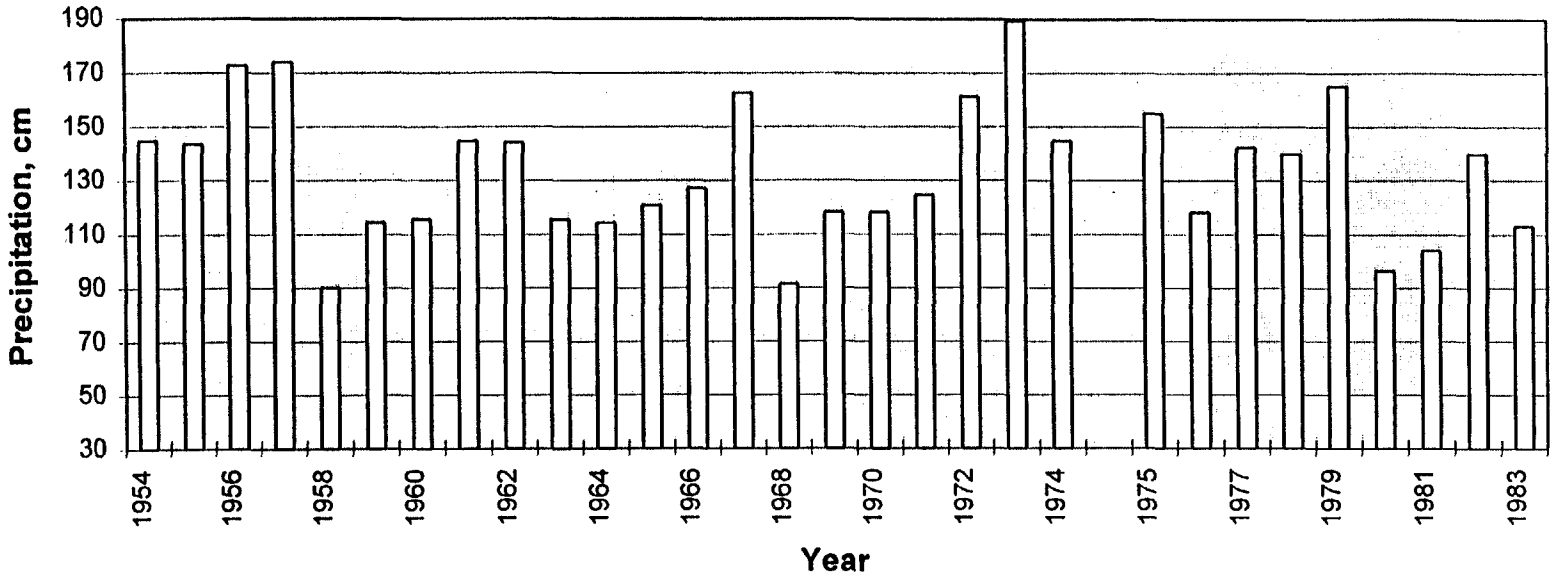

Webster and Bradley, 1988, Data Acquisition From:

1954-71: Air Resources Atmospheric Turbulence and Diffusion Laboratory, 1972.
1972-75: Gray Henderson, ORNL, written commun., 1976.
1976-80: Webster and others, 1982b
1981-83: Webster and McMaster, USGS, written communication, 1984.

Figure 2. Variability in annual precipitation from a number of monitoring sites surrounding Oak Ridge National Labs, Oak Ridge, TN. Revised from Webster and Bradley, 1988.

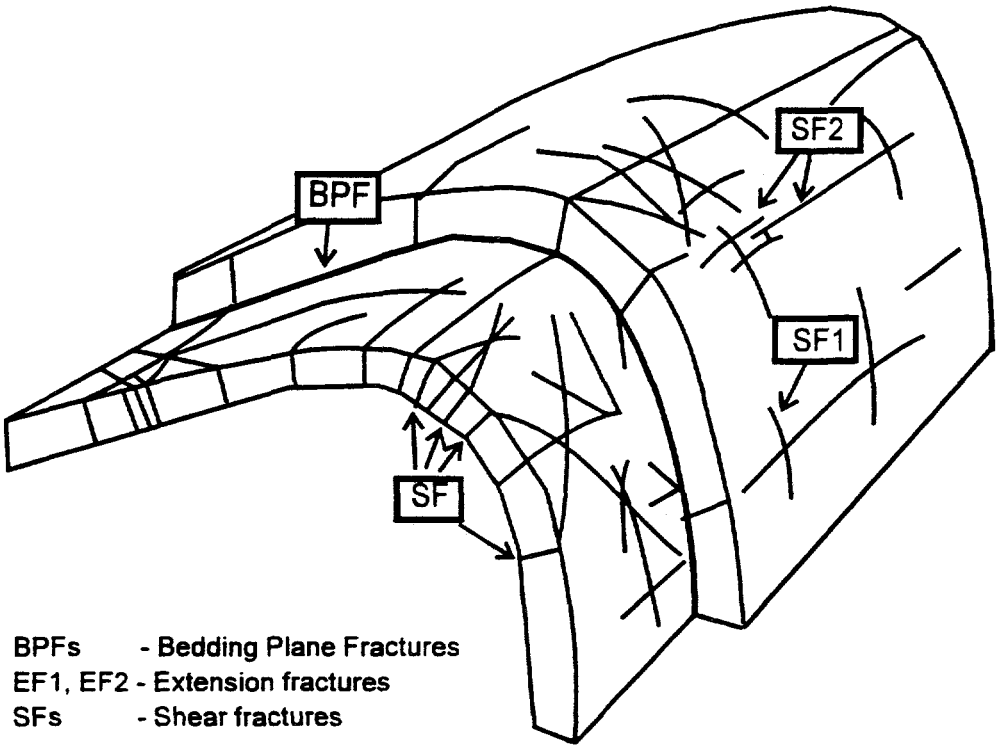

Figure 3. Schematic diagram of fold related fractures, taken directly from Dreier et al. (1987), which was modified from Price (1967).

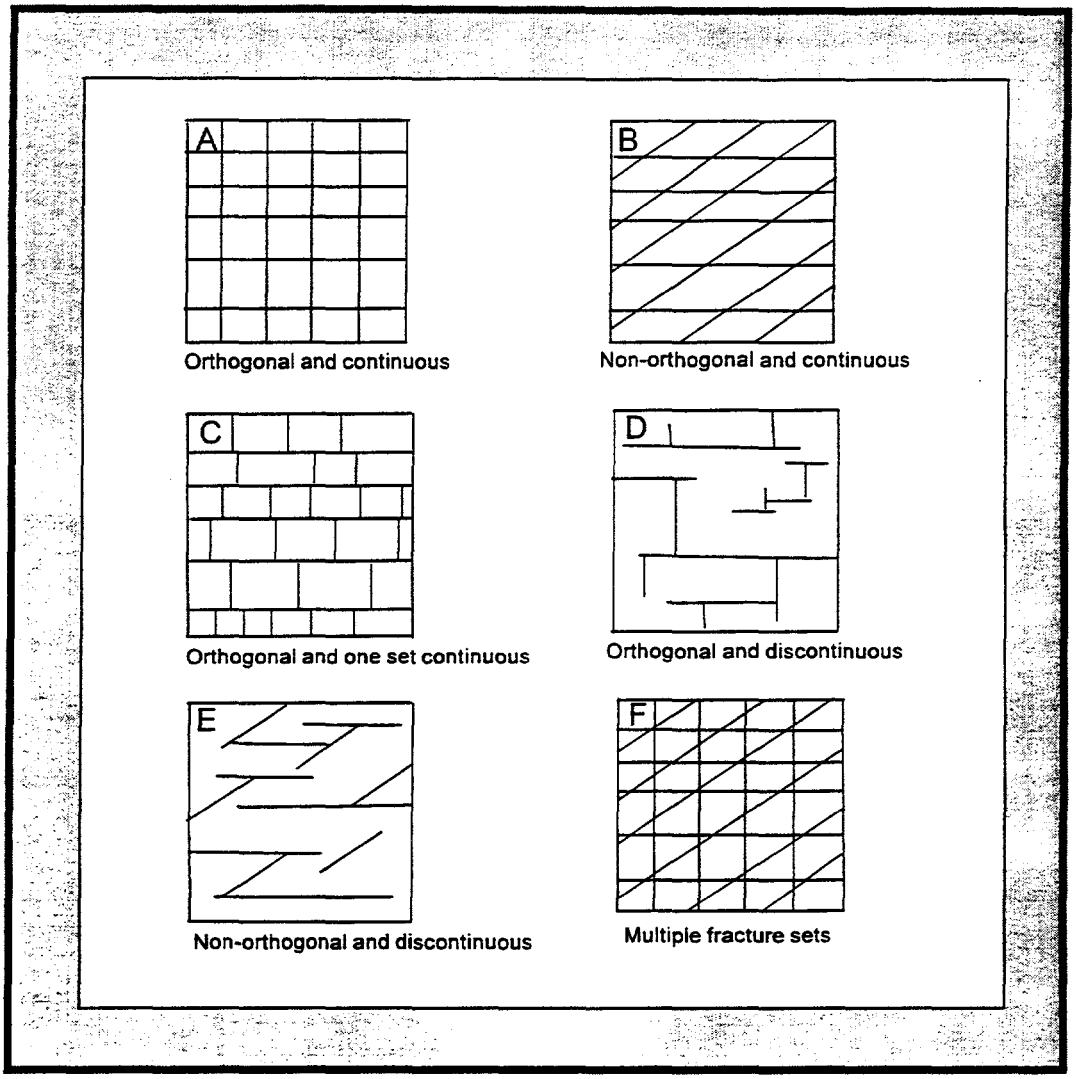

Figure 4. Fracture geometry styles observed on exposed bedding surfaces located at Oak Ridge Reservation (revised from Hatcher et al., 1992).

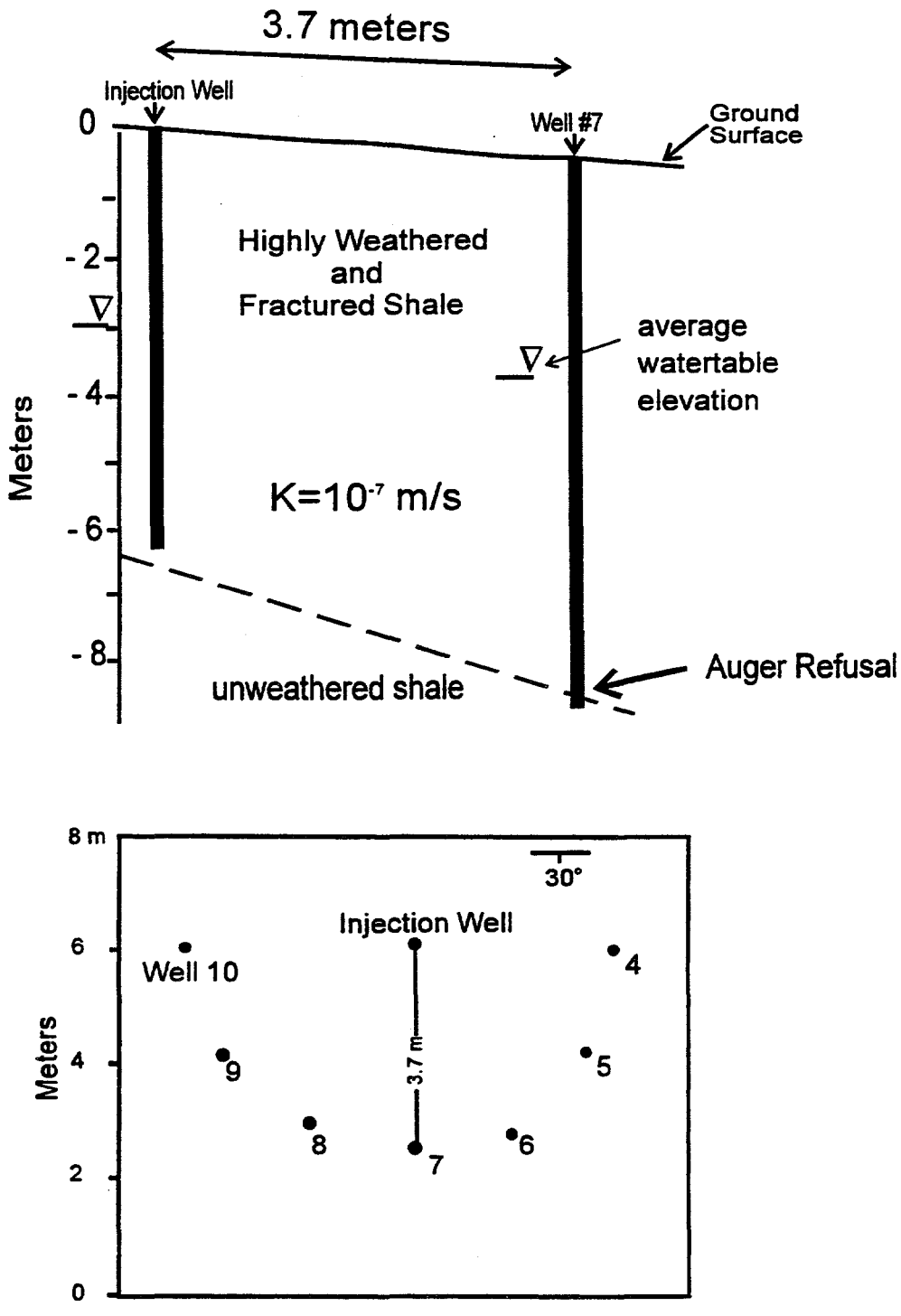

Figure 5. Cross-section and plan view of tracer experiment site near Burial Ground 4, Oak Ridge National Laboratory, Oak Ridge, TN.

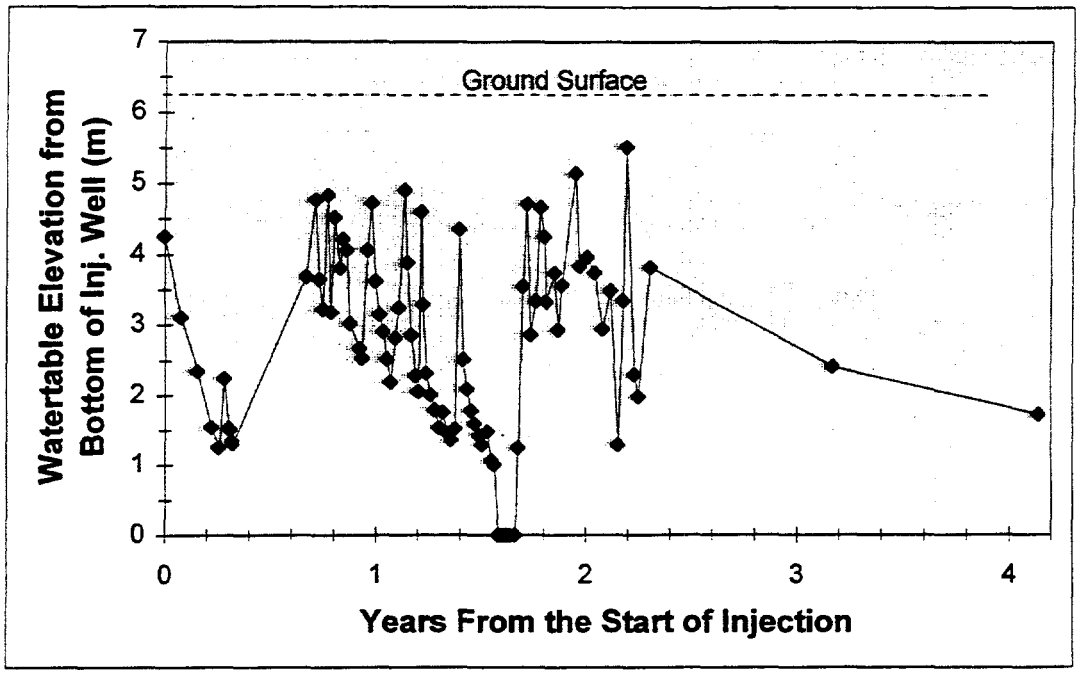

Figure 6. Water Table Data From Injection Well.

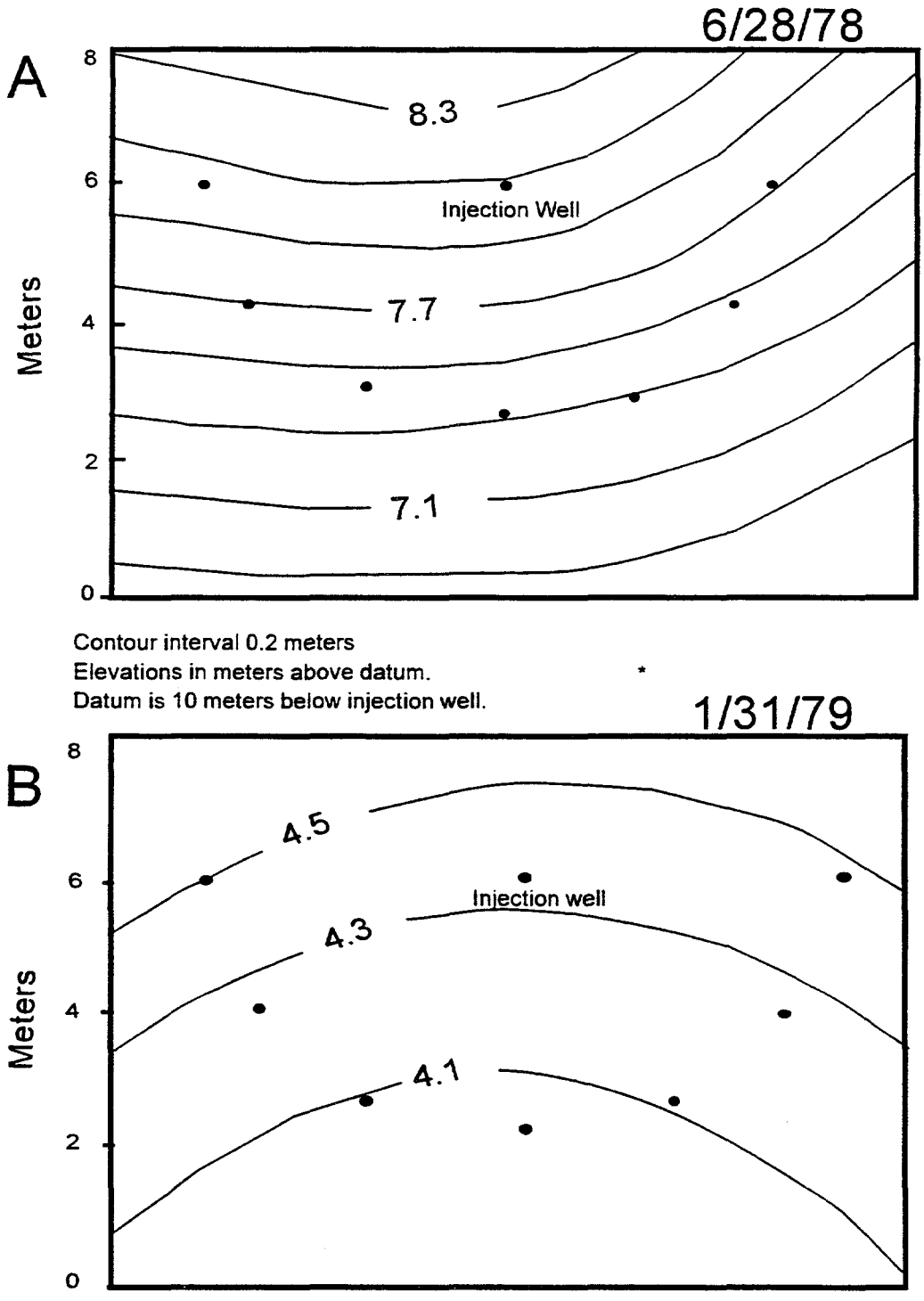

Figure 7. Contours of watertable elevation at the tracer experiment site adjacent to BG4 during A) a high and B) a low watertable period.

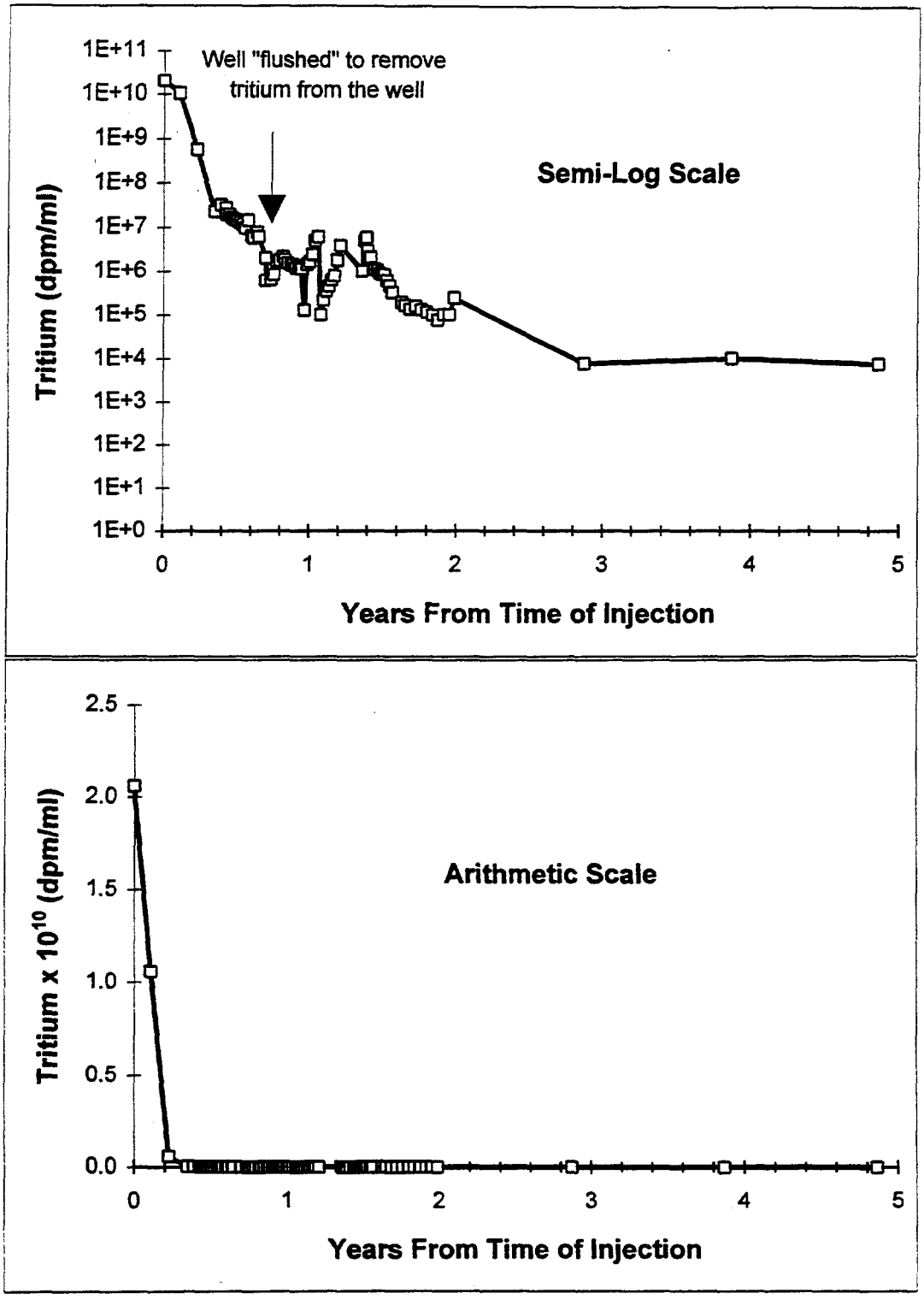

Figure 8. Tritium in the injection well.

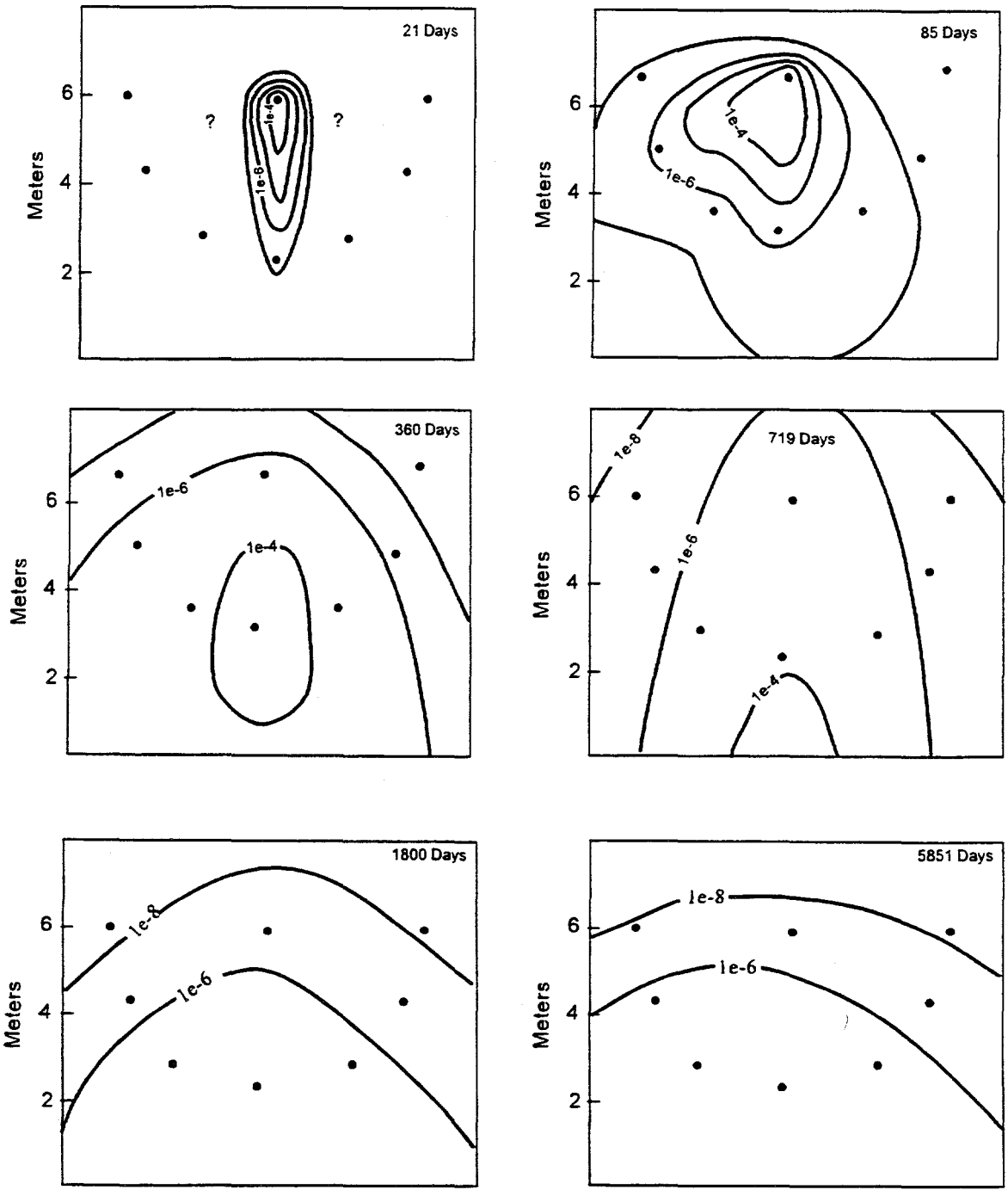

Contours are in log scale with an interval of 100

Figure 9. Contours of relative tritium concentration at six different times after addition of tritium into the injection well.

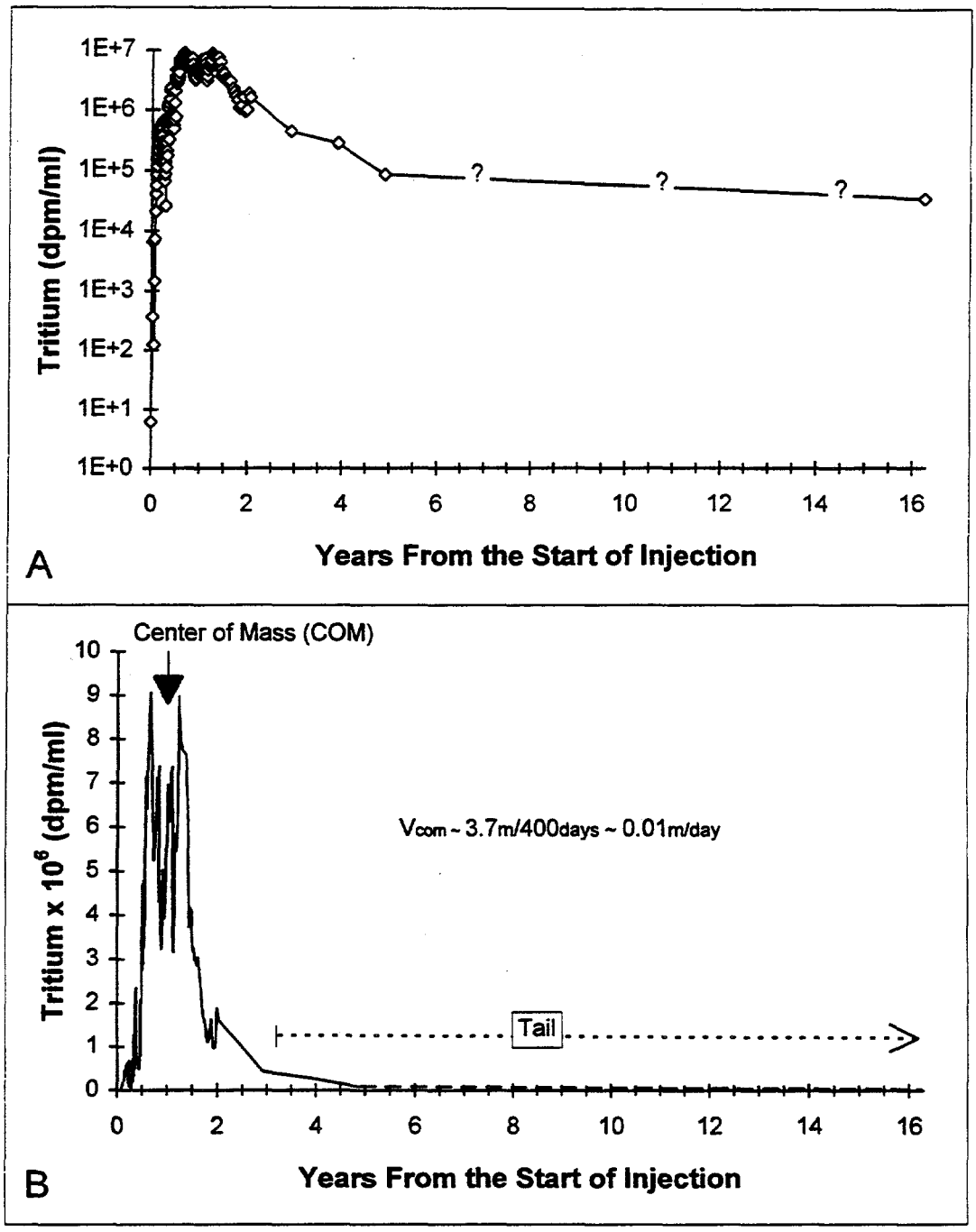

Figure 10. Tritium in monitoring well 7 (Near Burial Ground 4). Graph A gives a clear view of lower concentrations, and graph B shows the location of the Center of Mass (COM).

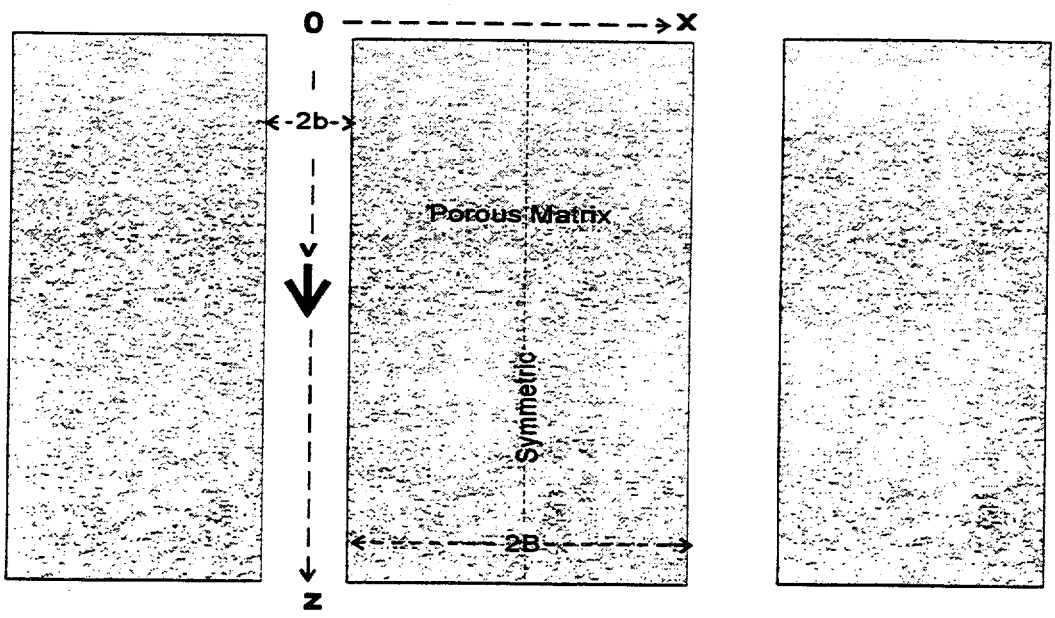

Figure 11. Hypothetical fractured system, from Sudicky and Frind, 1982.

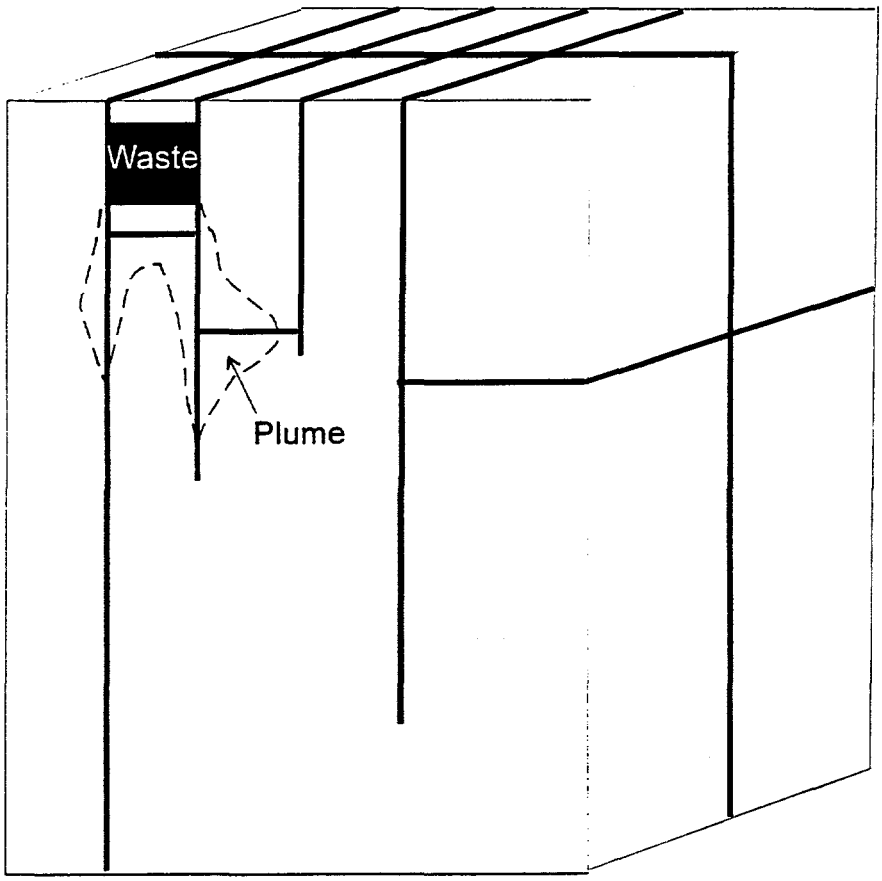

Figure 12. Typical system describing transport through fractured material. The vertical dimension was not considered for purposes of the thesis.

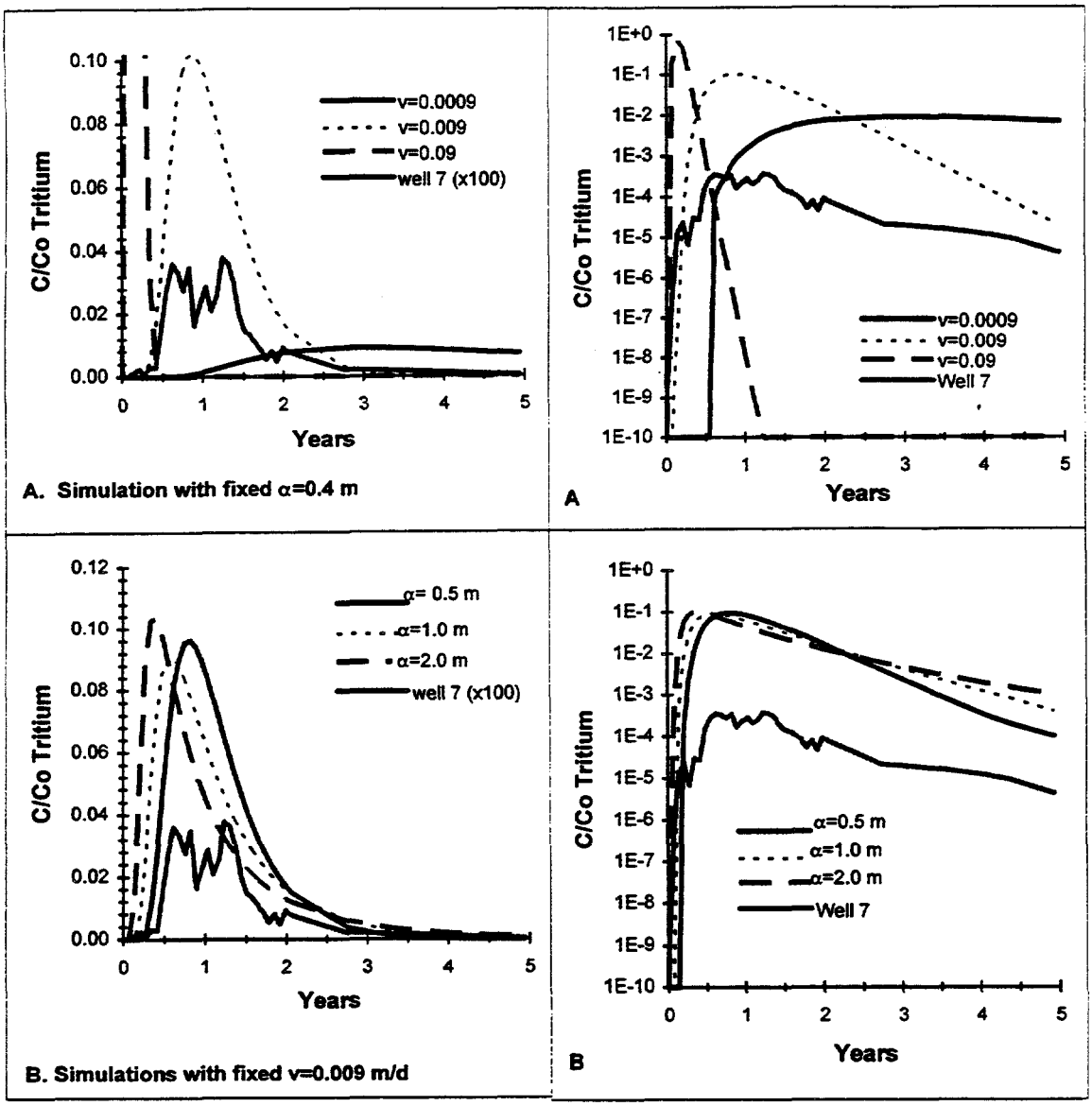

Figure 13. Varying v and α for one-dimensional EPM simulations.

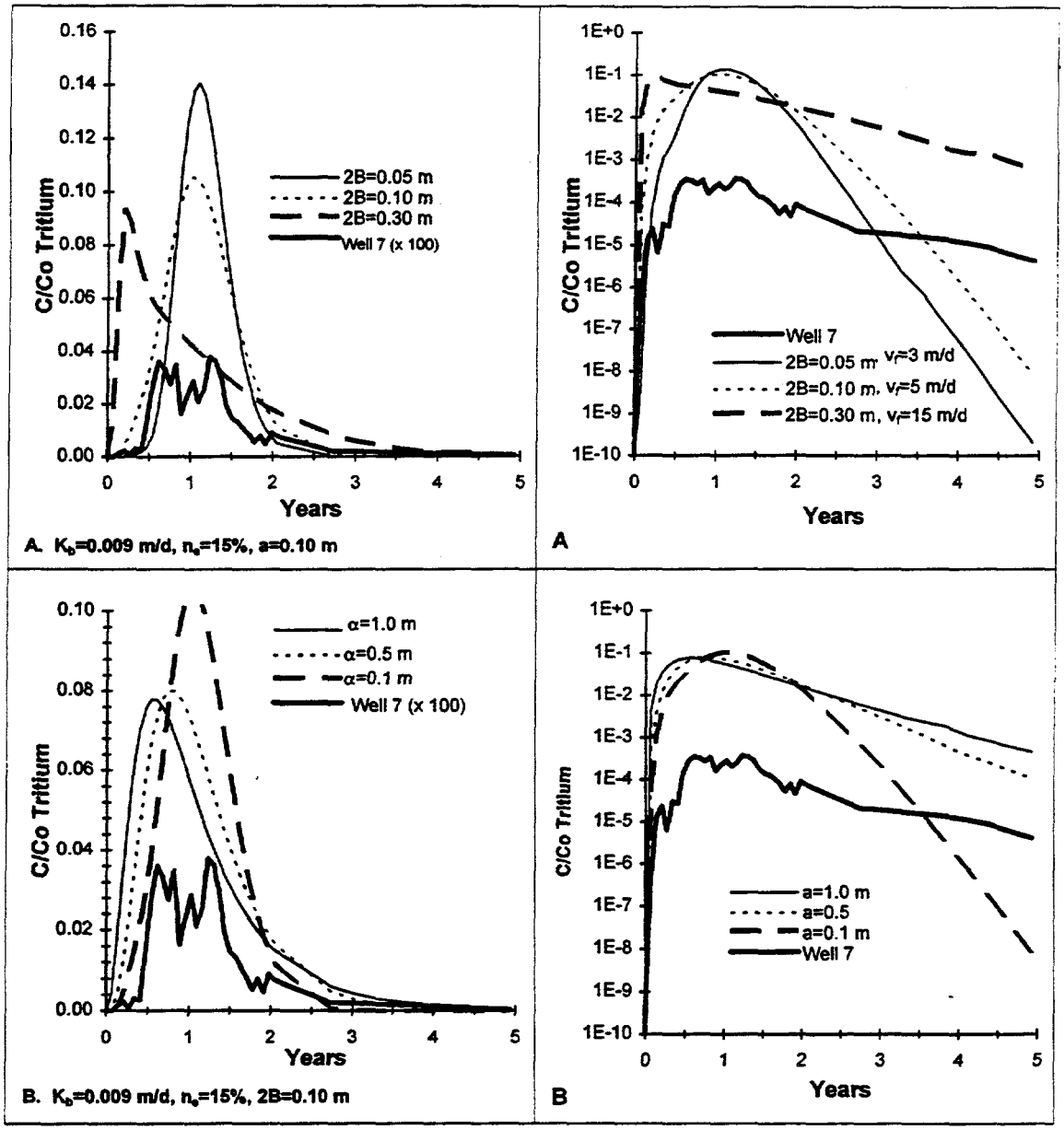

Figure 14. Varying fracture spacing, 2B (Graphs A), and fracture dispersivity, α, (Graphs B) for 1D-DFMD simulations.

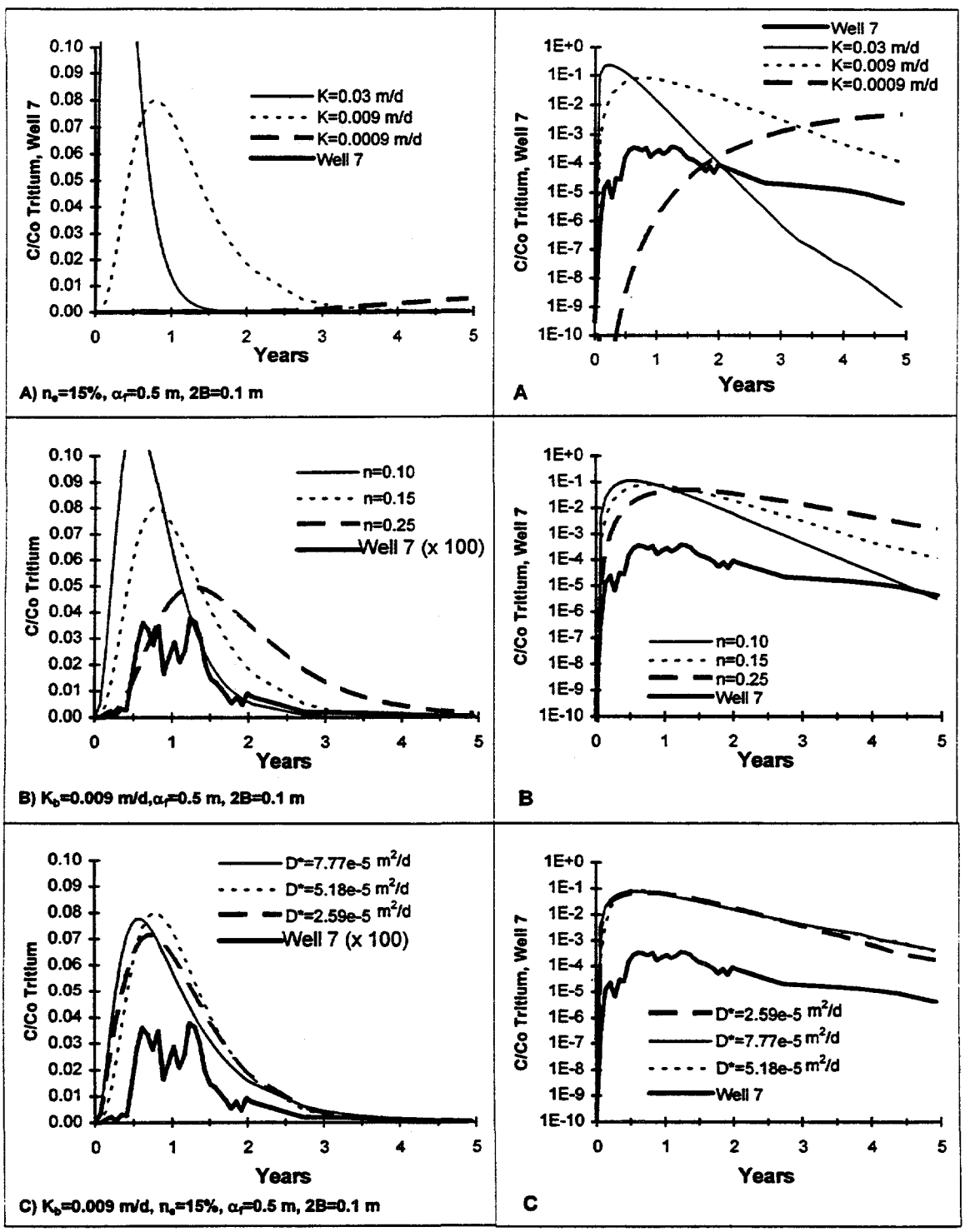

Figure 15. Varying bulk hydraulic conductivity, K_b, matrix porosity, n, and diffusion coefficient, D*, for 1D DFMD simulations.

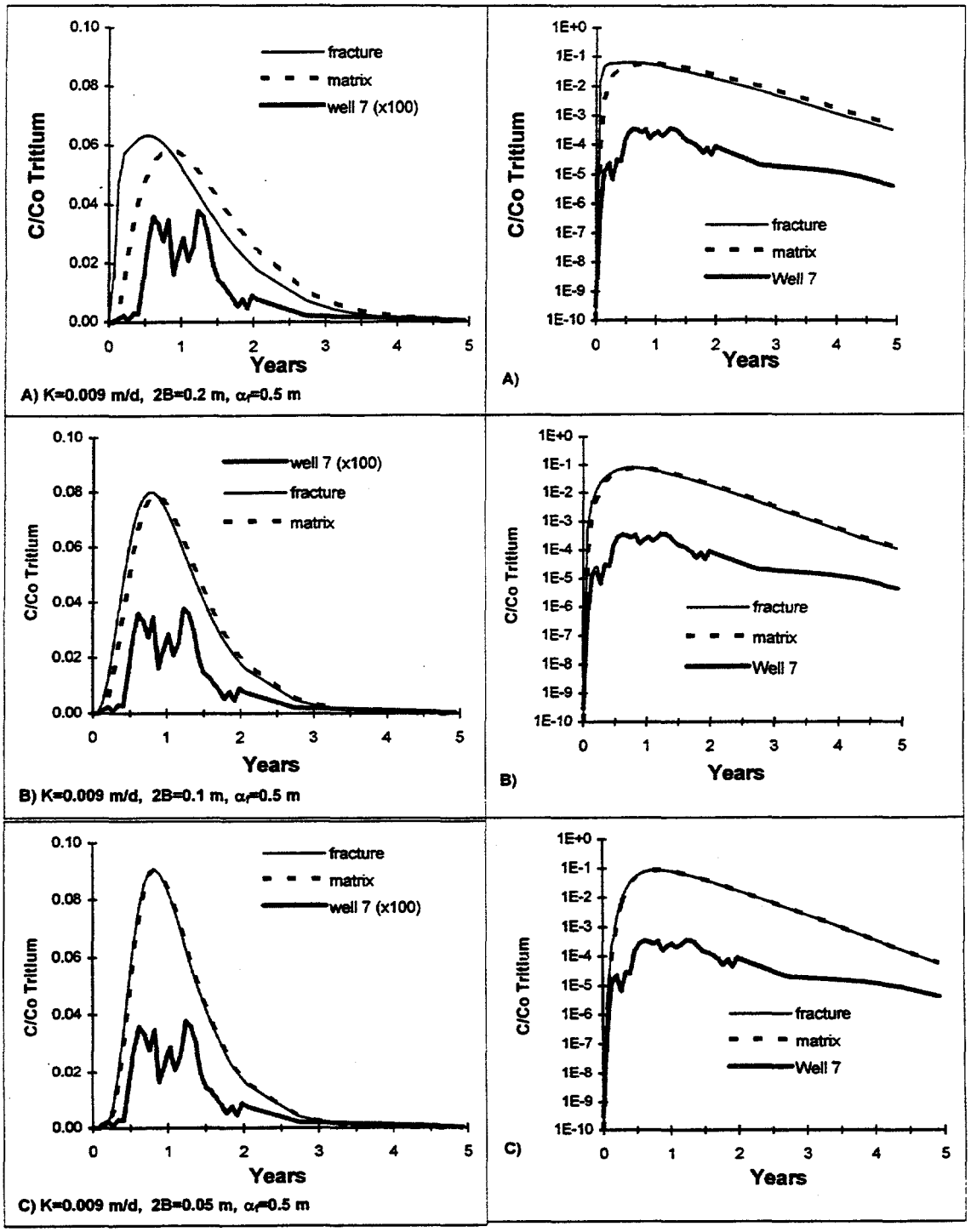

Figure 16. 1D-DFMD simulations showing concentrations in the fracture and in the matrix midway between fractures.

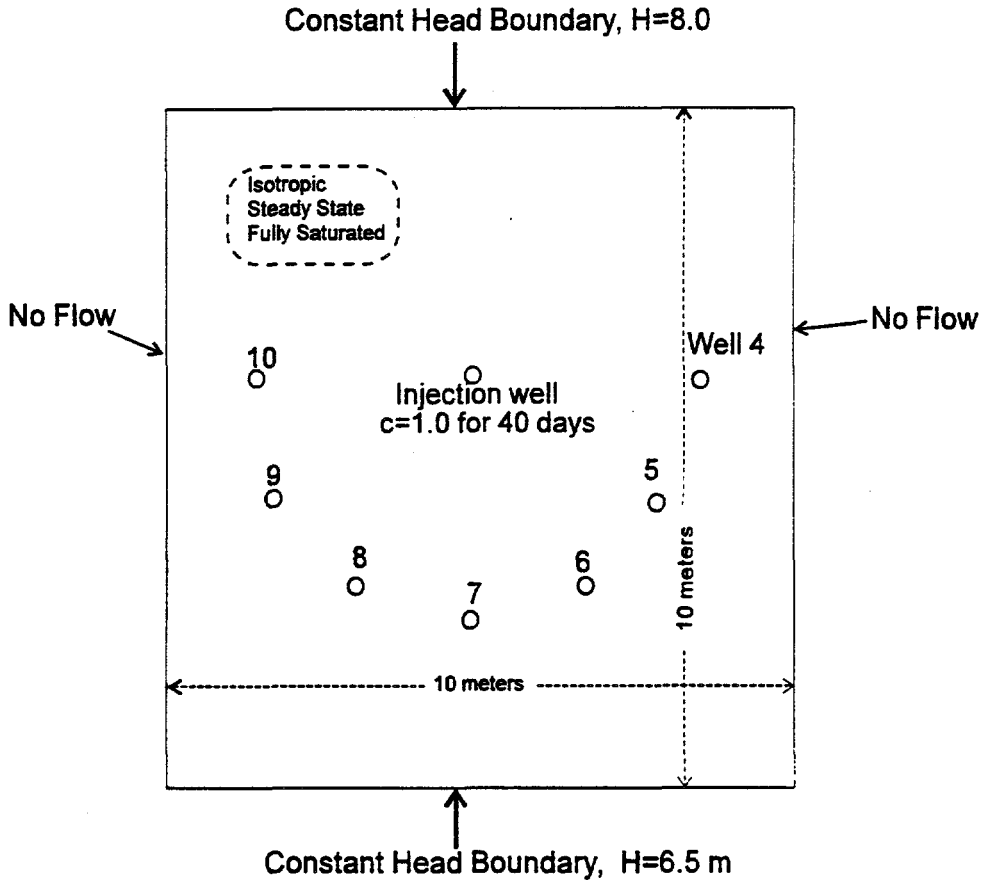

Figure 17. Graphical representation of two-dimensional grid used for EPM and discrete fracture FRAC3DVS simulations.

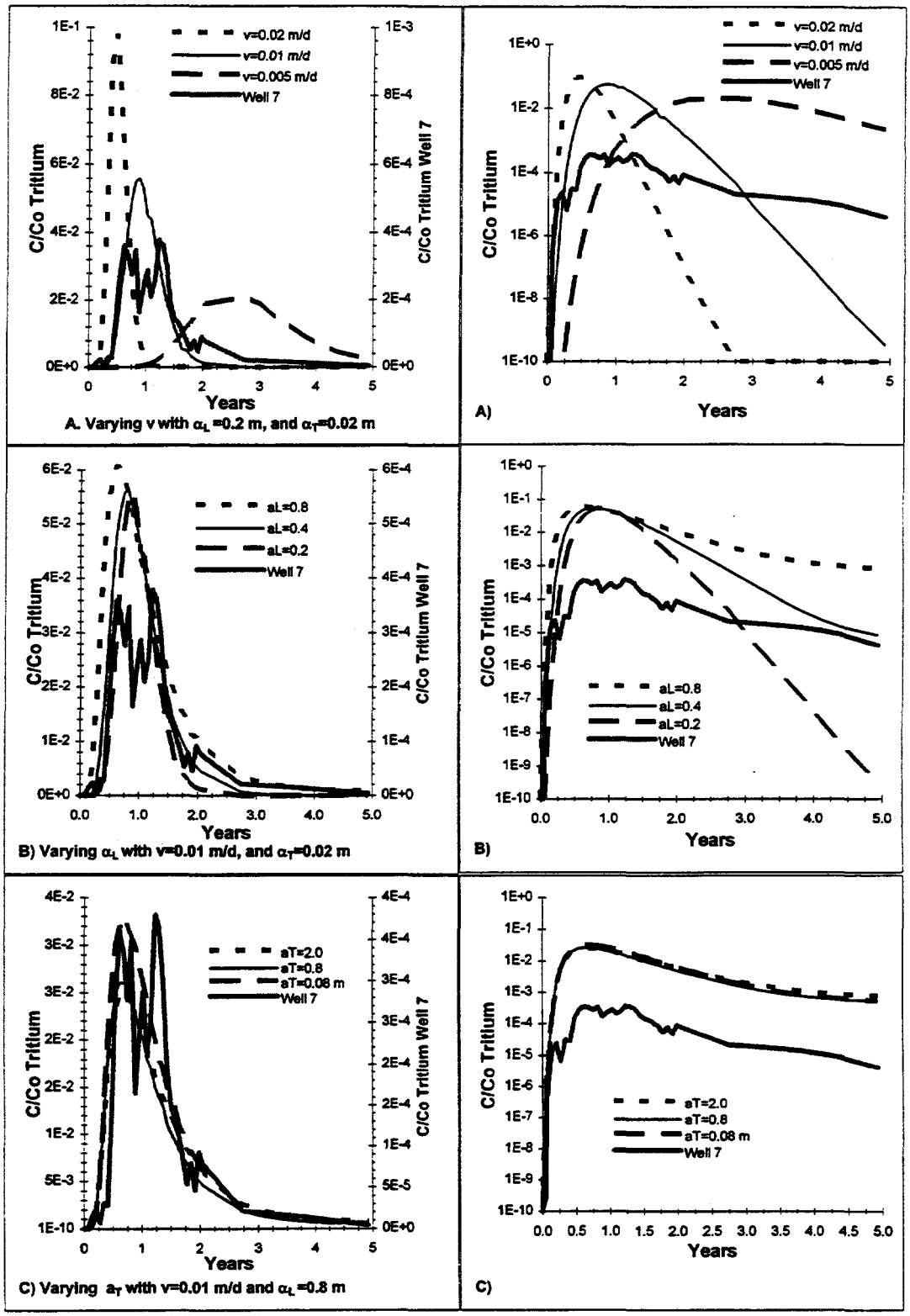

Figure 18. Observed and simulated break-through curves for well 7 using two-dimensional EPM model.

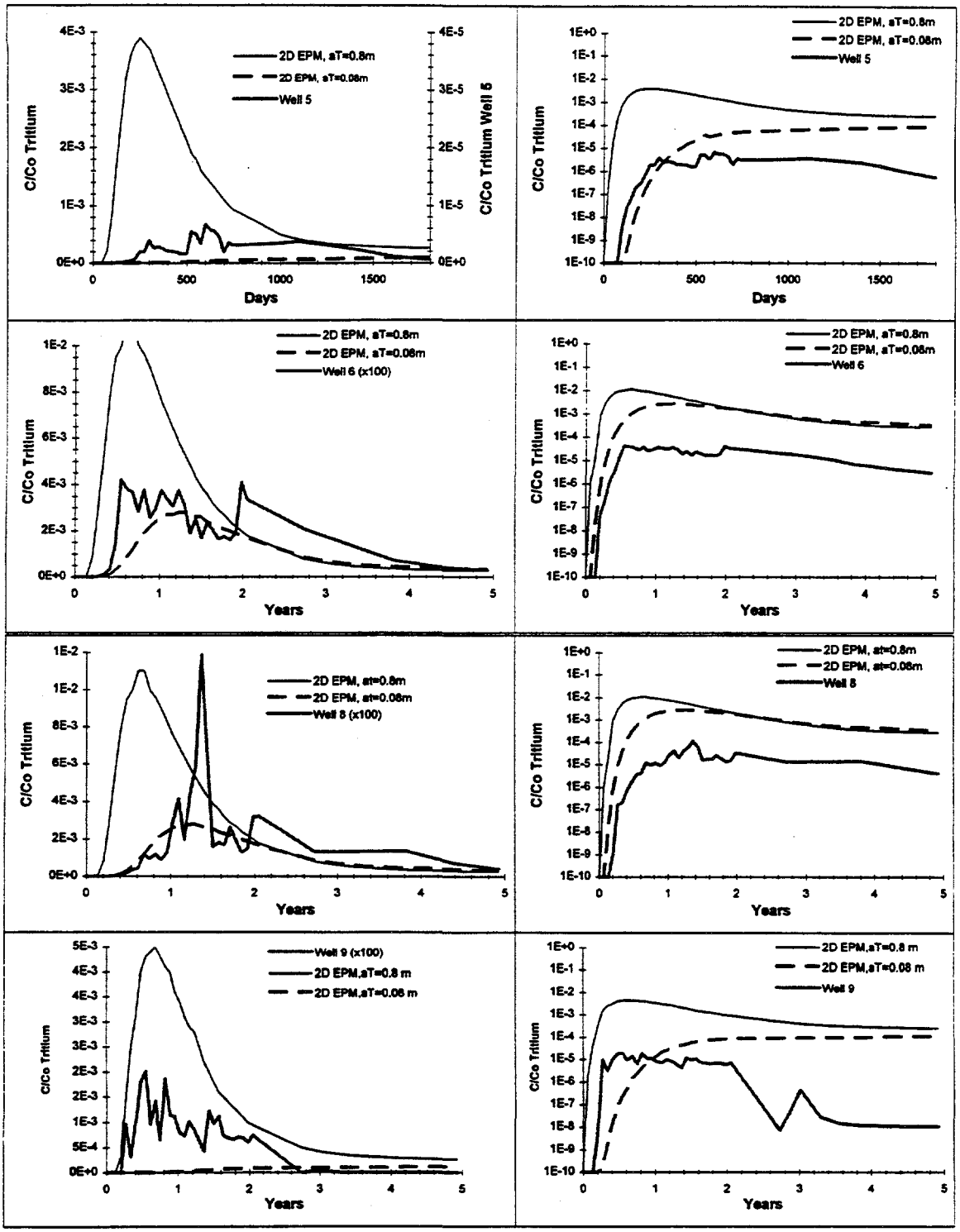

Figure 19. Two-dimensional EPM simulation results for monitoring wells 5, 6, 8 and 9 using v=0.01 m/d and α_L=0.8 m.

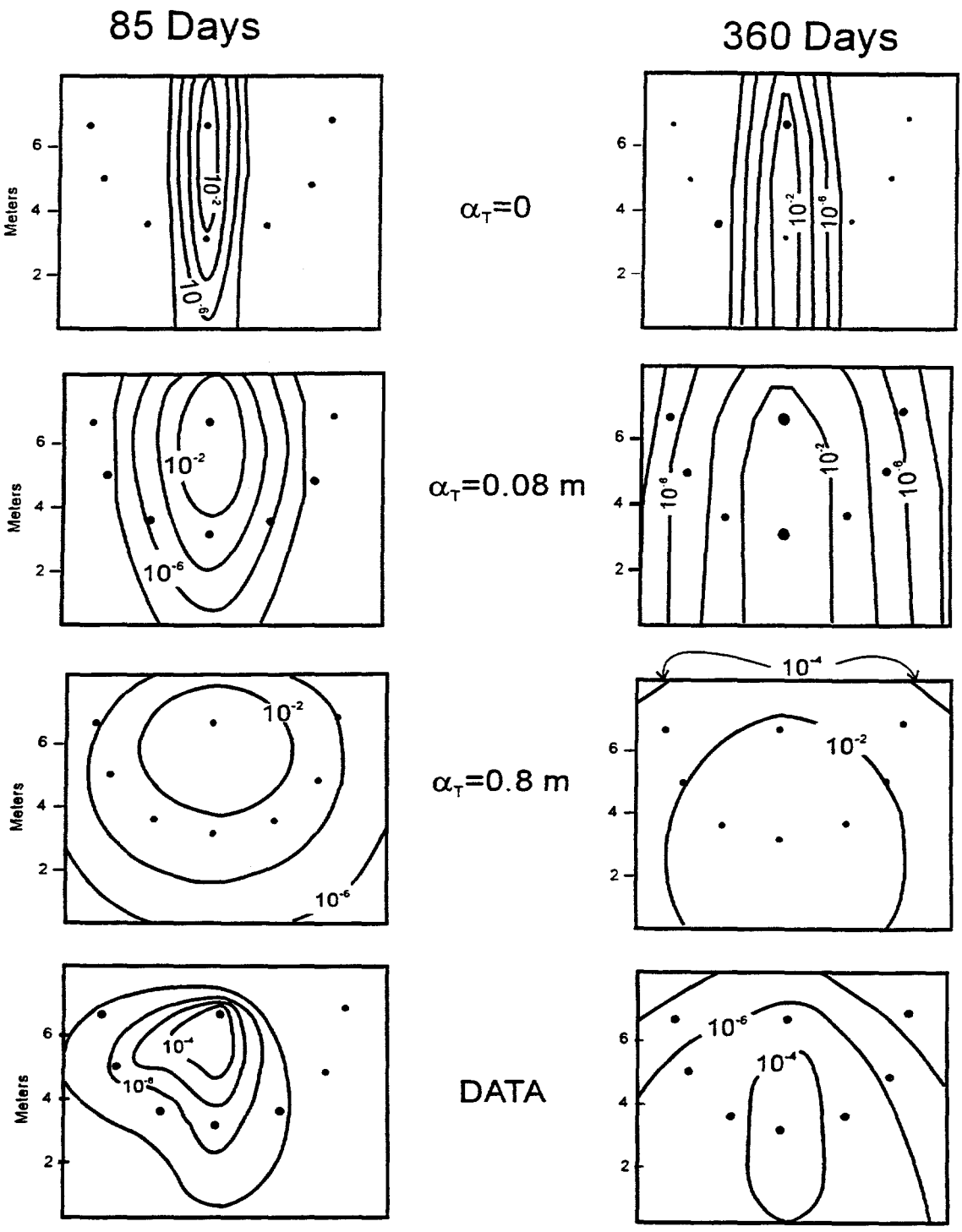

Figure 20. Two-dimensional EPM simulation results at 85 and 360 days, with v=0.01m/d, α_L=0.8 m, and varying α_T.

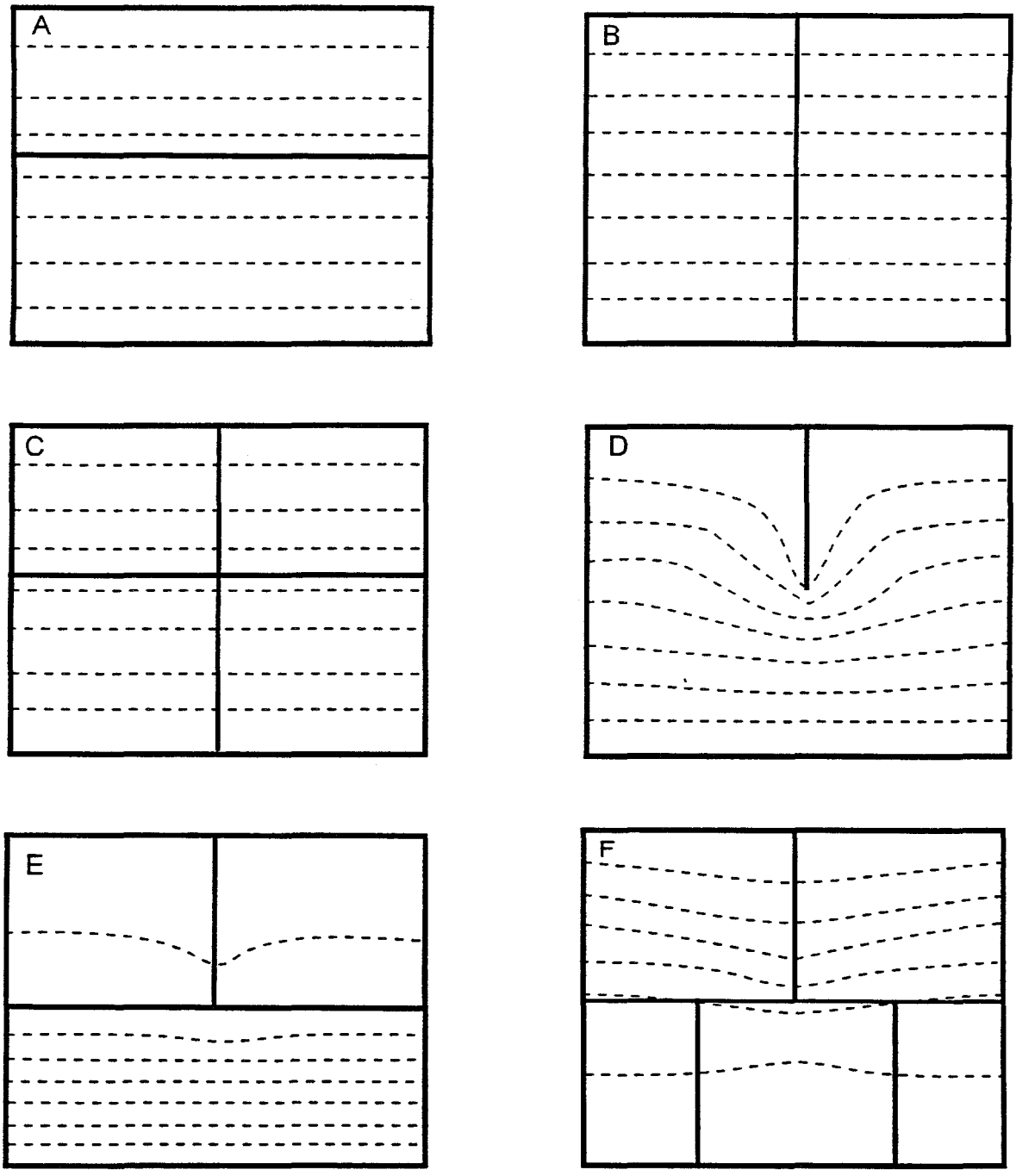

Figure 21. Fracture effects on head distribution using an aperture of 250 μm in a equivalent porous medium, with v=0.01 m/d (before addition of fractures)

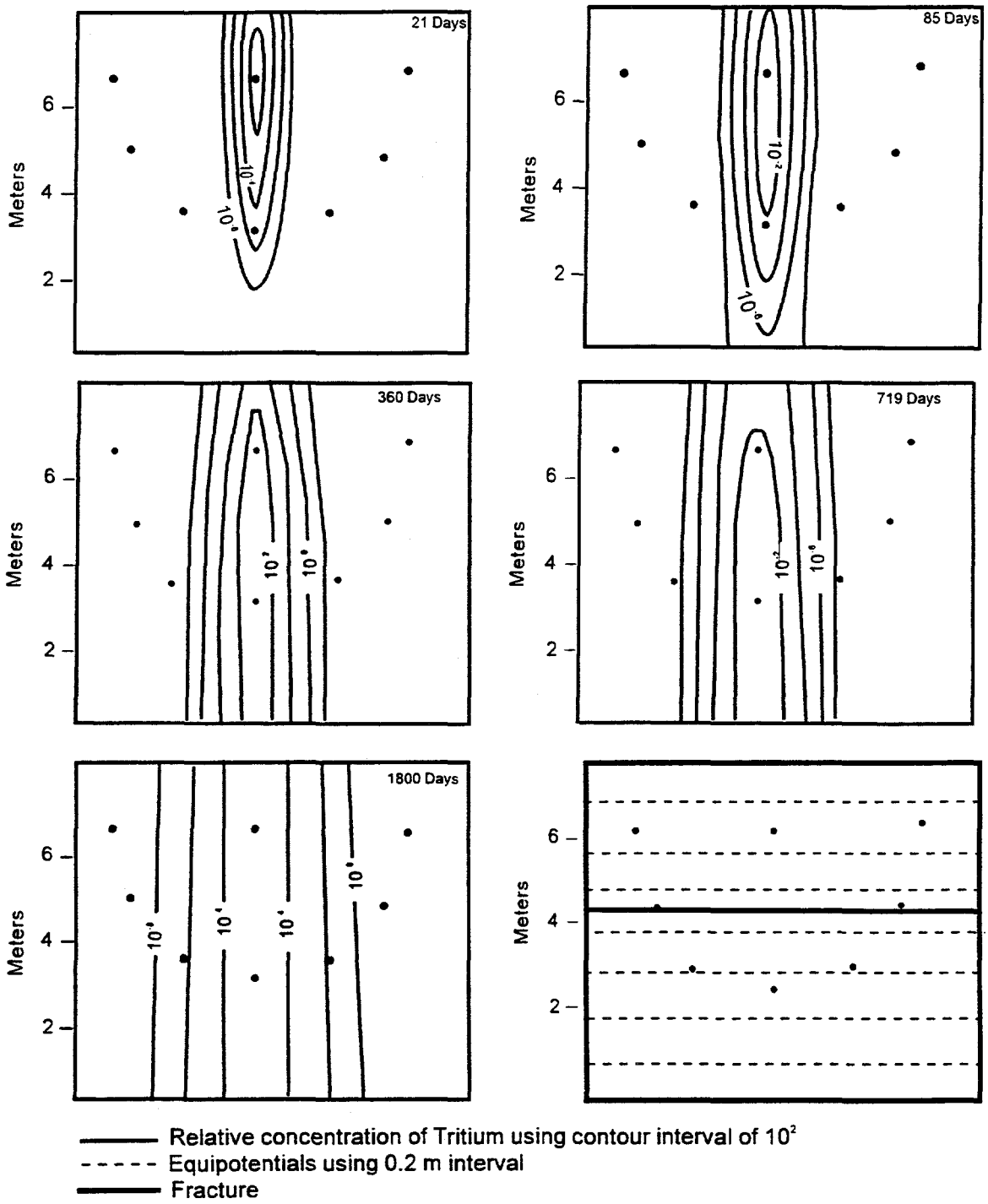

Figure 22. Simulation results for two-dimensional DF-EPM model, case A, using 2b=250 μm.

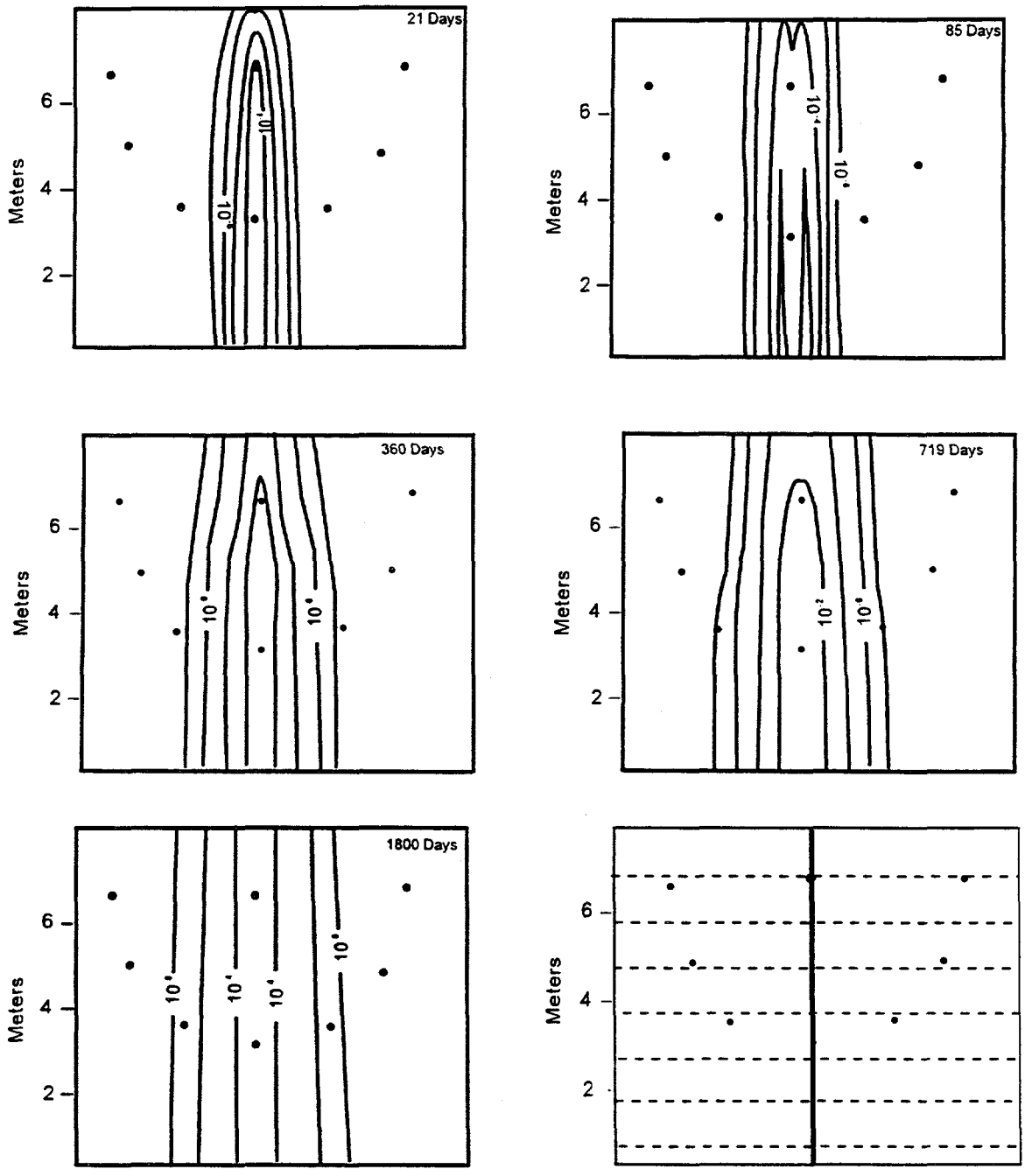

Figure 23. Simulation results for two-dimensional DF-EPM model, case B, using 2b=250 μm.

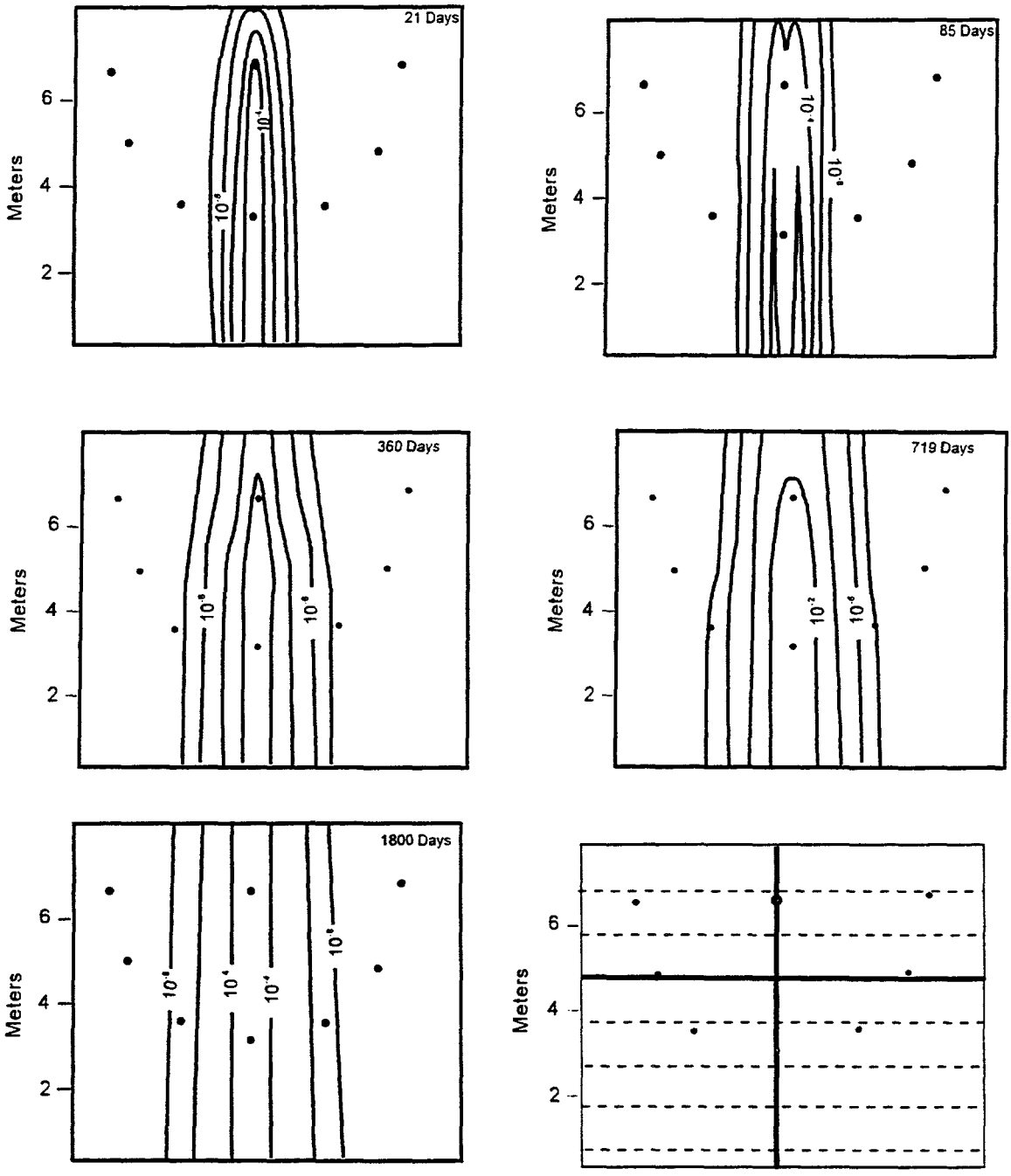

Figure 24. Simulation results for two-dimensional DF-EPM model, case C, using 2b=250 μm.

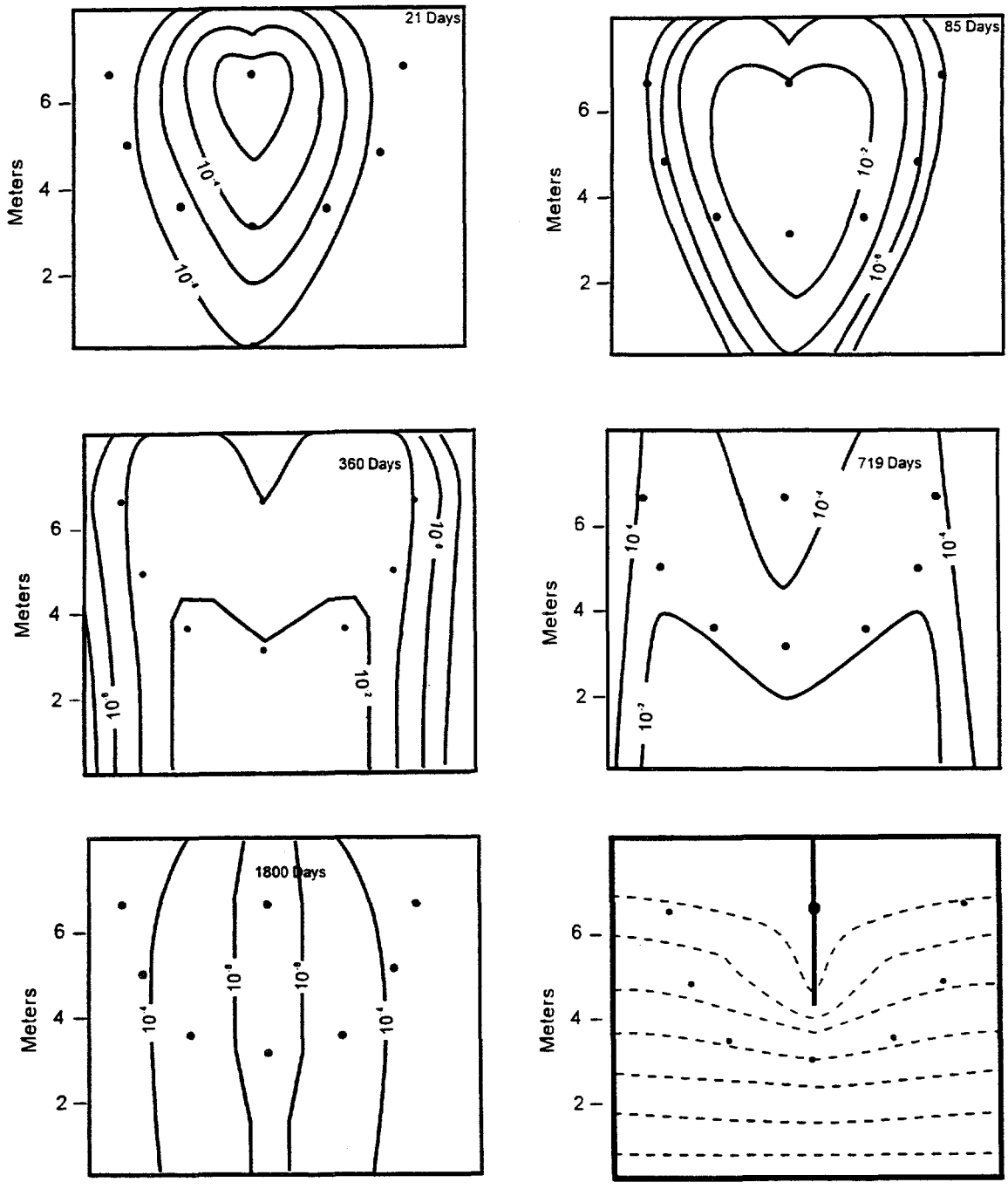

Figure 25. Simulation results for two-dimensional DF-EPM model, case D, using 2b=250μm.

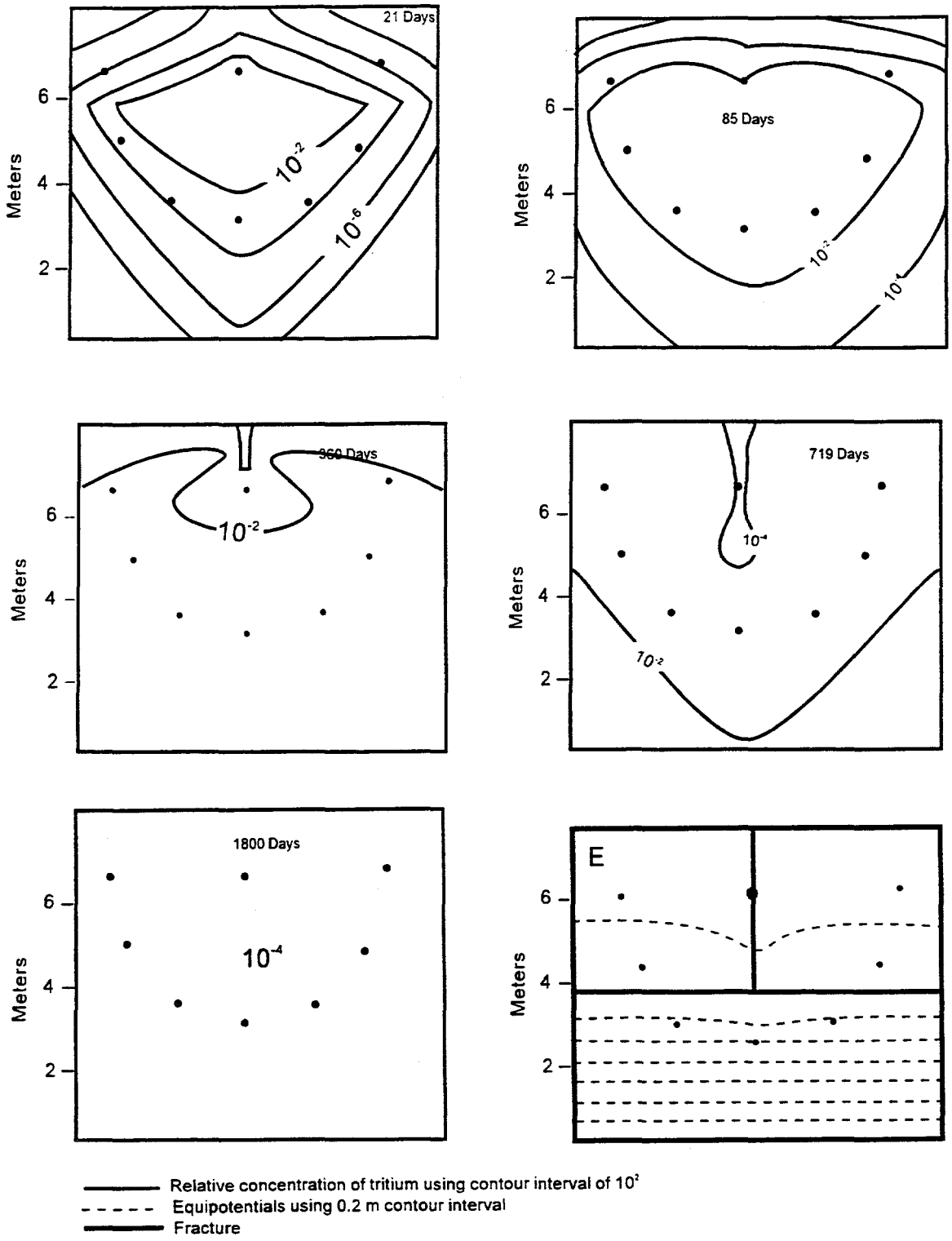

Figure 26. Simulation results for two-dimensional DF-EPM model, case E, using 2b=250 μm.

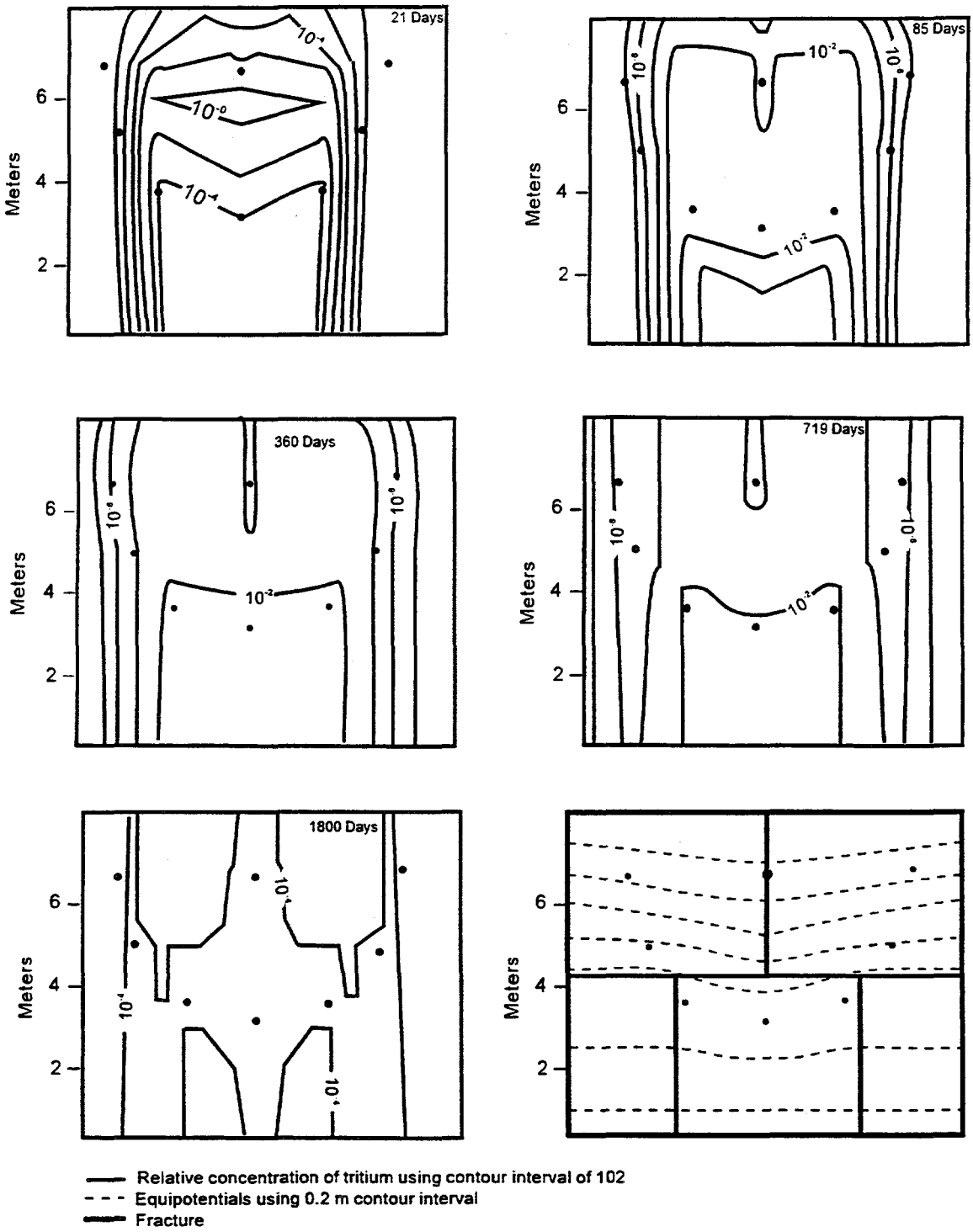

Figure 27. Simulation results for two-dimensional DF-EPM model, case F, using 2b=250 μm.

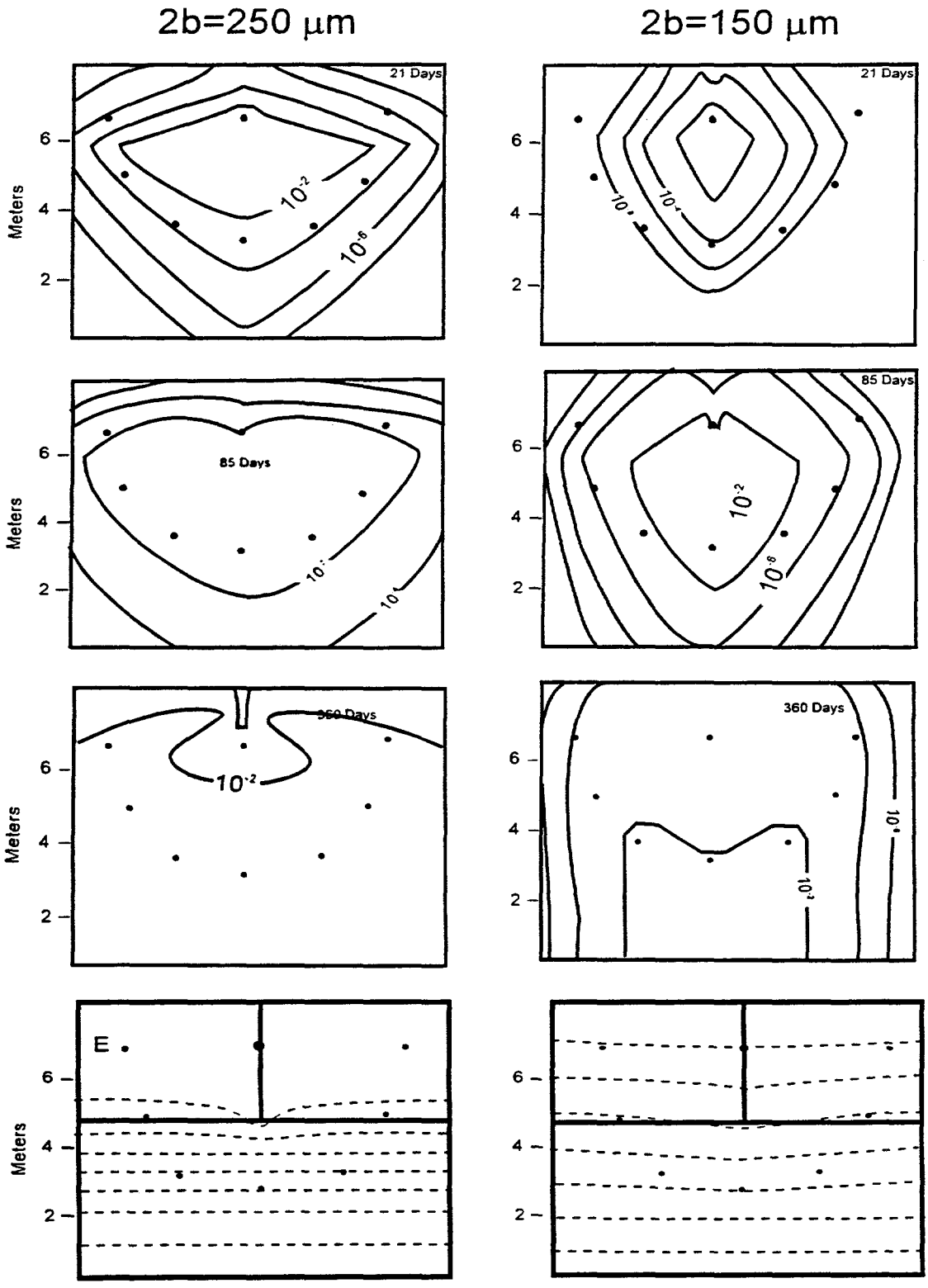

Figure 28. Simulations for case E with two different apertures.

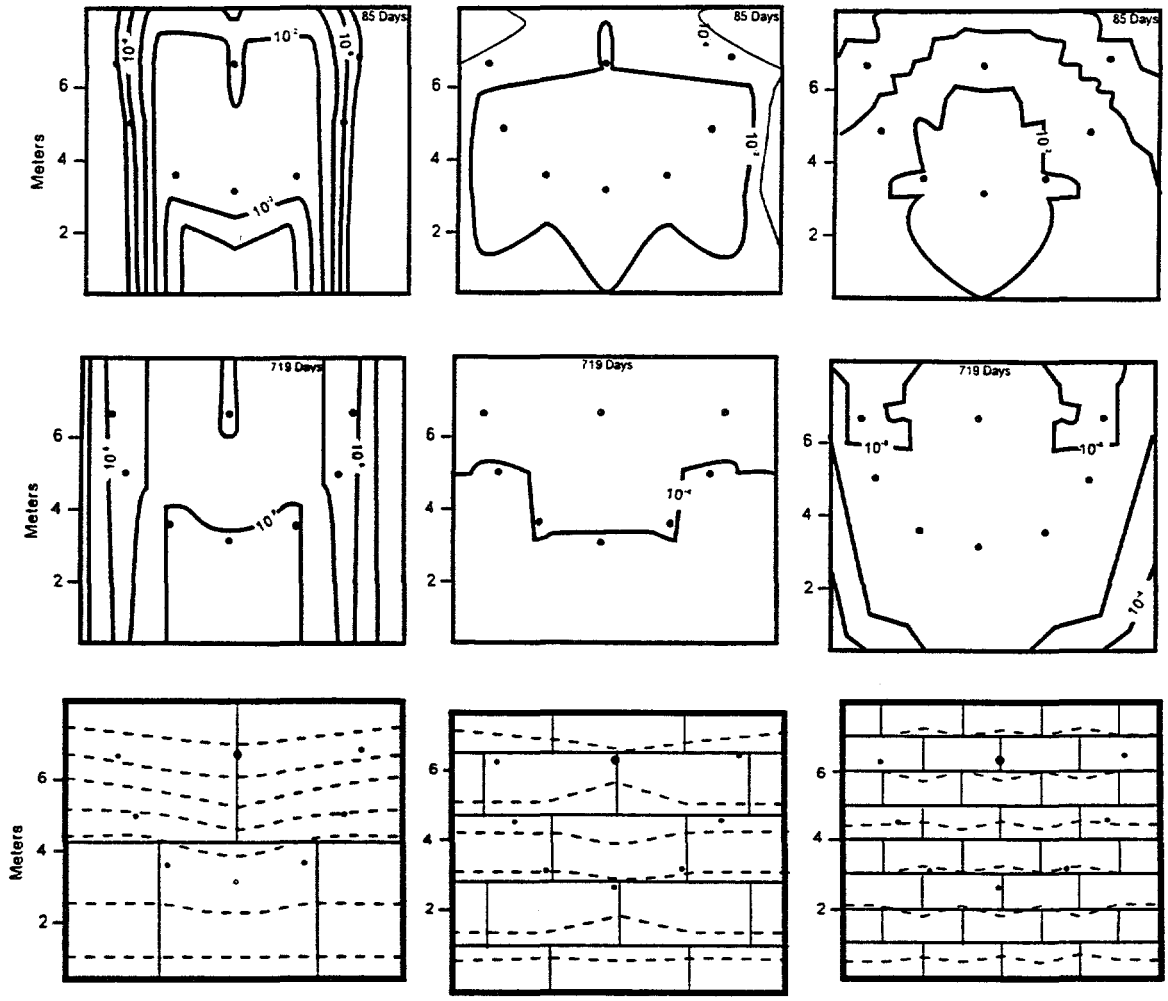

Figure 29. Simulation results for two-dimensional DF-EPM model using 2b=250μm and varying fracture spacing.

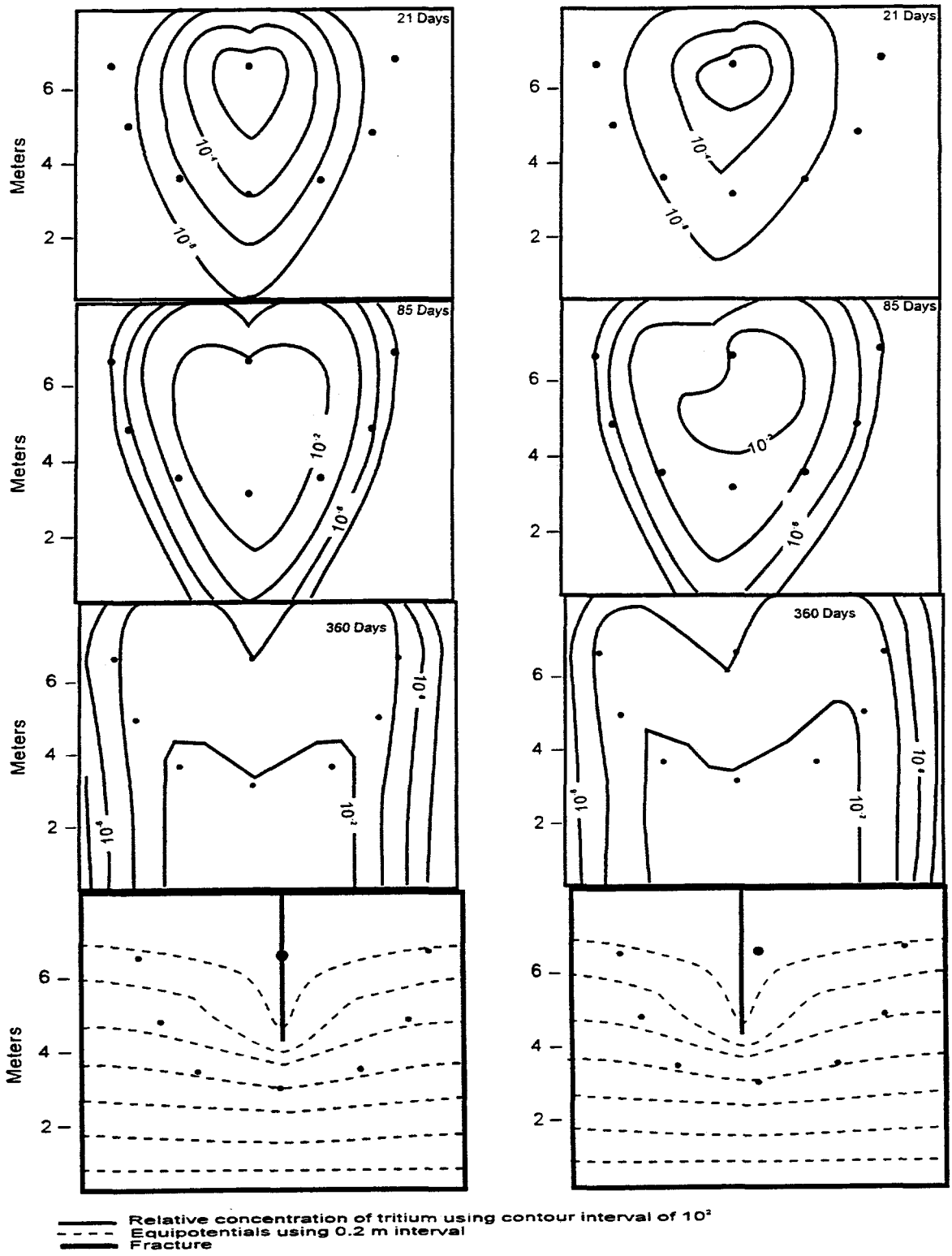

Figure 30. Simulation results for two-dimensional DF-EPM model, case D, using 2b=250μm, and varying fracture placement from source.

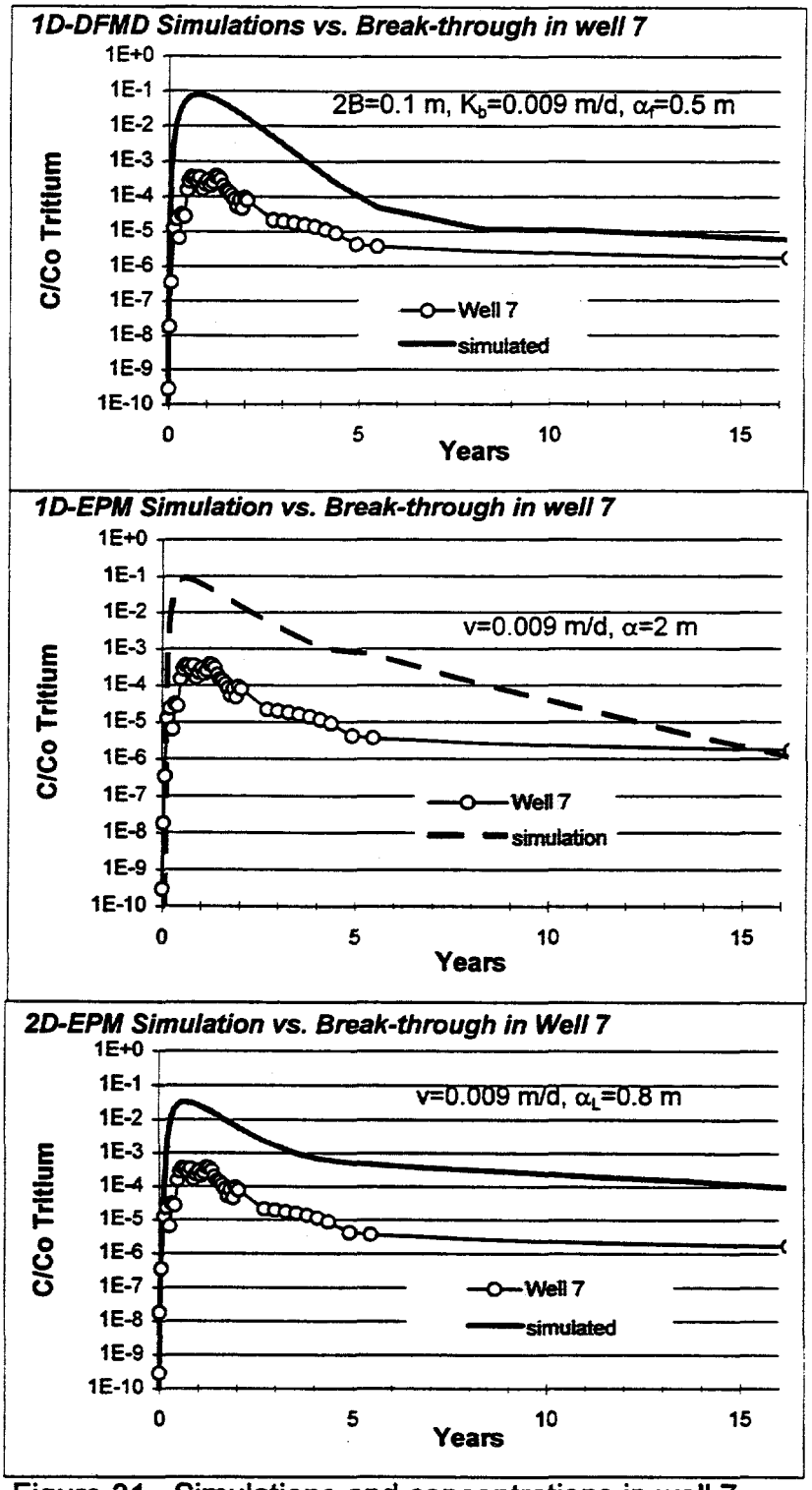

Figure 31. Simulations and concentrations in well 7 extending to 16 years.

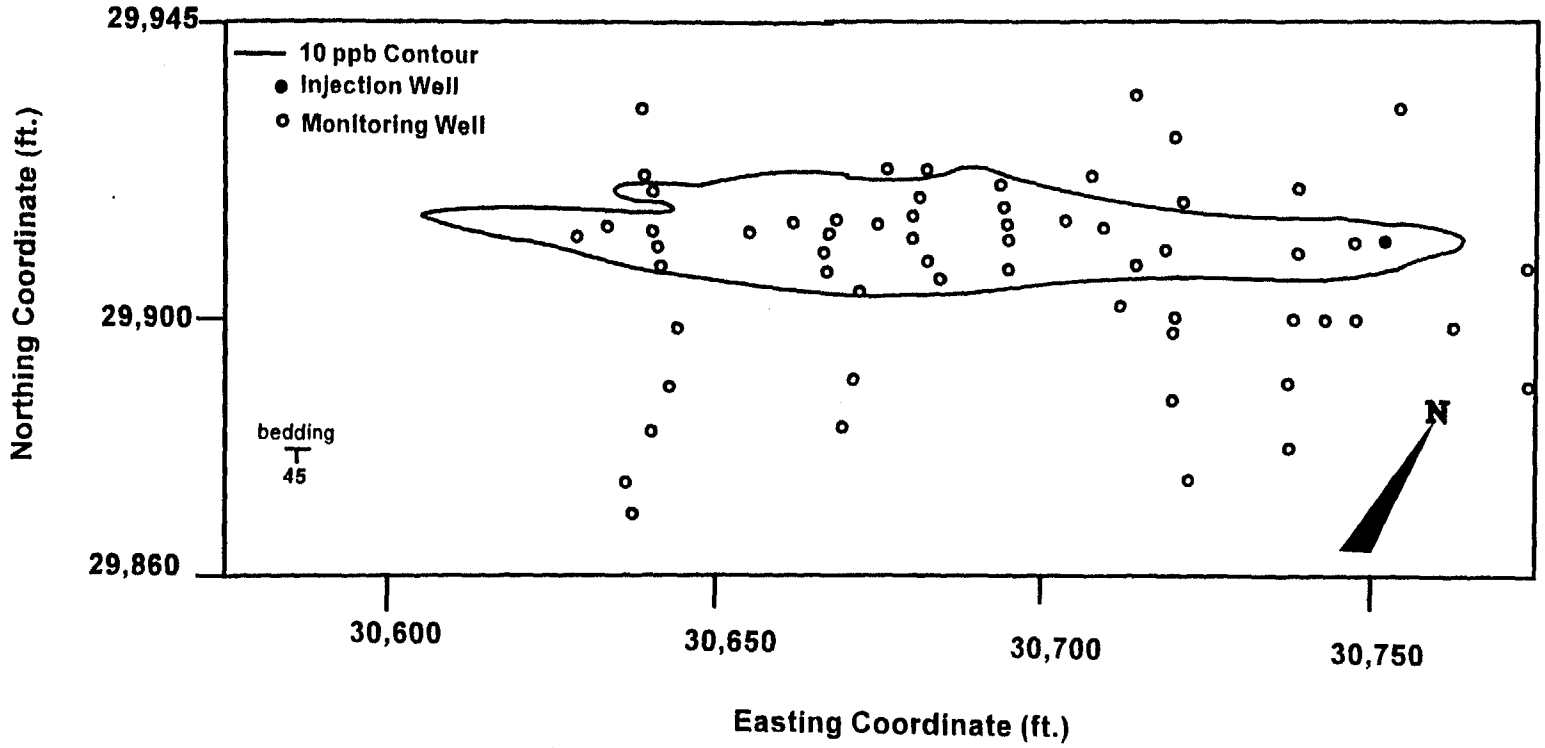

Figure 32. Rhodamine tracer plume at West Bear Creek Valley on the Oak Ridge Reservation, Oak Ridge, TN, showing the location of the 10 ppb contour (Revised from Sanford and Solomon, 1995).

APPENDIX B

CALCULATIONS

Contents

- Calculations of Water Residence Time in Injection Well
- Calculations Based on Measurements of Relative Mass

CALCULATIONS OF THE SOURCE FUNCTION

Calculations of Water Residence Time in Injection Well

The calculations below were performed to calculate the amount of time required for the volume of water in the injection well to be flushed out under natural gradient conditions. The well volume ,V, and the area ,A, both change as the water table fluctuates. At t=0, height of the water column above the bottom of the well is 4.2 m, and at approximately 94 days is 1.2 m. The average height of the water column during the first 94 days is 2.7 m. The cross-sectional area of the well is $(\pi r^2) = (\pi((0.089m)/2)^2 = 6.2x10^{-3}$ and volume of water in the well, V, is (πr^2) x (height of water column) = 0.017 m^3. The area of the well perpendicular to flow is 0.21 m^2. The average bulk hydraulic conductivity, K_b, measured in the at the field site is 0.0067 m/d, and the value measured in the injection well is 0.0048 m/d. The specific discharge, q, through the soil, is calculated by the following equation:

$$q = K_b i = \left(0.0048 \tfrac{m}{d}\right)(0.15) = 7.2x10^{-4} \tfrac{m}{d}$$

where i is the average hydraulic gradient from the injection well to well 7. The amount of time required for one well volume to be flushed out of the well is:

$$t = \frac{V}{Aq} = \frac{1.7x10^{-2} m^3}{\left(0.21 m^2\right)\left(7.2x10^{-4} \tfrac{m}{d}\right)} = 111 d .$$

*The area to which flow is perpendicular is defined as the product of the diameter of the well (0.089m) and the average water column height (2.7m)

Calculations Based on Measurements of Relative Mass

The "best fit" 2D-EPM simulation at 40 days (the end of the tracer injection) was used (see next page) to determine the amount of mass being input. Each contour of $1x10^{-0.1}$ beginning with a range of 10^{0}-$10^{-0.3}$ then from $0.10^{-0.3}$ - $10^{-0.04}$ and so on was used to measure the amount of volume per unit depth that the given contour encompasses. The following is the result of the mass calculations.

Average Log C/Co between adjacent concentration contours	A_c Area between contours =V/unit depth (m^3/m)	Relative mass (C/Co)x(V/unit depth)
0.15	0.098	0.069
0.35	0.17	0.076
0.45	0.24	0.085
0.55	0.30	0.085
0.65	0.40	0.90
0.75	0.44	0.078
0.85	0.49	0.069
0.95	0.48	0.054
1.25	0.99	0.055
1.75	1.27	0.023
2.25	1.34	0.0075
2.75	1.51	0.0027
3.25	1.51	0.00085
	TOTAL	0.70

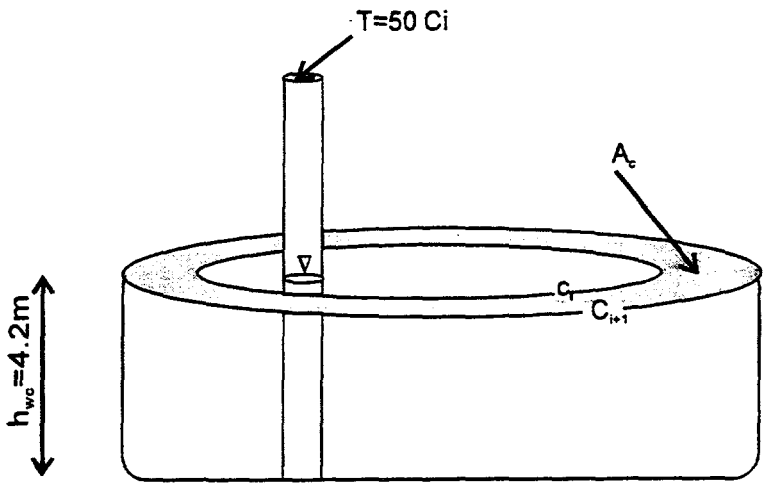

$$M_t = \frac{T}{A_{well}h}(n_e M) = \left(\frac{50Ci}{(6.2x10^{-3}m^2)(4.2m)}\right)(0.15)(0.70^{m^3}/_m) = 201^{Ci}/_m$$

$M_T = M_t \times h_p = (201 Ci/m)(2.7m) = 550$ Ci which is a factor of 11 larger than the amount of tritium added.

M_t=total tritium mass per unit thickness of plume

T=total tritium input = 50 Ci

A_{well}=cross-sectional area of the well = $6.2x10^{-3}m^2$

h_{wc}=height of the water column in well at start of experiment = 4.2 m

h_p=average thickness of plume during first 40 days of experiment = 2.7 m

n_e= effective porosity (assumes that solute is evenly spread through fractures and matrix = 0.15

A_c=area between adjacent contours of relative concentration (ex. between C_i and C_{i+1})

M_r= relative mass calculated from simulation after 40 days

$M = M_r \times n_e$ = total relative mass per unit thickness of plume

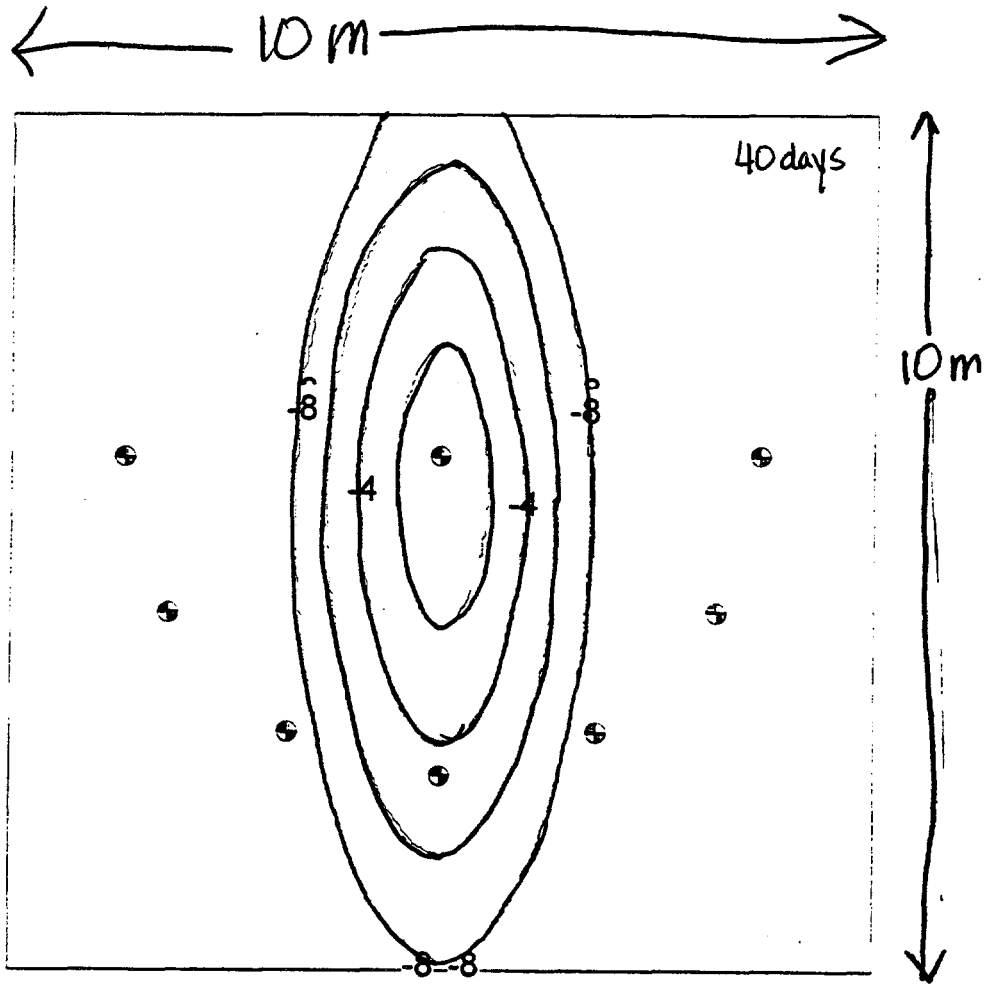

best-fit EPM

$V = 0.01$ $\eta_e = 0.15$

$\alpha_L = 0.8m$ $\frac{dh}{dl} = 0.15$

Individual Contour Area Calculated
0.9-1.0
0.8-1.0
0.7-1.0
0.6-1.0
0.5-1.0
0.4-1.0
0.3-1.0
761
number of small squares. Each square represents how
2.8×10⁻³ m³/m.

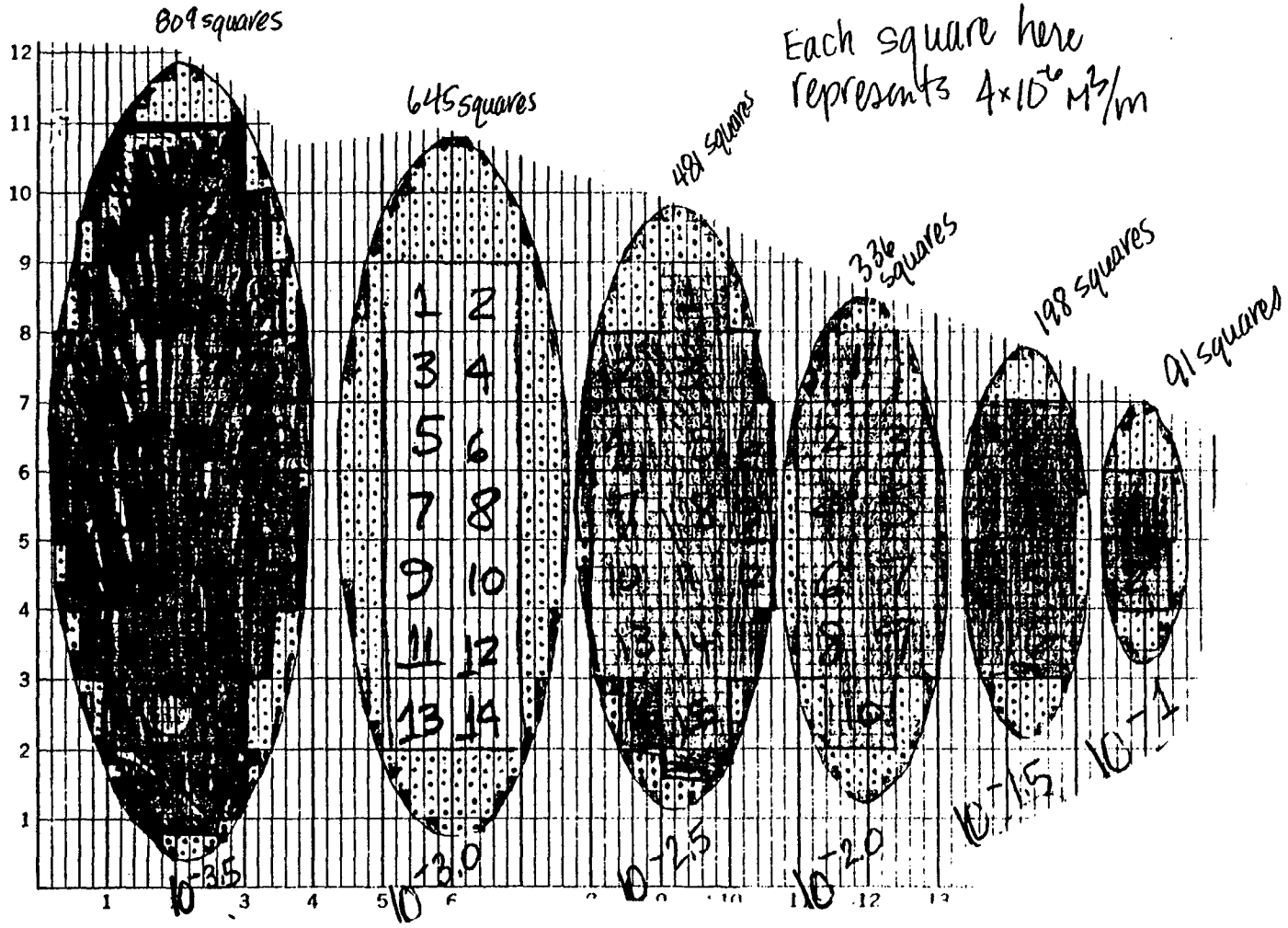
809 squares
645 squares
481 squares
336 squares
198 squares
91 squares
Each square here represents 4×10⁻⁶ m³/m
10⁻³·⁵
10⁻³·⁰
10⁻²·⁵
10⁻²·⁰
10⁻¹·⁵
10⁻¹·⁰

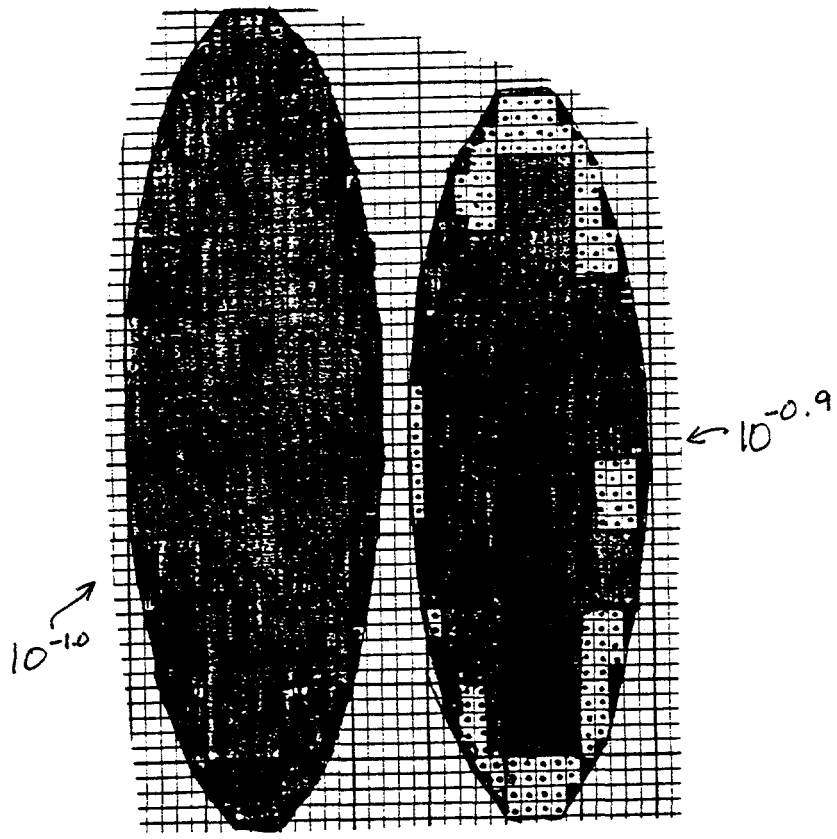

each square represents $3.2 \times 10^{-3} M^3/m$

APPENDIX C

ADDITIONAL SIMULATIONS USING FRAC3DVS

Contents

- Input data files for FRAC3DVS (version 1.3)
- Aperture study for simple truncated system

  fracture placement from the source study using one and two fractures parallel to flow and 1 meter spacing brickwork
- Study of two layers of different fracture spacing
- Suppliment to Figure 20; 3 additional times for best fit 2D EPM simulation

```
*** Group 1:Title ***
df.dat :
*** Group 2:Simulation control param ***
.false.      ; true if random grid generation
.true.       ; true if finite difference for blocks or prisms
.true.       ; true if mass balance
.true.       ; true if saturated
.true.       ; true if hydraulic head defines the problem
.true.       ; true if hydraulic head is outputted
.true.       ; true if transport is performed
.true.       ; true if simulation is performed
.false.      ; true if y-axis is vertical
.true.       ; true if generate grid
*** Group 3:Output control parameters ***
0,1,1,0,0,0,0, KPMSH,KPHEAD,KPCONC,KPVEL,KPSAT,KRESTAR,KPMASB
.true.       ; true if the above also echoes to unit 66 (ASCII)
*** Group 4:Grid data ***
.true.       ; true if generate grid from coordinates
101  NX
81,  NY
2,   NZ
.false.      ; true if the spacing is variable
10.0, 8.0, 2.0  ;xl,yl,zl (constant spacing)
*** Group 5:Physical parameters ***
.FALSE.      ; true if random k
.TRUE.       ; true if use coordinates to define property zones
1, NZONES
0.0, 10.0, 0.0, 8.0, 0.0, 2.0  ; xfrom,xto,yfrom,yto,zfrom,zto
1e-18, 1e-18, 1e-18, 0.00, 0.40  ;KX,KY,KZ,SS,por
*** Group 6: initial conditions ***
.false.      ; krestar
.true.       ; true if all init cond are default
8.0,         ; initial Head
*** Group 7:Output times ***
.false.      ; true if steady-state
0.0          ; tinit, time transport is started
1            ; nt_out, number of output times
0.5            ; output times (days)
0.5, 0.5       ; time weighting for flow then transport
5, 5         ; peclet crit, courant crit (when warnings occur)
.true.       ; automatic time step for transport (TCONTROL)
0.1          ; deltain, initial time step size for simulation
.false., 50.0, 1e-3 ; control_head, dhead_allowed, dhead_min_allowed
.false., 15.0, 1e-6 ; control_sat, dsat_allowed, dsat_min_allowed
.true., 15.0, 1e-6 ; control_conc, dconc_allowed, dconc_min_allowed (transient)
*** Group 8:Solver data ***
1.0d-30,1.0d-10,1.0d-30  ; RESIDUAL,RELATIVE,ABSOLUTE (ERRORS)
.false.      ; true if solver information
.true.       ; true if compute the residual
.false.      ; true if 2nd-order factorization
*** Group 9:Newton-Raphson parameters***
*** Group 10:Dirichlet nodes ***
.true.       ; true if dirichlet nodes
.true.       ; true if use coordinates to define 1st-type zones
2,           ; number of zones
0.0, 10.0, 8.0, 8.0, 0.0, 2.0 ; up hill boundary ("North" of 4-11)
1,           ; number of time intervals
.false.      ; function for head
8.0, -1.0, 1.0e10, ; prescribed head, time on, time off
0.0, 10.0, 0.0, 0.0, 0.0, 2.0 ; down hill boundary ("South" of 4-7)
1,           ; number of time intervals
.false.      ; function for head
6.8, -1.0, 1.0e10  ; prescribed head, time on, time off
*** Group 11: Second-type b.c. ***
.false.      ; true if 2nd-type b.c.
*** Group 12: Seepage face data ***
.False.
*** Group 13:Source/sink ***
.false.      ; true if inj/with wells
*** Group 14: Observ. well ***
.false.      ; true if observ wells
*** Group 15: Fracture data ***
.false.      ; true if fractured
*** Group 15b: Output Grids ***
.false.
*** Group 16: Simulation control param for transport ***
.true.       ; MASSBALC
.true.       ; XTERMS (dispersion)
.false.      ; CVOLUME
.false.      ; BIOCHEM
*** Group 17: Transport Output control parameters ***
0, 0         ; KWRITHC, KPMASBC
*** Group 18: Transport parameters ***
0.09         ; Longitudinal dispersivity, AL
0.001, 0.0001  ; horizontal and vertical dispersivity
1.0          ; tortuosity
1.60         ; Soil bulk density (kg/M^3)
*** Group 19: Transport parameters for the solute ***
1            ; NSPECIES
0            ; IBAT
.false.      ; KD_RAND, not random Kd
5.18e-05     ; DIFFRAC
2.209e-04    ; CLAMDA [1/T]
0            ; NPA
0.0          ; Distribution cofficient
*** Group 20: Initial conditions ***
.false.      ; KRESTARC
.true.       ; DEFAULT_IC
0.0          ; default initial concentration
*** Group 21: Orthomin solver data ***
1.0d-30, 1.0d-10, 1.0d-25 ;residual, relative and absolute convergence
.false.      ; solver info. output, ISOLV_INFOC
.false.      ; no upstream-weighting of velocities
1.0, 1.0, 1.0  ; weighting factor for x, y, & z directions (not used)
*** Group 22: Dirichlet node data ***
.true.       ; 1st type boundary conditions
.true.       ; true if use coordinates
1,           ; number of 1st type zones
1,           ; number of concentration intervals
1.0, 0.0, 40.0  ; conc, ton, toff
5.0, 5.0, 6.0, 6.0, 0.0, 2.0 ; extent in x/y/z grid
*** Group 23: 3rd-type boundary condition ***
.false.      ; no 3rd type boundary condition
*** Group 24: Concentration at Injection Wells ***
.false.      ; there is not an injection well
*** Group 25: Fracture data for transport ***
.false.      ; there are fractures for transport problem
*** Group 26: Immiscible phase dissolution Data ***
.false.      ; There is no dissolution
```

df ☐ No Fractures

$K_{x,y} = 0.02\ m/d$

$\alpha_L = 0.09m$ (matrix)

$\alpha_T = 0.01m$ "

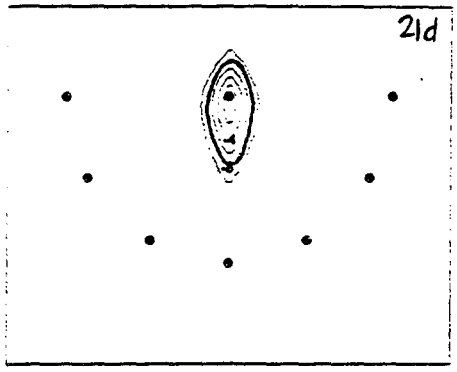

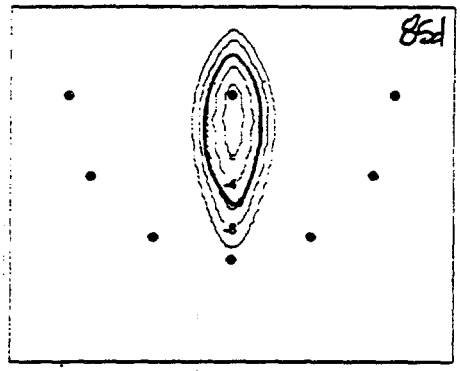

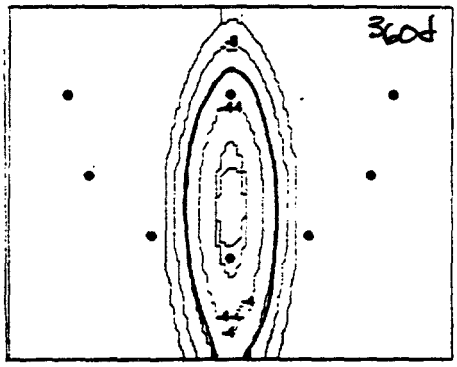

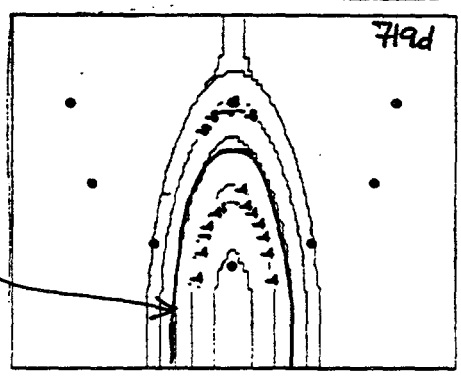

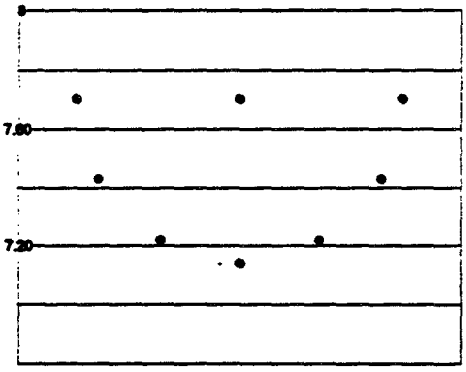

head distribution

FRAC3DVS-1.3 Input File

```
*** Group 1:Title ***
dfl.dat : simple truncated system, 2b=50μm
*** Group 2:Simulation control param ***
.false.      ; true if random grid generation
.true.       ; true if finite difference for blocks or prisms
.true.       ; true if mass balance
.true.       ; true if saturated
.true.       ; true if hydraulic head defines the problem
.true.       ; true if hydraulic head is outputted
.true.       ; true if transport is performed
.true.       ; true if simulation is performed
.false.      ; true if y-axis is vertical
.true.       ; true if generate grid
*** Group 3:Output control parameters ***
0,1,1,0,0,0,0, KPMSH,KPHEAD,KPCONC,KPVEL,KPSAT,KRESTAR,KPMASB
.true.       ; true if the above also echoes to unit 66 (ASCII)
*** Group 4:Grid data ***
.true.       ; true if generate grid from coordinates
101  NX
81,  NY
2,  NZ
.false.      ; true if the spacing is variable
10.0, 8.0, 2.0  ;xl,yl,zl (constant spacing)
*** Group 5:Physical parameters ***
.FALSE.      ; true if random k
.TRUE.       ; true if use coordinates to define property zones
1, NZONES
0.0, 10.0, 0.0, 8.0, 0.0, 2.0  ; xfrom,xto,yfrom,yto,zfrom,zto
1e-18, 1e-18, 1e-18, 0.00, 0.40  ;KX,KY,KZ,SS,por
*** Group 6: initial conditions ***
.false.      ; krestar
.true.       ; true if all init cond are default
8.0,         ; initial Head
*** Group 7:Output times ***
.false.      ; true if steady-state
0.0          ; tinit, time transport is started
1            ; nt_out, number of output times
0.5          ; output times (days)
0.5, 0.5     ; time weighting for flow then transport
5, 5         ; peclet crit, courant crit (when warnings occur)
.true.       ; automatic time step for transport (TCONTROL)
0.1          ; deltain, initial time step size for simulation
.false., 50.0, 1e-3 ; control_head, dhead_allowed, dhead_min_allowed
.false., 15.0, 1e-6 ; control_sat, dsat_allowed, dsat_min_allowed
.true., 15.0, 1e-6 ; control_conc, dconc_allowed, dconc_min_allowed
(transient)
*** Group 8:Solver data ***
1.0d-30,1.0d-10,1.0d-30  ; RESIDUAL,RELATIVE,ABSOLUTE
(ERRORS)
.false.      ; true if solver information
.true.       ; true if compute the residual
.false.      ; true if 2nd-order factorization
*** Group 9:Newton-Raphson parameters***
*** Group 10:Dirichlet nodes ***
.true.       ; true if dirichlet nodes
.true.       ; true if use coordinates to define 1st-type zones
2,           ; number of zones
0.0, 10.0, 8.0, 8.0, 0.0, 2.0 ; up hill boundary ("North" of 4-11)
1,           ; number of time intervals
.false.      ; function for head
8.0, -1.0, 1.0e10, ; prescribed head, time on, time off
0.0, 10.0, 0.0, 0.0, 0.0, 2.0 ; down hill boundary ("South" of 4-7)
1,           ; number of time intervals
.false.      ; function for head
6.8, -1.0, 1.0e10  ; prescribed head, time on, time off
*** Group 11: Second-type b.c. ***
.false.      ; true if 2nd-type b.c.
*** Group 12: Seepage face data ***
.False.
*** Group 13:Source/sink ***
.false.      ; true if inj/with wells
*** Group 14: Observ. well ***
.false.      ; true if observ wells
*** Group 15: Fracture data ***
.true.       ; true if fractured
2            ; nfrac_temp (number of fractures)
1000.0       ; fluid density
113.0        ; fluid viscosity
7.32e10      ; gravity
2            ; number of different fracture sets
.true.       ; the current set refers to fractures
0.0          ; spec. storage within the fracture
.true.       ; current set refers to fracture
0.0          ; spec. storage within fracture
5.0, 5.0, 0.0, 4.0, 0.0, 2.0, 5.0e-5, 3, 1 ; yz fracture
0.0, 10.0, 4.0, 4.0, 0.0, 2.0, 5.0e-5, 2, 1 ; xz fracture
*** Group 15b: Output Grids ***
.false.
*** Group 16: Simulation control param for transport ***
.true.       ; MASSBALC
.true.       ; XTERMS (dispersion)
.false.      ; CVOLUME
.false.      ; BIOCHEM
*** Group 17: Transport Output control parameters ***
0, 0         ; KWRITHC, KPMASBC
*** Group 18: Transport parameters ***
0.09         ; Longitudinal dispersivity, AL
0.001, 0.0001  ; horizontal and vertical dispersivity
1.0          ; tortuosity
1.60         ; Soil bulk density (kg/M^3)
*** Group 19: Transport parameters for the solute ***
1            ; NSPECIES
0            ; IBAT
.false.      ; KD_RAND, not random Kd
5.18e-05     ; DIFFRAC
2.209e-04    ; CLAMDA [1/T]
0            ; NPA
0.0          ; Distribution cofficient
*** Group 20: Initial conditions ***
.false.      ; KRESTARC
.true.       ; DEFAULT_IC
0.0          ; default initial concentration
*** Group 21: Orthomin solver data ***
1.0d-30, 1.0d-10, 1.0d-25 ;residual, relative and absolute convergence
.false.      ; solver info. output, ISOLV_INFOC
.false.      ; no upstream-weighting of velocities
1.0, 1.0, 1.0  ; weighting factor for x, y, & z directions (not used)
*** Group 22: Dirichlet node data ***
.true.       ; 1st type boundary conditions
.true.       ; true if use coordinates
1,           ; number of 1st type zones
1,           ; number of concentration intervals
1.0, 0.0, 40.0  ; conc, ton, toff
5.0, 5.0, 6.0, 6.0, 0.0, 2.0 ; extent in x/y/z grid
*** Group 23: 3rd-type boundary condition ***
.false.      ; no 3rd type boundary condition
*** Group 24: Concentration at Injection Wells ***
.false.      ; there is not an injection well
*** Group 25: Fracture data for transport ***
.true.       ; there are fractures for transport problem
0.2          ; αL for the first fracture set
0.001        ; αT for the first fracture set
1.0          ; R in the first fracture set
0.2          ; αL
0.001        ; αT
1.0          ; R
*** Group 26: Immiscible phase dissolution Data ***
.false.      ; There is no dissolution
```

df1 ⊞ 50μm
part of aperture study series
$K_{xH} = 0.02 M/d$
$\alpha_L = 0.09 m$ } Matrix
$\alpha_T = 0.001 m$ }
$\alpha_L = 0.3 m$ } Fracture
$\alpha_T = 0.001 m$ }

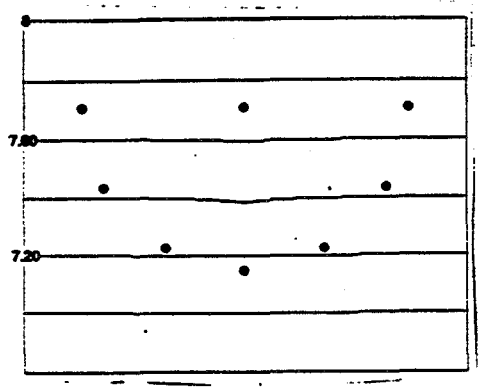

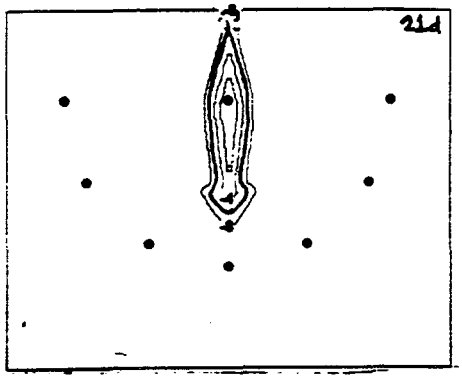

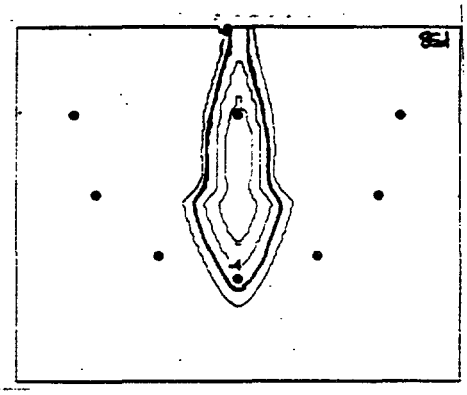

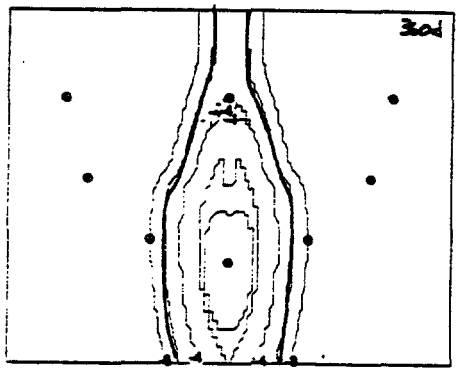

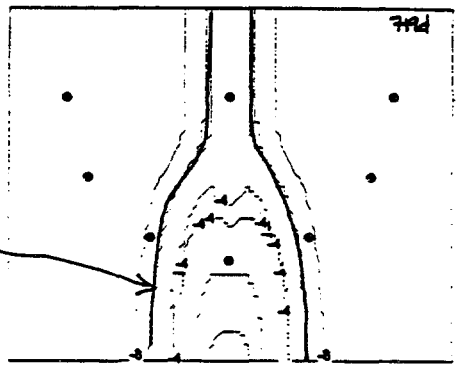

10^{-6} g/l

df2 ▯ 75μm

part of aperture study series

$K_{x,y} = 0.02\ m/d$

$\alpha_L = 0.09m$ } matrix
$\alpha_T = 0.001m$ }

$\alpha_L = 0.3m$ } fracture
$\alpha_T = 0.001m$ }

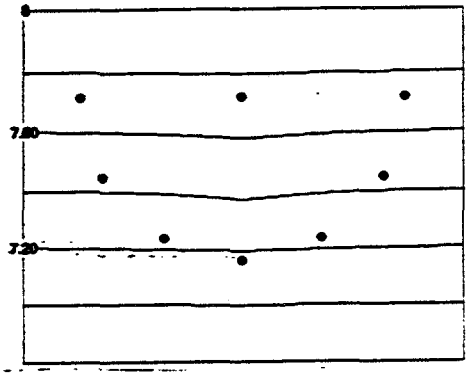

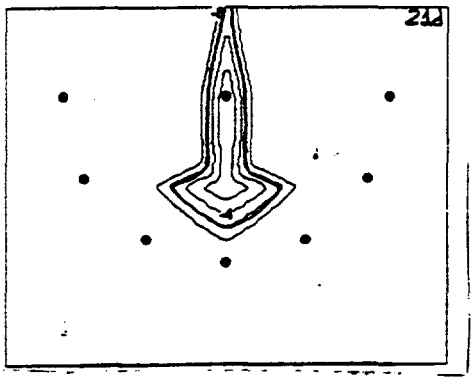

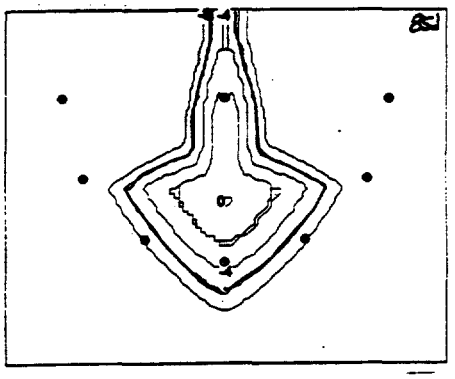

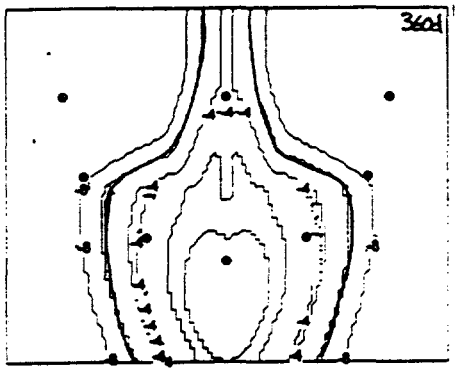

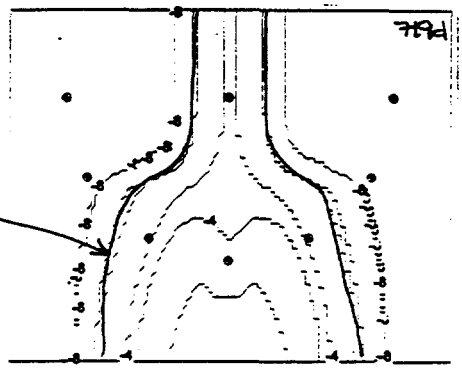

10^{-6} %

dfs 100μm

part of aperture study

$K_{x-y} = 0.02$ m/d

$\alpha_L = 0.09$m } Matrix $\alpha_L = 0.3$m } fracture

$\alpha_T = 0.001$m } $\alpha_T = 0.001$m }

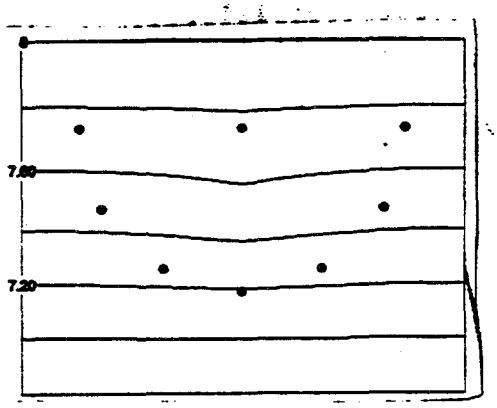

head distro.

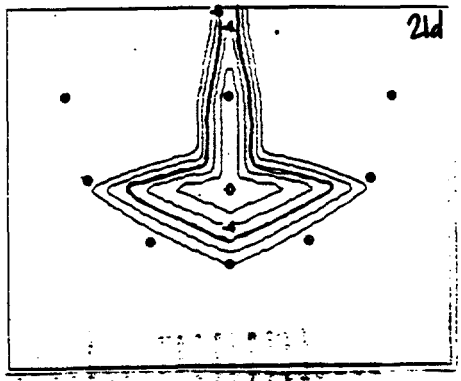

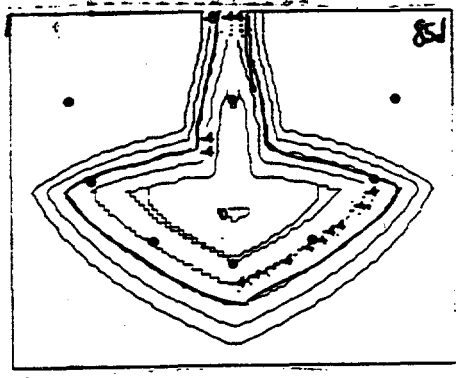

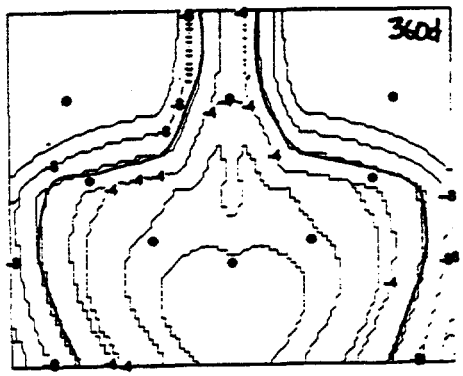

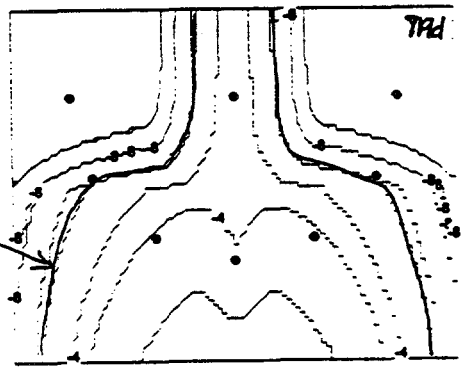

10 %

Program limitation w/ increasing 2b.

$K_{x=y} = 0.02 m/d$

$d_{L,matrix} = 0.09m$

$d_{L,frac} = 0.2m$

21 days

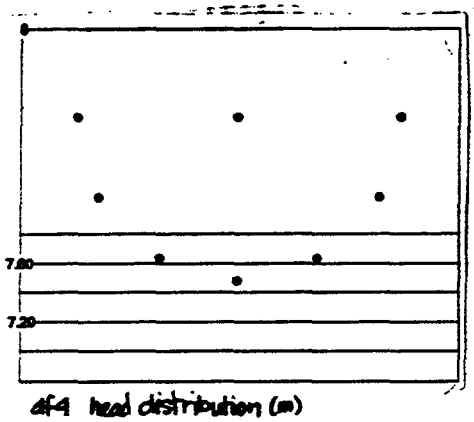

df4 head distribution (m)

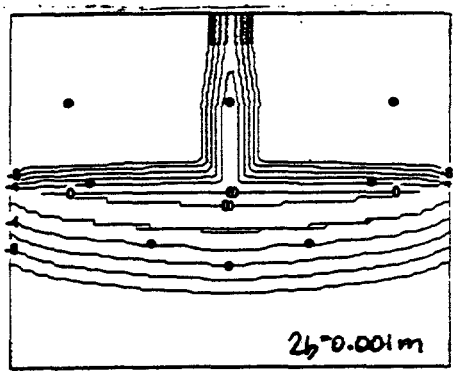

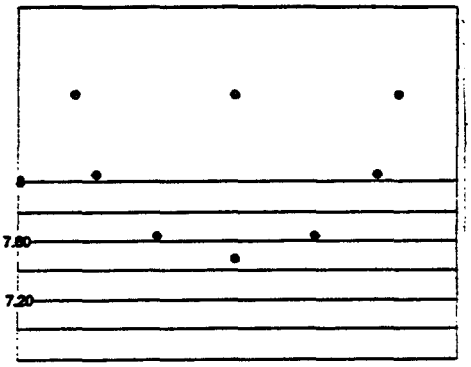

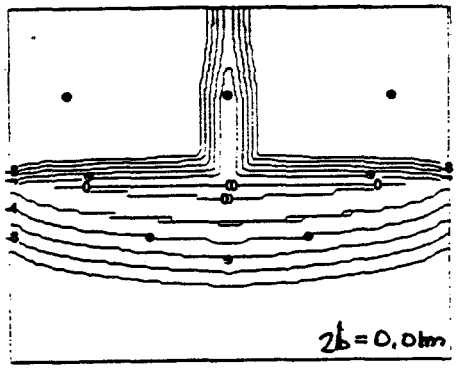

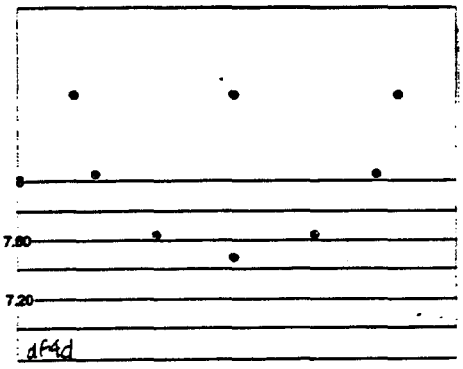

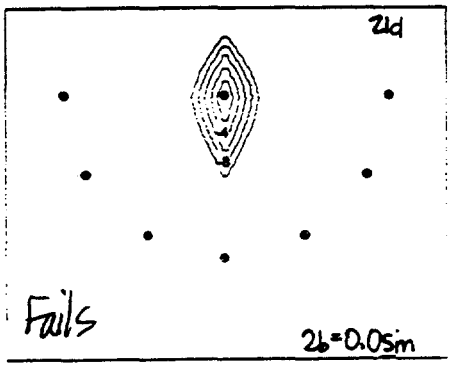

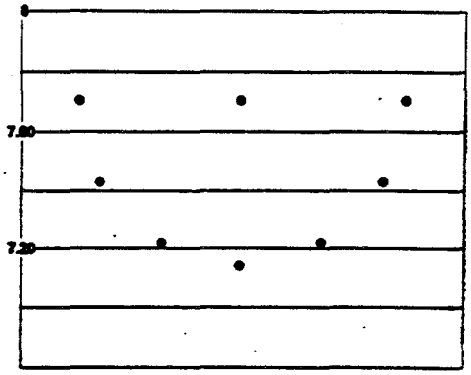

dfs_h

K_{xy} = 0.02HD

matrix: α_L = 0.09m α_T = 0.009m

fracture: α_L = 0.3m α_T = 0

T5pm

fract/inj well location study series

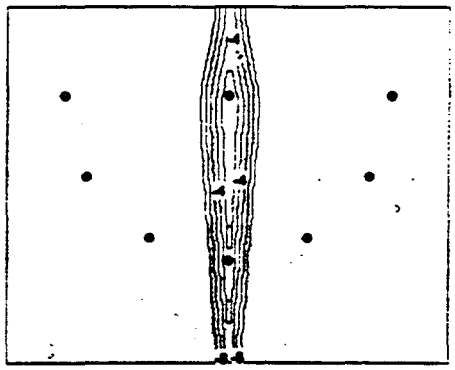

dfs_21

fracture/inj well location stable series

T5pm

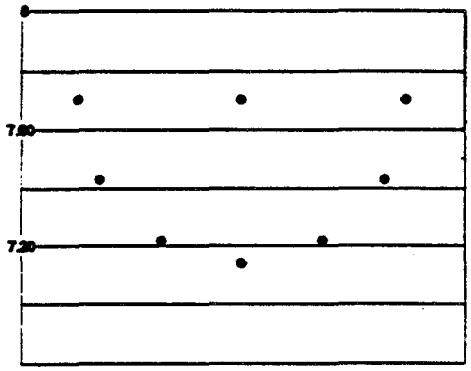

Fs_h

T5pm

fract/inj well location study series

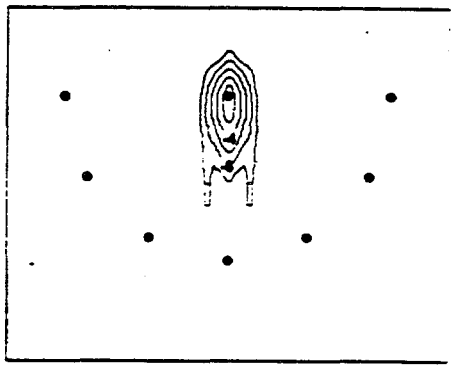

dfs_21

fract/inj well studies series

T5pm

2m

df7

brickwork, $2b = 1m$, $2b = 75\mu m$

Fracture intersects inj. well

$K_{x,y} = 0.02 m/d$ $\alpha_{L,matrix} = 0.09m$ $\alpha_{T,matrix} = 0.001m$

$\alpha_{L,fracture} = 0.30m$ $\alpha_{T,fracture} = 0.001m$

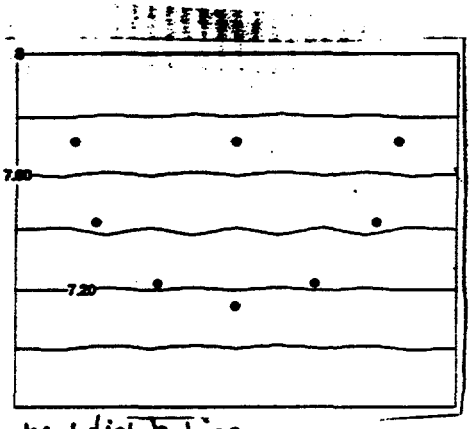

head distribution

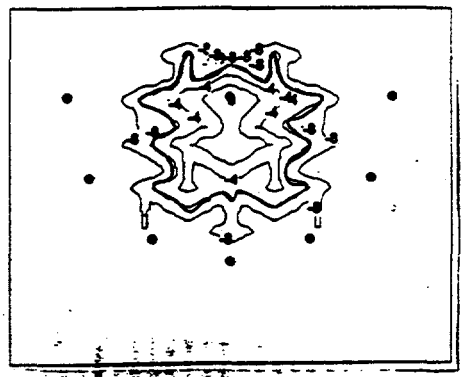

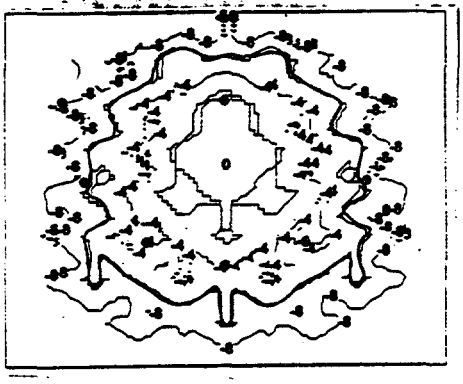

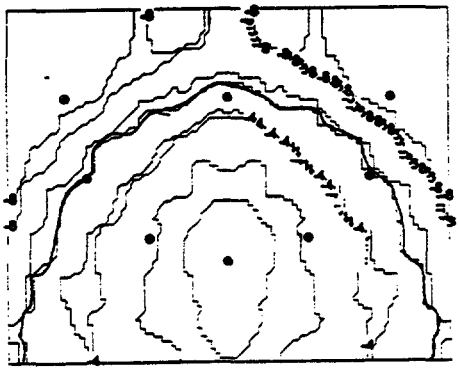

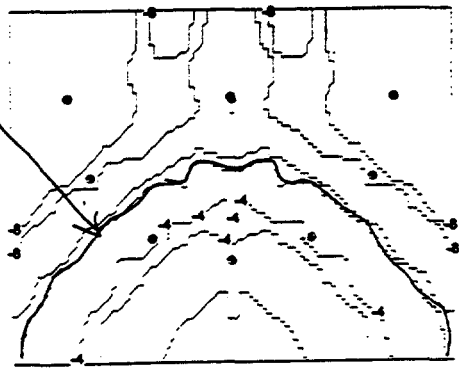

```
*** Group 1:Title ***
df7a.dat : cross-hatch 1m spacing; inj. well not penetrated by fracture
*** Group 2:Simulation control param ***
.false.      ; true if random grid generation
.true.       ; true if finite difference for blocks or prisms
.true.       ; true if mass balance
.true.       ; true if saturated
.true.       ; true if hydraulic head defines the problem
.true.       ; true if hydraulic head is outputted
.true.       ; true if transport is performed
.true.       ; true if simulation is performed
.false.      ; true if y-axis is vertical
.true.       ; true if generate grid
*** Group 3:Output control parameters ***
0,1,1,0,0,0,0,
KPMSH,KPHEAD,KPCONC,KPVEL,KPSAT,KRESTAR,KPMASB
.true.       ; true if the above also echoes to unit 66 (ASCII)
*** Group 4:Grid data ***
.true.       ; true if generate grid from coordinates
101  NX
81,  NY
2,  NZ
.false.      ; true if the spacing is variable
10.0, 8.0, 2.0  ;xl,yl,zl (constant spacing)
*** Group 5:Physical parameters ***
.FALSE.      ; true if random k
.TRUE.       ; true if use coordinates to define property zones
1, NZONES
0.0, 10.0, 0.0, 8.0, 0.0, 2.0  ; xfrom,xto,yfrom,yto,zfrom,zto
0.02, 0.02, 0.00001, 0.00, 0.40  ;KX,KY,KZ,SS,por
*** Group 6: initial conditions ***
.false.      ; krestar
.true.       ; true if all init cond are default
8.0,         ; initial Head
*** Group 7:Output times ***
.true.       ; true if steady-state
0.0          ; tinit, time transport is started
4            ; nt_out, number of output times
21,85,360,719   ; output times (days)
0.5, 0.5     ; time weighting for flow then transport
5, 5         ; peclet crit, courant crit (when warnings occur)
.true.       ; automatic time step for transport (TCONTROL)
0.1          ; deltain, initial time step size for simulation
.true., 15.0, 1e-6 ; control_conc, dconc_allowed, dconc_min_allowed (transient)
*** Group 8:Solver data ***
1.0d-30,1.0d-10,1.0d-30  ; RESIDUAL,RELATIVE,ABSOLUTE (ERRORS)
.false.      ; true if solver information
.true.       ; true if compute the residual
.false.      ; true if 2nd-order factorization
*** Group 9:Newton-Raphson parameters***
*** Group 10:Dirichlet nodes ***
.true.       ; true if dirichlet nodes
.true.       ; true if use coordinates to define 1st-type zones
2,           ; number of zones
0.0, 10.0, 8.0, 8.0, 0.0, 2.0 ; up hill boundary ("North" of 4-11)
1,           ; number of time intervals
.false.      ; function for head
8.0, -1.0, 1.0e10, ; prescribed head, time on, time off
0.0, 10.0, 0.0, 0.0, 0.0, 2.0 ; down hill boundary ("South" of 4-7)
1,           ; number of time intervals
.false.      ; function for head
6.8, -1.0, 1.0e10   ; prescribed head, time on, time off
*** Group 11: Second-type b.c. ***
.false.      ; true if 2nd-type b.c.
*** Group 12: Seepage face data ***
.False.
*** Group 13:Source/sink ***
.false.      ; true if inj/with wells
*** Group 14: Observ. well ***
.false.      ; true if observ wells
*** Group 15: Fracture data ***
.true.       ; true if fractured
43           ; nfrac_temp - number of fractures
1000.0       ; fluid density (rho)
113.0        ; visc
7.32e10      ; grav.
2            ; number of different sets of fractures
.true.       ; the current set refers to fractures
0.0          ; spec. storage within the fracture
.true.       ; the current set refers to fractures
0.0          ; spec. storage within the fracture
2.0, 2.0, 1.5, 2.5, 0.0, 2.0,  7.5e-5, 3, 1 ; yz fracture
4.0, 4.0, 1.5, 2.5, 0.0, 2.0,  7.5e-5, 3, 1 ; yz fracture
6.0, 6.0, 1.5, 2.5, 0.0, 2.0,  7.5e-5, 3, 1 ; yz fracture
8.0, 8.0, 1.5, 2.5, 0.0, 2.0,  7.5e-5, 3, 1 ; yz fracture
1.0, 1.0, 2.5, 3.5, 0.0, 2.0,  7.5e-5, 3, 1 ; yz fracture
3.0, 3.0, 2.5, 3.5, 0.0, 2.0,  7.5e-5, 3, 1 ; yz fracture
5.0, 5.0, 2.5, 3.5, 0.0, 2.0,  7.5e-5, 3, 1 ; yz fracture
7.0, 7.0, 2.5, 3.5, 0.0, 2.0,  7.5e-5, 3, 1 ; yz fracture
9.0, 9.0, 2.5, 3.5, 0.0, 2.0,  7.5e-5, 3, 1 ; yz fracture
2.0, 2.0, 3.5, 4.5, 0.0, 2.0,  7.5e-5, 3, 1 ; yz fracture
4.0, 4.0, 3.5, 4.5, 0.0, 2.0,  7.5e-5, 3, 1 ; yz fracture
6.0, 6.0, 3.5, 4.5, 0.0, 2.0,  7.5e-5, 3, 1 ; yz fracture
8.0, 8.0, 3.5, 4.5, 0.0, 2.0,  7.5e-5, 3, 1 ; yz fracture
1.0, 1.0, 4.5, 5.5, 0.0, 2.0,  7.5e-5, 3, 1 ; yz fracture
3.0, 3.0, 4.5, 5.5, 0.0, 2.0,  7.5e-5, 3, 1 ; yz fracture
5.0, 5.0, 4.5, 5.5, 0.0, 2.0,  7.5e-5, 3, 1 ; yz fracture
7.0, 7.0, 4.5, 5.5, 0.0, 2.0,  7.5e-5, 3, 1 ; yz fracture
9.0, 9.0, 4.5, 5.5, 0.0, 2.0,  7.5e-5, 3, 1 ; yz fracture
2.0, 2.0, 5.5, 6.5, 0.0, 2.0,  7.5e-5, 3, 1 ; yz fracture
4.0, 4.0, 5.5, 6.5, 0.0, 2.0,  7.5e-5, 3, 1 ; yz fracture
6.0, 6.0, 5.5, 6.5, 0.0, 2.0,  7.5e-5, 3, 1 ; yz fracture
8.0, 8.0, 5.5, 6.5, 0.0, 2.0,  7.5e-5, 3, 1 ; yz fracture
1.0, 1.0, 6.5, 7.5, 0.0, 2.0,  7.5e-5, 3, 1 ; yz fracture
3.0, 3.0, 6.5, 7.5, 0.0, 2.0,  7.5e-5, 3, 1 ; yz fracture
5.0, 5.0, 6.5, 7.5, 0.0, 2.0,  7.5e-5, 3, 1 ; yz fracture
7.0, 7.0, 6.5, 7.5, 0.0, 2.0,  7.5e-5, 3, 1 ; yz fracture
9.0, 9.0, 6.5, 7.5, 0.0, 2.0,  7.5e-5, 3, 1 ; yz fracture
0.0, 10.0, 0.5, 0.5, 0.0, 2.0, 7.5e-5, 2, 1 ; yz fracture
0.0, 10.0, 1.5, 1.5, 0.0, 2.0, 7.5e-5, 2, 1 ; yz fracture
0.0, 10.0, 2.5, 2.5, 0.0, 2.0, 7.5e-5, 2, 1 ; yz fracture
0.0, 10.0, 3.5, 3.5, 0.0, 2.0, 7.5e-5, 2, 1 ; yz fracture
0.0, 10.0, 4.5, 4.5, 0.0, 2.0, 7.5e-5, 2, 1 ; yz fracture
0.0, 10.0, 5.5, 5.5, 0.0, 2.0, 7.5e-5, 2, 1 ; yz fracture
0.0, 10.0, 6.5, 6.5, 0.0, 2.0, 7.5e-5, 2, 1 ; yz fracture
*** Group 15b: Output Grids ***
.false.
*** Group 16: Simulation control param for transport ***
.true.       ; MASSBALC
.true.       ; XTERMS (dispersion)
.false.      ; CVOLUME
.false.      ; BIOCHEM
*** Group 17: Transport Output control parameters ***
0, 0         ; KWRITHC, KPMASBC
*** Group 18: Transport parameters ***
0.09         ; Longitudinal dispersivity, AL
0.01, 0.0    ; horizontal and vertical dispersivity
1.0          ; tortuosity
1.60         ; Soil bulk density (kg/M^3)
*** Group 19: Transport parameters for the solute ***
1            ; NSPECIES
0            ; IBAT
.false.      ; KD_RAND, not random Kd
5.18e-05     ; DIFFRAC
2.209e-04    ; CLAMDA [1/T]
0            ; NPA
0.0          ; Distribution cofficient
*** Group 20: Initial conditions ***
.false.      ; KRESTARC
.true.       ; DEFAULT_IC
0.0          ; default initial concentration
*** Group 21: Orthomin solver data ***
1.0d-30, 1.0d-10, 1.0d-25 ;residual, relative and absolute convergence
.false.      ; solver info. output, ISOLV_INFOC
.false.      ; no upstream-weighting of velocities
1.0, 1.0, 1.0   ; weighting factor for x, y, & z directions (not used)
*** Group 22: Dirichlet node data ***
.true.       ; 1st type boundary conditions
.true.       ; true if use coordinates
1,           ; number of 1st type zones
1,           ; number of concentration intervals
1.0, 0.0, 40.0  ; conc, ton, toff
5.0, 5.0, 6.0, 6.0, 0.0, 2.0 ; extent in x/y/z grid
*** Group 23: 3rd-type boundary condition ***
.false.      ; no 3rd type boundary condition
*** Group 24: Concentration at Injection Wells ***
.false.      ; there is not an injection well
*** Group 25: Fracture data for transport ***
.true.       ; there are fractures for transport problem
0.3          ; al (dispersivity in the fractures)
0.001        ; at
1.0          ; retardation
0.3          ; al (dispersivity in the fractures)
0.001        ; at
1.0          ; retardation
*** Group 26: Immiscible phase dissolution Data ***
.false.      ; There is no dissolution
```

df7a

brickwork, 2B=1m, 2b=75μm

Fracture does not intersect inj. well

$K_{x,y}$=0.02m/d $\alpha_{L,matrix}$=0.01m $\alpha_{T,matrix}$=0.001m

$\alpha_{L,fracture}$=0.3m $\alpha_{T,fracture}$=0.001m

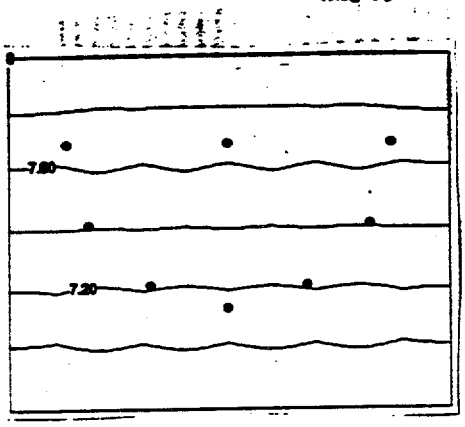

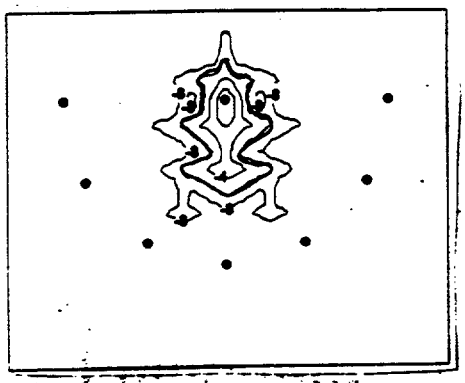

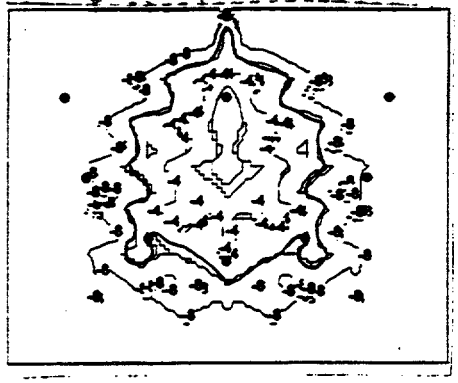

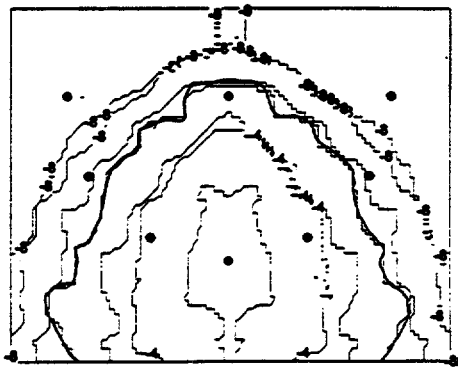

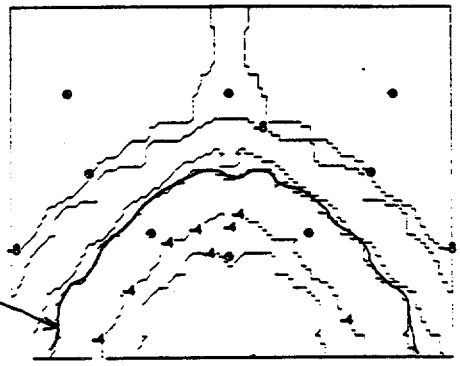

*** Group 1:Title *** fracture spacing study
df8.dat : ~~grid size study with small grid and one set of bricks~~
*** Group 2:Simulation control param ***
.false. ; true if random grid generation
.true. ; true if finite difference for blocks or prisms
.true. ; true if mass balance
.true. ; true if saturated
.true. ; true if hydraulic head defines the problem
.true. ; true if hydraulic head is outputted
.true. ; true if transport is performed
.true. ; true if simulation is performed
.false. ; true if y-axis is vertical
.true. ; true if generate grid
*** Group 3:Output control parameters ***
0,1,1,0,0,0,0,
KPMSH,KPHEAD,KPCONC,KPVEL,KPSAT,KRESTAR,KPMASB
.true. ; true if the above also echoes to unit 66 (ASCII)
*** Group 4:Grid data ***
.true. ; true if generate grid from coordinates
101 NX
81, NY
2, NZ
.false. ; true if the spacing is variable
10.0, 8.0, 2.0 ;xl,yl,zl (constant spacing)
*** Group 5:Physical parameters ***
.FALSE. ; true if random k
.TRUE. ; true if use coordinates to define property zones
1, NZONES
0.0, 10.0, 0.0, 8.0, 0.0, 2.0 ; xfrom,xto,yfrom,yto,zfrom,zto
0.02, 0.02, 0.00001, 0.00, 0.40 ;KX,KY,KZ,SS,por
*** Group 6: initial conditions ***
.false. ; krestar
.true. ; true if all init cond are default
8.0, ; initial Head
*** Group 7:Output times ***
.false. ; true if steady-state
0.0 ; tinit, time transport is started
4 ; nt_out, number of output times
21,85,360,719 ; output times (days)
0.5, 0.5 ; time weighting for flow then transport
5, 5 ; peclet crit, courant crit (when warnings occur)
.true. ; automatic time step for transport (TCONTROL)
0.1 ; deltain, initial time step size for simulation
.false., 50.0, 1e-3 ; control_head, dhead_allowed, dhead_min_allowed
.false., 15.0, 1e-6 ; control_sat, dsat_allowed, dsat_min_allowed
.true., 15.0, 1e-6 ; control_conc, dconc_allowed, dconc_min_allowed (transient)
*** Group 8:Solver data ***
1.0d-30,1.0d-10,1.0d-30 ; RESIDUAL,RELATIVE,ABSOLUTE (ERRORS)
.false. ; true if solver information
.true. ; true if compute the residual
.false. ; true if 2nd-order factorization
*** Group 9:Newton-Raphson parameters***
*** Group 10:Dirichlet nodes ***
.true. ; true if dirichlet nodes
.true. ; true if use coordinates to define 1st-type zones
2, ; number of zones
0.0, 10.0, 8.0, 8.0, 0.0, 2.0 ; up hill boundary ("North" of 4-11)
1, ; number of time intervals
.false. ; function for head
8.0, -1.0, 1.0e10, ; prescribed head, time on, time off
0.0, 10.0, 0.0, 0.0, 0.0, 2.0 ; down hill boundary ("South" of 4-7)
1, ; number of time intervals
.false. ; function for head
6.8, -1.0, 1.0e10 ; prescribed head, time on, time off
*** Group 11: Second-type b.c. ***
.false. ; true if 2nd-type b.c.
*** Group 12: Seepage face data ***
.False.
*** Group 13:Source/sink ***
.false. ; true if inj/with wells
*** Group 14: Observ. well ***
.false. ; true if observ wells
*** Group 15: Fracture data ***
.true. ; true if fractured
19 ; nfrac_temp - number of fractures
1000.0 ; fluid density (rho)
113.0 ; visc
7.32e10 ; grav.
2 ; number of different sets of fractures
.true. ; the current set refers to fractures
0.0 ; spec. storage within the fracture
.true. ; the current set refers to fractures
0.0 ; spec. storage within the fracture
1.0, 1.0, 5.0, 6.0, 0.0, 2.0, 1e-4, 3, 1 ; yz fracture
2.0, 2.0, 5.0, 6.0, 0.0, 2.0, 1e-4, 3, 1 ; yz fracture
3.0, 3.0, 5.0, 6.0, 0.0, 2.0, 1e-4, 3, 1 ; yz fracture
4.0, 4.0, 5.0, 6.0, 0.0, 2.0, 1e-4, 3, 1 ; yz fracture
5.0, 5.0, 5.0, 6.0, 0.0, 2.0, 1e-4, 3, 1 ; yz fracture
6.0, 6.0, 5.0, 6.0, 0.0, 2.0, 1e-4, 3, 1 ; yz fracture
7.0, 7.0, 5.0, 6.0, 0.0, 2.0, 1e-4, 3, 1 ; yz fracture
8.0, 8.0, 5.0, 6.0, 0.0, 2.0, 1e-4, 3, 1 ; yz fracture
9.0, 9.0, 5.0, 6.0, 0.0, 2.0, 1e-4, 3, 1 ; yz fracture
1.4, 1.4, 4.0, 5.0, 0.0, 2.0, 1e-4, 3, 1 ; yz fracture
2.8, 2.8, 4.0, 5.0, 0.0, 2.0, 1e-4, 3, 1 ; yz fracture
4.2, 4.2, 4.0, 5.0, 0.0, 2.0, 1e-4, 3, 1 ; yz fracture
5.6, 5.6, 4.0, 5.0, 0.0, 2.0, 1e-4, 3, 1 ; yz fracture
7.0, 7.0, 4.0, 5.0, 0.0, 2.0, 1e-4, 3, 1 ; yz fracture
8.4, 8.4, 4.0, 5.0, 0.0, 2.0, 1e-4, 3, 1 ; yz fracture
9.8, 9.8, 4.0, 5.0, 0.0, 2.0, 1e-4, 3, 1 ; yz fracture
0.0, 10.0, 4.0, 4.0, 0.0, 2.0, 1e-4, 2, 1 ; xz fracture
0.0, 10.0, 5.0, 5.0, 0.0, 2.0, 1e-4, 2, 1 ; xz fracture
0.0, 10.0, 6.0, 6.0, 0.0, 2.0, 1e-4, 2, 1 ; xz fracture
*** Group 15b: Output Grids ***
.false.
*** Group 16: Simulation control param for transport ***
.true. ; MASSBALC
.true. ; XTERMS (dispersion)
.false. ; CVOLUME
.false. ; BIOCHEM
*** Group 17: Transport Output control parameters ***
0, 0 ; KWRITHC, KPMASBC
*** Group 18: Transport parameters ***
0.09 ; Longitudinal dispersivity, AL
0.001, 0.0001 ; horizontal and vertical dispersivity
1.0 ; tortuosity
1.60 ; Soil bulk density (kg/M^3)
*** Group 19: Transport parameters for the solute ***
1 ; NSPECIES
0 ; IBAT
.false. ; KD_RAND, not random Kd
5.18e-05 ; DIFFRAC
2.209e-04 ; CLAMDA [1/T]
0 ; NPA
0.0 ; Distribution cofficient
*** Group 20: Initial conditions ***
.false. ; KRESTARC
.true. ; DEFAULT_IC
0.0 ; default initial concentration
*** Group 21: Orthomin solver data ***
1.0d-30, 1.0d-10, 1.0d-25 ;residual, relative and absolute convergence
.false. ; solver info. output, ISOLV_INFOC
.false. ; no upstream-weighting of velocities
1.0, 1.0, 1.0 ; weighting factor for x, y, & z directions (not used)
*** Group 22: Dirichlet node data ***
.true. ; 1st type boundary conditions
.true. ; true if use coordinates
1, ; number of 1st type zones
1, ; number of concentration intervals
1.0, 0.0, 40.0 ; conc, ton, toff
5.0, 5.0, 6.0, 6.0, 0.0, 2.0 ; extent in x/y/z grid
*** Group 23: 3rd-type boundary condition ***
.false. ; no 3rd type boundary condition
*** Group 24: Concentration at Injection Wells ***
.false. ; there is not an injection well
*** Group 25: Fracture data for transport ***
.true. ; there are fractures for transport problem
0.2 ; al (dispersivity in the fractures)
0.001 ; at
1.0 ; retardation
0.2 ; al (dispersivity in the fractures)
0.001 ; at
1.0 ; retardation
*** Group 26: Immiscible phase dissolution Data ***
.false. ; There is no dissolution

df8

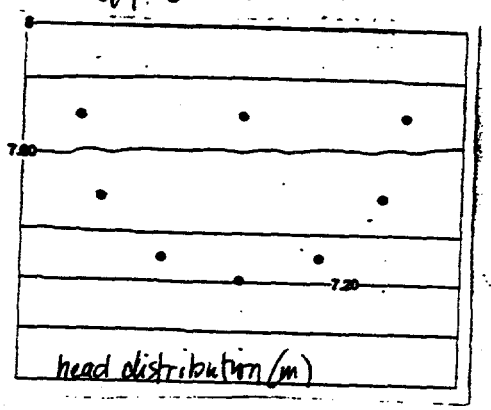

Study of 2 layers of different fracture spacing

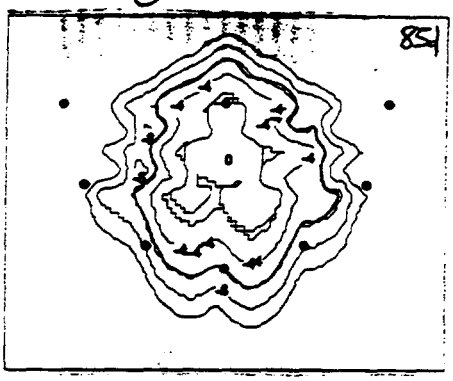

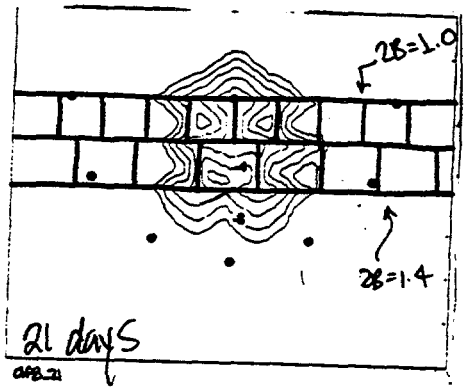

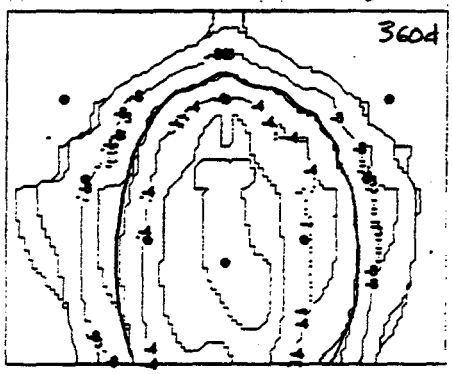

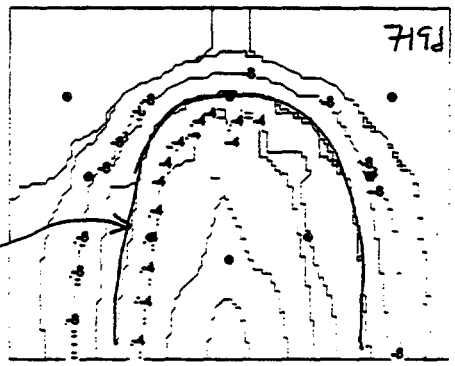

```
*** Group 1:Title ***
df9.dat : 2 different layers
*** Group 2:Simulation control param ***
.false.      ; true if random grid generation
.true.       ; true if finite difference for blocks or prisms
.true.       ; true if mass balance
.true.       ; true if saturated
.true.       ; true if hydraulic head defines the problem
.true.       ; true if hydraulic head is outputted
.true.       ; true if transport is performed
.true.       ; true if simulation is performed
.false.      ; true if y-axis is vertical
.true.       ; true if generate grid
*** Group 3:Output control parameters ***
0,1,1,0,0,0,0, KPMSH,KPHEAD,KPCONC,KPVEL,KPSAT,KRESTAR,KPMASB
.true.      ; true if the above also echoes to unit 66 (ASCII)
*** Group 4:Grid data ***
.true.       ; true if generate grid from coordinates
101  NX
81,  NY
2,  NZ
.false.      ; true if the spacing is variable
10.0, 8.0, 2.0  ;xl,yl,zl (constant spacing)
*** Group 5:Physical parameters ***
.FALSE.      ; true if random k
.TRUE.       ; true if use coordinates to define property zones
1, NZONES
0.0, 10.0, 0.0, 8.0, 0.0, 2.0  ; xfrom,xto,yfrom,yto,zfrom,zto
1e-18, 1e-18, 1e-18, 0.00, 0.40  ;KX,KY,KZ,SS,por
*** Group 6: initial conditions ***
.false.      ; krestar
.true.       ; true if all init cond are default
8.0,         ; initial Head
*** Group 7:Output times ***
.false.      ; true if steady-state
0.0          ; tinit, time transport is started
1            ; nt_out, number of output times
0.5          ; output times (days)
0.5, 0.5     ; time weighting for flow then transport
5, 5         ; peclet crit, courant crit (when warnings occur)
.true.       ; automatic time step for transport (TCONTROL)
0.1          ; deltain, initial time step size for simulation
.false., 50.0, 1e-3 ; control_head, dhead_allowed, dhead_min_allowed
.false., 15.0, 1e-6 ; control_sat, dsat_allowed, dsat_min_allowed
.true., 15.0, 1e-6 ; control_conc, dconc_allowed, dconc_min_allowed (transient)
*** Group 8:Solver data ***
1.0d-30,1.0d-10,1.0d-30  ; RESIDUAL,RELATIVE,ABSOLUTE (ERRORS)
.false.      ; true if solver information
.true.       ; true if compute the residual
.false.      ; true if 2nd-order factorization
*** Group 9:Newton-Raphson parameters***
*** Group 10:Dirichlet nodes ***
.true.       ; true if dirichlet nodes
.true.       ; true if use coordinates to define 1st-type zones
2,           ; number of zones
0.0, 10.0, 8.0, 8.0, 0.0, 2.0 ; up hill boundary ("North" of 4-11)
1,           ; number of time intervals
.false.      ; function for head
8.0, -1.0, 1.0e10, ; prescribed head, time on, time off
0.0, 10.0, 0.0, 0.0, 0.0, 2.0 ; down hill boundary ("South" of 4-7)
1,           ; number of time intervals
.false.      ; function for head
6.8, -1.0, 1.0e10   ; prescribed head, time on, time off
*** Group 11: Second-type b.c. ***
.false.       ; true if 2nd-type b.c.
*** Group 12: Seepage face data ***
.False.
*** Group 13:Source/sink ***
.false.      ; true if inj/with wells
*** Group 14: Observ. well ***
.false.      ; true if observ wells
*** Group 15: Fracture data ***
.true.       ; true if fractured
17                          ; nfrac_temp - number of fractures
1000.0                      ; fluid density (rho)
113.0                       ; visc
7.32e10                     ; grav.
2                           ; number of different sets of fractures
.true.                      ; the current set refers to fractures
0.0                         ; spec. storage within the fracture
.true.                      ; the current set refers to fractures
0.0                         ; spec. storage within the fracture
1.0,  1.0, 4.0, 8.0, 0.0, 2.0, 1e-4, 3, 1 ; yz fracture
2.0,  2.0, 4.0, 8.0, 0.0, 2.0, 1e-4, 3, 1 ; yz fracture
3.0,  3.0, 4.0, 8.0, 0.0, 2.0, 1e-4, 3, 1 ; yz fracture
4.0,  4.0, 4.0, 8.0, 0.0, 2.0, 1e-4, 3, 1 ; yz fracture
5.0,  5.0, 4.0, 8.0, 0.0, 2.0, 1e-4, 3, 1 ; yz fracture
6.0,  6.0, 4.0, 8.0, 0.0, 2.0, 1e-4, 3, 1 ; yz fracture
7.0,  7.0, 4.0, 8.0, 0.0, 2.0, 1e-4, 3, 1 ; yz fracture
8.0,  8.0, 4.0, 8.0, 0.0, 2.0, 1e-4, 3, 1 ; yz fracture
9.0,  9.0, 4.0, 8.0, 0.0, 2.0, 1e-4, 3, 1 ; yz fracture
1.4, 1.4 , 0, 4.0, 0.0, 2.0, 1e-4, 3, 1 ; yz fracture
2.8, 2.8, 0, 4.0, 0.0, 2.0, 1e-4, 3, 1 ; yz fracture
4.2, 4.2, 0, 4.0, 0.0, 2.0, 1e-4, 3, 1 ; yz fracture
5.6, 5.6, 0, 4.0, 0.0, 2.0, 1e-4, 3, 1 ; yz fracture
7.0, 7.0, 0, 4.0, 0.0, 2.0, 1e-4, 3, 1 ; yz fracture
8.4, 8.4, 0, 4.0, 0.0, 2.0, 1e-4, 3, 1 ; yz fracture
9.8, 9.8, 0, 4.0, 0.0, 2.0, 1e-4, 3, 1 ; yz fracture
0.0,10.0, 4.0, 0.0, 2.0, 1e-4, 3, 1 ; yz fracture
*** Group 15b: Output Grids ***
.false.
*** Group 16: Simulation control param for transport ***
.true.       ; MASSBALC
.true.       ; XTERMS (dispersion)
.false.      ; CVOLUME
.false.      ; BIOCHEM
*** Group 17: Transport Output control parameters ***
0, 0         ; KWRITHC, KPMASBC
*** Group 18: Transport parameters ***
0.09         ; Longitudinal dispersivity, AL
0.001, 0.0001  ; horizontal and vertical dispersivity
1.0          ; tortuosity
1.60         ; Soil bulk density (kg/M^3)
*** Group 19: Transport parameters for the solute ***
1            ; NSPECIES
0            ; IBAT
.false.      ; KD_RAND, not random Kd
5.18e-05      ; DIFFRAC
2.209e-04     ; CLAMDA [1/T]
0          ; NPA
0.0          ; Distribution cofficient
*** Group 20: Initial conditions ***
.false.      ; KRESTARC
.true.       ; DEFAULT_IC
0.0          ; default initial concentration
*** Group 21: Orthomin solver data ***
1.0d-30, 1.0d-10, 1.0d-25 ;residual, relative and absolute convergence
.false.      ; solver info. output, ISOLV_INFOC
.false.      ; no upstream-weighting of velocities
1.0, 1.0, 1.0  ; weighting factor for x, y, & z directions (not used)
*** Group 22: Dirichlet node data ***
.true.       ; 1st type boundary conditions
.true.       ; true if use coordinates
1,           ; number of 1st type zones
1,           ; number of concentration intervals
1.0, 0.0, 40.0  ; conc, ton, toff
5.0, 5.0, 6.0, 6.0, 0.0, 2.0 ; extent in x/y/z grid
*** Group 23: 3rd-type boundary condition ***
.false.      ; no 3rd type boundary condition
*** Group 24: Concentration at Injection Wells ***
.false.      ; there is not an injection well
*** Group 25: Fracture data for transport ***
.true.       ; there are fractures for transport problem
0.2                         ; al (dispersivity in the fractures)
0.001                       ; at
1.0                         ; retardation
0.2                         ; al (dispersivity in the fractures)
0.001                       ; at
1.0                         ; retardation
*** Group 26: Immiscible phase dissolution Data ***
.false.      ; There is no dissolution
```

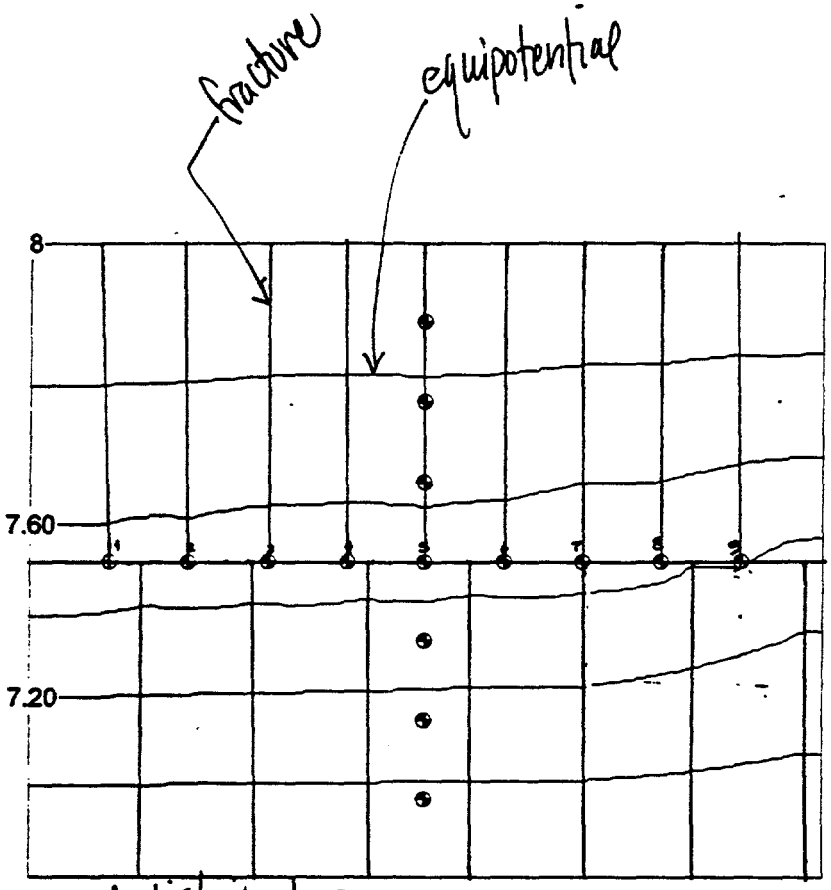

head distribution

df9

$K_{x,y,z} \rightarrow 0$

$2b = 100\mu m$

```
*** Group 1:Title ***
df10.dat : increasing 2B
*** Group 2:Simulation control param ***
.false.      ; true if random grid generation
.true.       ; true if finite difference for blocks or prisms
.true.       ; true if mass balance
.true.       ; true if saturated
.true.       ; true if hydraulic head defines the problem
.true.       ; true if hydraulic head is outputted
.true.       ; true if transport is performed
.true.       ; true if simulation is performed
.false.      ; true if y-axis is vertical
.true.       ; true if generate grid
*** Group 3:Output control parameters ***
0,1,1,1,0,0,1,
KPMSH,KPHEAD,KPCONC,KPVEL,KPSAT,KRESTAR,KPMASB
.true.       ; true if the above also echoes to unit 66 (ASCII)
*** Group 4:Grid data ***
.true.       ; true if generate grid from coordinates
101  NX
81,  NY
2,  NZ
.false.      ; true if the spacing is variable
10.0, 8.0, 2.0  ;xl,yl,zl (constant spacing)
*** Group 5:Physical parameters ***
.FALSE.      ; true if random k
.TRUE.       ; true if use coordinates to define property zones
1, NZONES
0.0, 10.0, 0.0, 8.0, 0.0, 2.0  ; xfrom,xto,yfrom,yto,zfrom,zto
1e-18, 1e-18, 1e-18, 0.00, 0.40  ;KX,KY,KZ,SS,por
*** Group 6: initial conditions ***
.false.      ; krestar
.true.       ; true if all init cond are default
8.0,         ; initial Head
*** Group 7:Output times ***
.false.      ; true if steady-state
0.0          ; tinit, time transport is started
1            ; nt_out, number of output times
0.5          ; output times (days)
0.5, 0.5     ; time weighting for flow then transport
5, 5         ; peclet crit, courant crit (when warnings occur)
.true.       ; automatic time step for transport (TCONTROL)
0.1          ; deltain, initial time step size for simulation
.false., 50.0, 1e-3 ; control_head, dhead_allowed, dhead_min_allowed
.false., 15.0, 1e-6 ; control_sat, dsat_allowed, dsat_min_allowed
.true., 15.0, 1e-6 ; control_conc, dconc_allowed, dconc_min_allowed (transient)
*** Group 8:Solver data ***
1.0d-30,1.0d-10,1.0d-30  ; RESIDUAL,RELATIVE,ABSOLUTE (ERRORS)
.false.      ; true if solver information
.true.       ; true if compute the residual
.false.      ; true if 2nd-order factorization
*** Group 9:Newton-Raphson parameters***
*** Group 10:Dirichlet nodes ***
.true.       ; true if dirichlet nodes
.true.       ; true if use coordinates to define 1st-type zones
2,           ; number of zones
0.0, 10.0, 8.0, 8.0, 0.0, 2.0 ; up hill boundary ("North" of 4-11)
1,           ; number of time intervals
.false.      ; function for head
8.0, -1.0, 1.0e10, ; prescribed head, time on, time off
0.0, 10.0, 0.0, 0.0, 0.0, 2.0 ; down hill boundary ("South" of 4-7)
1,           ; number of time intervals
.false.      ; function for head
6.8, -1.0, 1.0e10  ; prescribed head, time on, time off
*** Group 11: Second-type b.c. ***
.false.      ; true if 2nd-type b.c.
*** Group 12: Seepage face data ***
.False.
*** Group 13:Source/sink ***
.false.      ; true if inj/with wells
*** Group 14: Observ. well ***
.false.      ; true if observ wells
*** Group 15: Fracture data ***
.true.       ; true if fractured
29                          ; nfrac_temp - number of fractures
1000.0                      ; fluid density (rho)
113.0                       ; visc
7.32e10                     ; grav.
2                           ; number of different sets of fractures
.true.                      ; the current set refers to fractures
0.0                         ; spec. storage within the fracture
.true.                      ; the current set refers to fractures
0.0                         ; spec. storage within the fracture
1.0,  1.0, 4.0, 8.0, 0.0, 2.0, 1e-4, 3, 1 ; yz fracture
2.0,  2.0, 4.0, 8.0, 0.0, 2.0, 1e-4, 3, 1 ; yz fracture
3.0,  3.0, 4.0, 8.0, 0.0, 2.0, 1e-4, 3, 1 ; yz fracture
4.0,  4.0, 4.0, 8.0, 0.0, 2.0, 1e-4, 3, 1 ; yz fracture
5.0,  5.0, 4.0, 8.0, 0.0, 2.0, 1e-4, 3, 1 ; yz fracture
6.0,  6.0, 4.0, 8.0, 0.0, 2.0, 1e-4, 3, 1 ; yz fracture
7.0,  7.0, 4.0, 8.0, 0.0, 2.0, 1e-4, 3, 1 ; yz fracture
8.0,  8.0, 4.0, 8.0, 0.0, 2.0, 1e-4, 3, 1 ; yz fracture
9.0,  9.0, 4.0, 8.0, 0.0, 2.0, 1e-4, 3, 1 ; yz fracture
0.5, 0.5, 0, 4.0, 0.0, 2.0, 1e-4, 3, 1 ; yz fracture
1.0, 1.0, 0, 4.0, 0.0, 2.0, 1e-4, 3, 1 ; yz fracture
1.5, 1.5, 0, 4.0, 0.0, 2.0, 1e-4, 3, 1 ; yz fracture
2.0, 2.0, 0, 4.0, 0.0, 2.0, 1e-4, 3, 1 ; yz fracture
2.5, 2.5, 0, 4.0, 0.0, 2.0, 1e-4, 3, 1 ; yz fracture
3.0, 3.0, 0, 4.0, 0.0, 2.0, 1e-4, 3, 1 ; yz fracture
3.5, 3.5, 0, 4.0, 0.0, 2.0, 1e-4, 3, 1 ; yz fracture
4.0, 4.0, 0, 4.0, 0.0, 2.0, 1e-4, 3, 1 ; yz fracture
4.5, 4.5, 0, 4.0, 0.0, 2.0, 1e-4, 3, 1 ; yz fracture
5.0, 5.0, 0, 4.0, 0.0, 2.0, 1e-4, 3, 1 ; yz fracture
5.5, 5.5, 0, 4.0, 0.0, 2.0, 1e-4, 3, 1 ; yz fracture
6.0, 6.0, 0, 4.0, 0.0, 2.0, 1e-4, 3, 1 ; yz fracture
6.5, 6.5, 0, 4.0, 0.0, 2.0, 1e-4, 3, 1 ; yz fracture
7.0, 7.0, 0, 4.0, 0.0, 2.0, 1e-4, 3, 1 ; yz fracture
7.5, 7.5, 0, 4.0, 0.0, 2.0, 1e-4, 3, 1 ; yz fracture
8.0, 8.0, 0, 4.0, 0.0, 2.0, 1e-4, 3, 1 ; yz fracture
8.5, 8.5, 0, 4.0, 0.0, 2.0, 1e-4, 3, 1 ; yz fracture
9.0, 9.0, 0, 4.0, 0.0, 2.0, 1e-4, 3, 1 ; yz fracture
9.5, 9.5, 0, 4.0, 0.0, 2.0, 1e-4, 3, 1 ; yz fracture
0.0, 10.0, 4.0, 4.0, 0.0, 2.0, 1e-4, 2, 1 ; xz fracture
*** Group 15b: Output Grids ***
.false.
*** Group 16: Simulation control param for transport ***
.true.       ; MASSBALC
.true.       ; XTERMS (dispersion)
.false.      ; CVOLUME
.false.      ; BIOCHEM
*** Group 17: Transport Output control parameters ***
0, 0         ; KWRITHC, KPMASBC
*** Group 18: Transport parameters ***
0.09         ; Longitudinal dispersivity, AL
0.001, 0.0001  ; horizontal and vertical dispersivity
1.0          ; tortuosity
1.60         ; Soil bulk density (kg/M^3)
*** Group 19: Transport parameters for the solute ***
1            ; NSPECIES
0            ; IBAT
.false.      ; KD_RAND, not random Kd
5.18e-05     ; DIFFRAC
2.209e-04    ; CLAMDA [1/T]
0            ; NPA
0.0          ; Distribution cofficient
*** Group 20: Initial conditions ***
.false.      ; KRESTARC
.true.       ; DEFAULT_IC
0.0          ; default initial concentration
*** Group 21: Orthomin solver data ***
1.0d-30, 1.0d-10, 1.0d-25 ;residual, relative and absolute convergence
.false.      ; solver info. output, ISOLV_INFOC
.false.      ; no upstream-weighting of velocities
1.0, 1.0, 1.0  ; weighting factor for x, y, & z directions (not used)
*** Group 22: Dirichlet node data ***
.true.       ; 1st type boundary conditions
.true.       ; true if use coordinates
1,           ; number of 1st type zones
1,           ; number of concentration intervals
1.0, 0.0, 40.0  ; conc, ton, toff
5.0, 5.0, 6.0, 6.0, 0.0, 2.0 ; extent in x/y/z grid
*** Group 23: 3rd-type boundary condition ***
.false.      ; no 3rd type boundary condition
*** Group 24: Concentration at Injection Wells ***
.false.      ; there is not an injection well
*** Group 25: Fracture data for transport ***
.true.       ; there are fractures for transport problem
0.2                         ; al (dispersivity in the fractures)
0.001                       ; at
1.0                         ; retardation
0.2                         ; al (dispersivity in the fractures)
0.001                       ; at
1.0                         ; retardation
*** Group 26: Immiscible phase dissolution Data ***
.false.      ; There is no dissolution
```

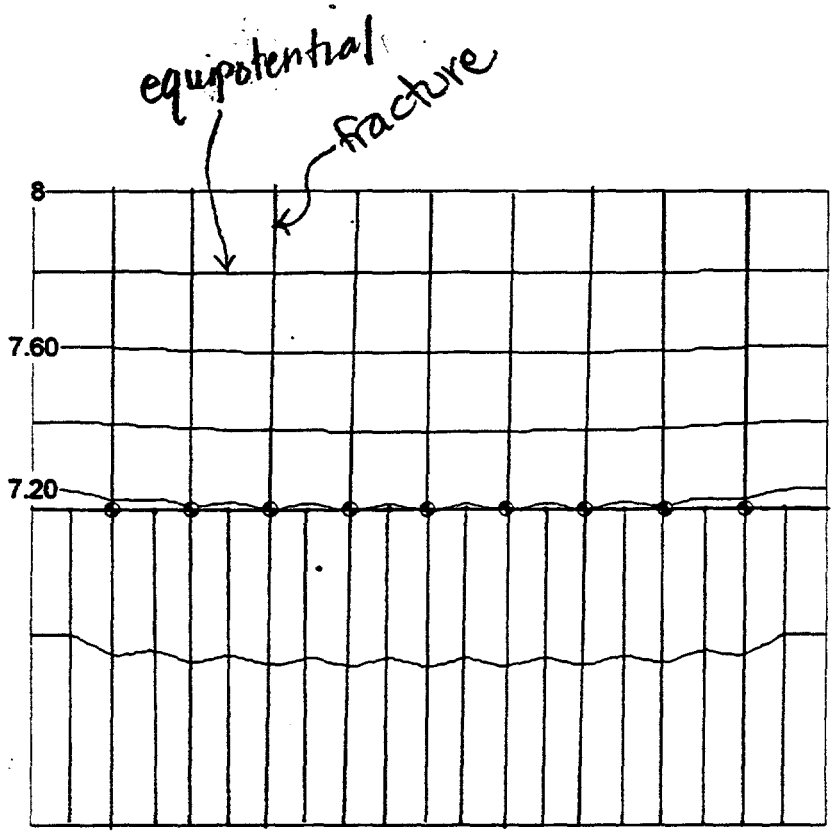

head distribution

df10

$K \rightarrow 0$
$K_{x,y,z}$

$2b = 100\mu m$

```
*** Group 1:Title ***
df11.dat :
*** Group 2:Simulation control param ***
.false.      ; true if random grid generation
.true.       ; true if finite difference for blocks or prisms
.true.       ; true if mass balance
.true.       ; true if saturated
.true.       ; true if hydraulic head defines the problem
.true.       ; true if hydraulic head is outputted
.true.       ; true if transport is performed
.true.       ; true if simulation is performed
.false.      ; true if y-axis is vertical
.true.       ; true if generate grid
*** Group 3:Output control parameters ***
0,1,1,0,0,0,0,
KPMSH,KPHEAD,KPCONC,KPVEL,KPSAT,KRESTAR,KPMASB
.true.       ; true if the above also echoes to unit 66 (ASCII)
*** Group 4:Grid data ***
.true.       ; true if generate grid from coordinates
101  NX
81,  NY
2,   NZ
.false.      ; true if the spacing is variable
10.0, 8.0, 2.0  ;xl,yl,zl (constant spacing)
*** Group 5:Physical parameters ***
.FALSE.      ; true if random k
.TRUE.       ; true if use coordinates to define property zones
1, NZONES
0.0, 10.0, 0.0, 8.0, 0.0, 2.0  ; xfrom,xto,yfrom,yto,zfrom,zto
0.02, 0.02, 1e-18, 0.00, 0.40  ;KX,KY,KZ,SS,por
*** Group 6: initial conditions ***
.false.      ; krestar
.true.       ; true if all init cond are default
8.0,         ; initial Head
*** Group 7:Output times ***
.false.      ; true if steady-state
0.0          ; tinit, time transport is started
4            ; nt_out, number of output times
21,85,360,719   ; output times (days)
0.5, 0.5     ; time weighting for flow then transport
5, 5         ; peclet crit, courant crit (when warnings occur)
.true.       ; automatic time step for transport (TCONTROL)
0.1          ; deltain, initial time step size for simulation
.false., 50.0, 1e-3 ; control_head, dhead_allowed, dhead_min_allowed
.false., 15.0, 1e-6 ; control_sat, dsat_allowed, dsat_min_allowed
.true., 15.0, 1e-6 ; control_conc, dconc_allowed, dconc_min_allowed (transient)
*** Group 8:Solver data ***
1.0d-30,1.0d-10,1.0d-30  ; RESIDUAL,RELATIVE,ABSOLUTE (ERRORS)
.false.      ; true if solver information
.true.       ; true if compute the residual
.false.      ; true if 2nd-order factorization
*** Group 9:Newton-Raphson parameters***
*** Group 10:Dirichlet nodes ***
.true.       ; true if dirichlet nodes
.true.       ; true if use coordinates to define 1st-type zones
2,           ; number of zones
0.0, 10.0, 8.0, 8.0, 0.0, 2.0 ; up hill boundary ("North" of 4-11)
1,           ; number of time intervals
.false.      ; function for head
8.0, -1.0, 1.0e10, ; prescribed head, time on, time off
0.0, 10.0, 0.0, 0.0, 0.0, 2.0 ; down hill boundary ("South" of 4-7)
1,           ; number of time intervals
.false.      ; function for head
6.8, -1.0, 1.0e10   ; prescribed head, time on, time off
*** Group 11: Second-type b.c. ***
.false.      ; true if 2nd-type b.c.
*** Group 12: Seepage face data ***
.False.
*** Group 13:Source/sink ***
.false.      ; true if inj/with wells
*** Group 14: Observ. well ***
.false.      ; true if observ wells
*** Group 15: Fracture data ***
.true.       ; true if fractured
17                          ; nfrac_temp - number of fractures
1000.0                      ; fluid density (rho)
113.0                       ; visc
7.32e10                     ; grav.
2                           ; number of different sets of fractures
.true.                      ; the current set refers to fractures
0.0                         ; spec. storage within the fracture
.true.                      ; the current set refers to fractures
0.0                         ; spec. storage within the fracture
1.0,  1.0, 0.0, 4.0, 0.0, 2.0, 1e-4, 3, 1 ; yz fracture
2.0,  2.0, 0.0, 4.0, 0.0, 2.0, 1e-4, 3, 1 ; yz fracture
3.0,  3.0, 0.0, 4.0, 0.0, 2.0, 1e-4, 3, 1 ; yz fracture
4.0,  4.0, 0.0, 4.0, 0.0, 2.0, 1e-4, 3, 1 ; yz fracture
5.0,  5.0, 0.0, 4.0, 0.0, 2.0, 1e-4, 3, 1 ; yz fracture
6.0,  6.0, 0.0, 4.0, 0.0, 2.0, 1e-4, 3, 1 ; yz fracture
7.0,  7.0, 0.0, 4.0, 0.0, 2.0, 1e-4, 3, 1 ; yz fracture
8.0,  8.0, 0.0, 4.0, 0.0, 2.0, 1e-4, 3, 1 ; yz fracture
9.0,  9.0, 0.0, 4.0, 0.0, 2.0, 1e-4, 3, 1 ; yz fracture
1.4,  1.4, 4.0, 8.0, 0.0, 2.0, 1e-4, 3, 1 ; yz fracture
2.8,  2.8, 4.0, 8.0, 0.0, 2.0, 1e-4, 3, 1 ; yz fracture
4.2,  4.2, 4.0, 8.0, 0.0, 2.0, 1e-4, 3, 1 ; yz fracture
5.6,  5.6, 4.0, 8.0, 0.0, 2.0, 1e-4, 3, 1 ; yz fracture
7.0,  7.0, 4.0, 8.0, 0.0, 2.0, 1e-4, 3, 1 ; yz fracture
8.4,  8.4, 4.0, 8.0, 0.0, 2.0, 1e-4, 3, 1 ; yz fracture
9.8,  9.8, 4.0, 8.0, 0.0, 2.0, 1e-4, 3, 1 ; yz fracture
0.0, 10.0, 4.0, 4.0, 0.0, 2.0, 1e-4, 2, 1 ; xz fracture
*** Group 15b: Output Grids ***
.false.
*** Group 16: Simulation control param for transport ***
.true.       ; MASSBALC
.true.       ; XTERMS (dispersion)
.false.      ; CVOLUME
.false.      ; BIOCHEM
*** Group 17: Transport Output control parameters ***
0, 0         ; KWRITHC, KPMASBC
*** Group 18: Transport parameters ***
0.15         ; Longitudinal dispersivity, AL
0.0, 0.0     ; horizontal and vertical dispersivity
1.0          ; tortuosity
1.60         ; Soil bulk density (kg/M^3)
*** Group 19: Transport parameters for the solute ***
1            ; NSPECIES
0            ; IBAT
.false.      ; KD_RAND, not random Kd
5.18e-05     ; DIFFRAC
2.209e-04    ; CLAMDA [1/T]
0            ; NPA
0.0          ; Distribution cofficient
*** Group 20: Initial conditions ***
.false.      ; KRESTARC
.true.       ; DEFAULT_IC
0.0          ; default initial concentration
*** Group 21: Orthomin solver data ***
1.0d-30, 1.0d-10, 1.0d-25 ;residual, relative and absolute convergence
.false.      ; solver info. output, ISOLV_INFOC
.false.      ; no upstream-weighting of velocities
1.0, 1.0, 1.0   ; weighting factor for x, y, & z directions (not used)
*** Group 22: Dirichlet node data ***
.true.       ; 1st type boundary conditions
.true.       ; true if use coordinates
1,           ; number of 1st type zones
1,           ; number of concentration intervals
1.0, 0.0, 40.0  ; conc, ton, toff
5.0, 5.0, 6.0, 6.0, 0.0, 2.0 ; extent in x/y/z grid
*** Group 23: 3rd-type boundary condition ***
.false.      ; no 3rd type boundary condition
*** Group 24: Concentration at Injection Wells ***
.false.      ; there is not an injection well
*** Group 25: Fracture data for transport ***
.true.       ; there are fractures for transport problem
0.2                         ; al (dispersivity in the fractures)
0.0                         ; at
1.0                         ; retardation
0.2                         ; al (dispersivity in the fractures)
0.0                         ; at
1.0                         ; retardation
*** Group 26: Immiscible phase dissolution Data ***
.false.      ; There is no dissolution
```

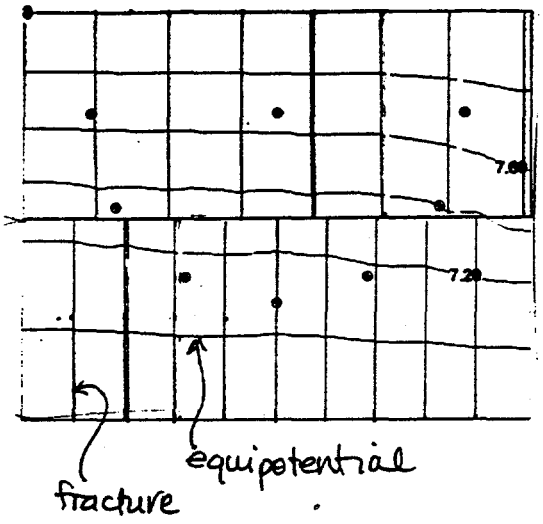

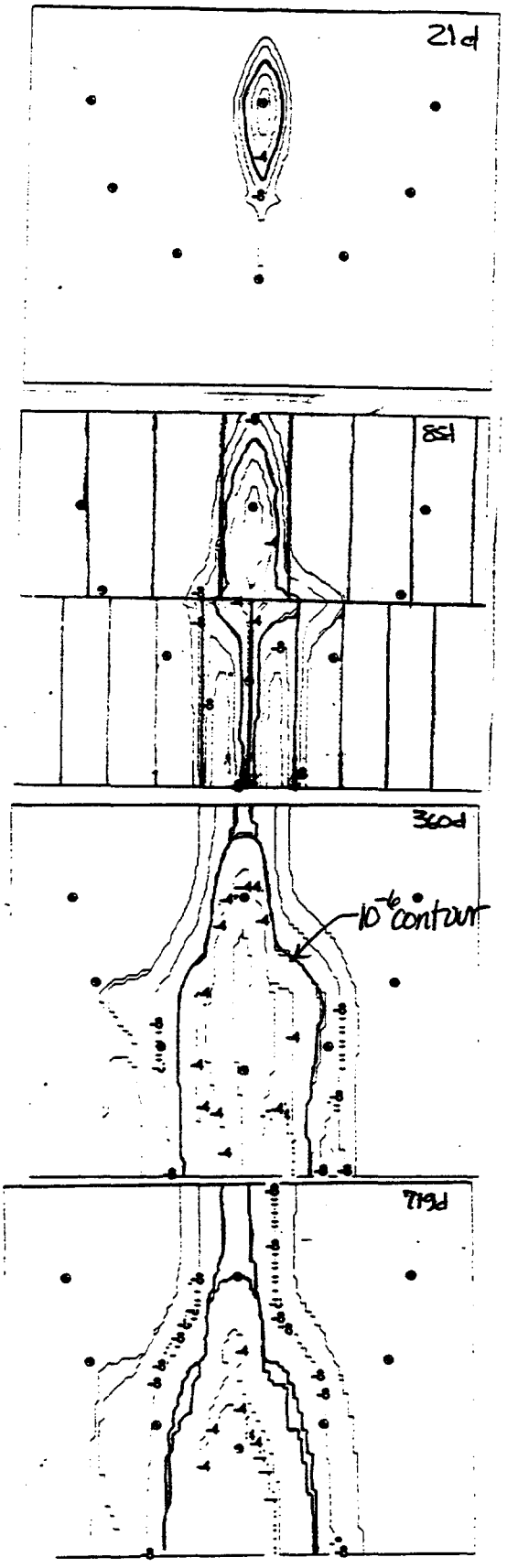

$K_{x,y} = 0.02$ Md

$2b = 100\,\mu m$

$\alpha_L = 0.15$ m
$\alpha_T = 0$ } matrix

$\alpha_{L,f} = 0.2$ m
$\alpha_{T,f} = 0$ } fracture

```
*** Group 1:Title ***
df12.dat :
*** Group 2:Simulation control param ***
.false.      ; true if random grid generation
.true.       ; true if finite difference for blocks or prisms
.true.       ; true if mass balance
.true.       ; true if saturated
.true.       ; true if hydraulic head defines the problem
.true.       ; true if hydraulic head is outputted
.true.       ; true if transport is performed
.true.       ; true if simulation is performed
.false.      ; true if y-axis is vertical
.true.       ; true if generate grid
*** Group 3:Output control parameters ***
0,1,1,0,0,0,0,
KPMSH,KPHEAD,KPCONC,KPVEL,KPSAT,KRESTAR,KPMASB
.true.       ; true if the above also echoes to unit 66 (ASCII)
*** Group 4:Grid data ***
.true.       ; true if generate grid from coordinates
101 NX
81, NY
2, NZ
.false.      ; true if the spacing is variable
10.0, 8.0, 2.0  ;xl,yl,zl (constant spacing)
*** Group 5:Physical parameters ***
.FALSE.      ; true if random k
.TRUE.       ; true if use coordinates to define property zones
1, NZONES
0.0, 10.0, 0.0, 8.0, 0.0, 2.0  ; xfrom,xto,yfrom,yto,zfrom,zto
0.02, 0.02, 1e-18, 0.00, 0.40  ;KX,KY,KZ,SS,por
*** Group 6: initial conditions ***
.false.      ; krestar
.true.       ; true if all init cond are default
8.0,         ; initial Head
*** Group 7:Output times ***
.false.      ; true if steady-state
0.0          ; tinit, time transport is started
4            ; nt_out, number of output times
21,85,360,719   ; output times (days)
0.5, 0.5     ; time weighting for flow then transport
5, 5         ; peclet crit, courant crit (when warnings occur)
.true.       ; automatic time step for transport (TCONTROL)
0.1          ; deltain, initial time step size for simulation
.false., 50.0, 1e-3 ; control_head, dhead_allowed, dhead_min_allowed
.false., 15.0, 1e-6 ; control_sat, dsat_allowed, dsat_min_allowed
.true., 15.0, 1e-6 ; control_conc, dconc_allowed, dconc_min_allowed (transient)
*** Group 8:Solver data ***
1.0d-30,1.0d-10,1.0d-30  ; RESIDUAL,RELATIVE,ABSOLUTE (ERRORS)
.false.      ; true if solver information
.true.       ; true if compute the residual
.false.      ; true if 2nd-order factorization
*** Group 9:Newton-Raphson parameters***
*** Group 10:Dirichlet nodes ***
.true.       ; true if dirichlet nodes
.true.       ; true if use coordinates to define 1st-type zones
2,           ; number of zones
0.0, 10.0, 8.0, 8.0, 0.0, 2.0 ; up hill boundary ("North" of 4-11)
1,           ; number of time intervals
.false.      ; function for head
8.0, -1.0, 1.0e10, ; prescribed head, time on, time off
0.0, 10.0, 0.0, 0.0, 0.0, 2.0 ; down hill boundary ("South" of 4-7)
1,           ; number of time intervals
.false.      ; function for head
6.8, -1.0, 1.0e10   ; prescribed head, time on, time off
*** Group 11: Second-type b.c. ***
.false.      ; true if 2nd-type b.c.
*** Group 12: Seepage face data ***
.False.
*** Group 13:Source/sink ***
.false.      ; true if inj/with wells
*** Group 14: Observ. well ***
.false.      ; true if observ wells
*** Group 15: Fracture data ***
.true.       ; true if fractured
3                          ; nfrac_temp - number of fractures
1000.0                     ; fluid density (rho)
113.0                      ; visc
7.32e10                    ; grav.
2                          ; number of different sets of fractures
.true.                     ; the current set refers to fractures
0.0                        ; spec. storage within the fracture
.true.                     ; the current set refers to fractures
0.0                        ; spec. storage within the fracture
5.0, 5.0, 4.0, 8.0, 0.0, 2.0, 1e-4, 3, 1 ; yz fracture
6.0, 6.0, 0.0, 4.0, 0.0, 2.0, 1e-4, 3, 1 ; yz fracture
0.0, 10.0, 4.0, 4.0, 0.0, 2.0, 1e-4, 2, 1 ; xz fracture
*** Group 15b: Output Grids ***
.false.
*** Group 16: Simulation control param for transport ***
.true.       ; MASSBALC
.true.       ; XTERMS (dispersion)
.false.      ; CVOLUME
.false.      ; BIOCHEM
*** Group 17: Transport Output control parameters ***
0, 0         ; KWRITHC, KPMASBC
*** Group 18: Transport parameters ***
0.15         ; Longitudinal dispersivity, AL
0.0, 0.      ; horizontal and vertical dispersivity
1.0          ; tortuosity
1.60         ; Soil bulk density (kg/M^3)
*** Group 19: Transport parameters for the solute ***
1            ; NSPECIES
0            ; IBAT
.false.      ; KD_RAND, not random Kd
5.18e-05     ; DIFFRAC
2.209e-04    ; CLAMDA [1/T]
0            ; NPA
0.0          ; Distribution cofficient
*** Group 20: Initial conditions ***
.false.      ; KRESTARC
.true.       ; DEFAULT_IC
0.0          ; default initial concentration
*** Group 21: Orthomin solver data ***
1.0d-30, 1.0d-10, 1.0d-25 ;residual, relative and absolute convergence
.false.      ; solver info. output, ISOLV_INFOC
.false.      ; no upstream-weighting of velocities
1.0, 1.0, 1.0   ; weighting factor for x, y, & z directions (not used)
*** Group 22: Dirichlet node data ***
.true.       ; 1st type boundary conditions
.true.       ; true if use coordinates
1,           ; number of 1st type zones
1,           ; number of concentration intervals
1.0, 0.0, 40.0  ; conc, ton, toff
5.0, 5.0, 6.0, 6.0, 0.0, 2.0 ; extent in x/y/z grid
*** Group 23: 3rd-type boundary condition ***
.false.      ; no 3rd type boundary condition
*** Group 24: Concentration at Injection Wells ***
.false.      ; there is not an injection well
*** Group 25: Fracture data for transport ***
.true.       ; there are fractures for transport problem
0.2                        ; al (dispersivity in the fractures)
0.0                        ; at
1.0                        ; retardation
0.2                        ; al (dispersivity in the fractures)
0.0                        ; at
1.0                        ; retardation
*** Group 26: Immiscible phase dissolution Data ***
.false.      ; There is no dissolution
```

df12

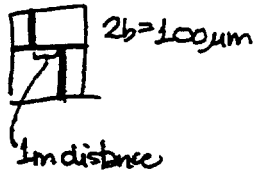

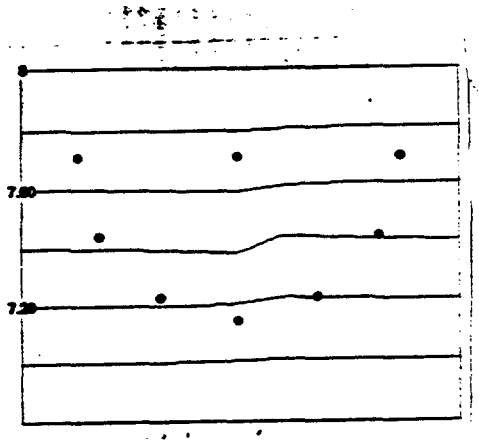

head distribution

$K_{x,y} = 0.02 M/d$

$\alpha_L = 0.15m$ } Matrix
$\alpha_T = 0$ }

$\alpha_{L,f} = 0.2m$ } fracture
$\alpha_{T,f} = 0$ }

$2b = 100\mu m$

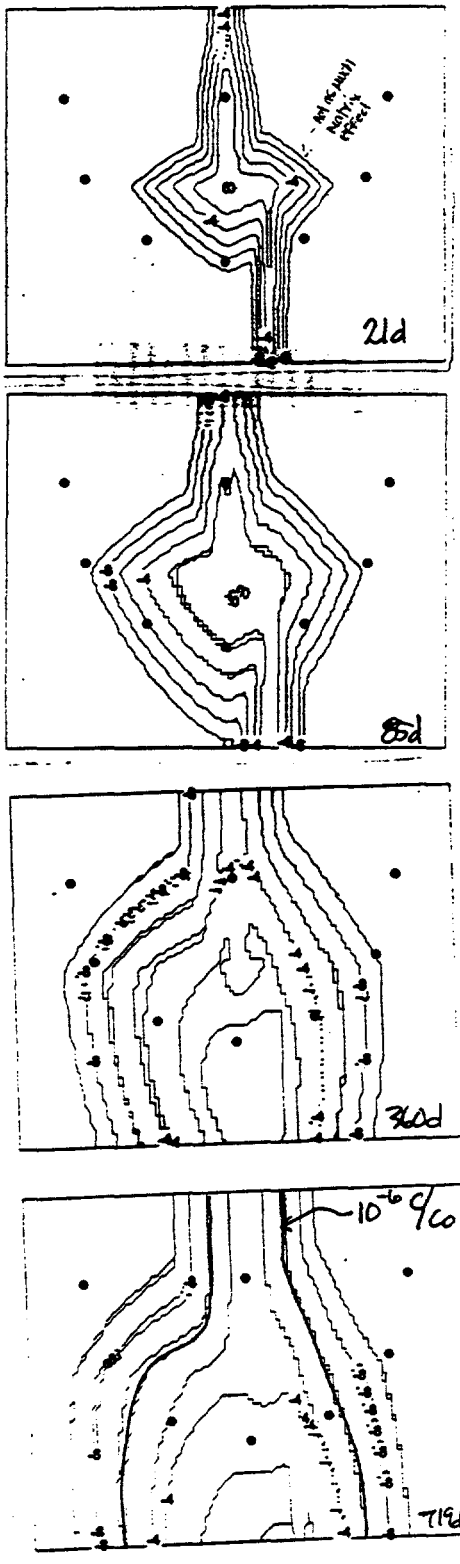

```
*** Group 1:Title ***
df13.dat :
*** Group 2:Simulation control param ***
.false.      ; true if random grid generation
.true.       ; true if finite difference for blocks or prisms
.true.       ; true if mass balance
.true.       ; true if saturated
.true.       ; true if hydraulic head defines the problem
.true.       ; true if hydraulic head is outputted
.true.       ; true if transport is performed
.true.       ; true if simulation is performed
.false.      ; true if y-axis is vertical
.true.       ; true if generate grid
*** Group 3:Output control parameters ***
0,1,1,0,0,0,0,
KPMSH,KPHEAD,KPCONC,KPVEL,KPSAT,KRESTAR,KPMASB
.true.       ; true if the above also echoes to unit 66 (ASCII)
*** Group 4:Grid data ***
.true.       ; true if generate grid from coordinates
101  NX
81,  NY
2,  NZ
.false.      ; true if the spacing is variable
10.0, 8.0, 2.0  ;xl,yl,zl (constant spacing)
*** Group 5:Physical parameters ***
.FALSE.      ; true if random k
.TRUE.       ; true if use coordinates to define property zones
1, NZONES
0.0, 10.0, 0.0, 8.0, 0.0, 2.0  ; xfrom,xto,yfrom,yto,zfrom,zto
0.02, 0.02, 1e-18, 0.00, 0.40  ;KX,KY,KZ,SS,por
*** Group 6: initial conditions ***
.false.      ; krestar
.true.       ; true if all init cond are default
8.0,         ; initial Head
*** Group 7:Output times ***
.false.      ; true if steady-state
0.0          ; tinit, time transport is started
4            ; nt_out, number of output times
21,85,360,719   ; output times (days)
0.5, 0.5     ; time weighting for flow then transport
5, 5         ; peclet crit, courant crit (when warnings occur)
.true.       ; automatic time step for transport (TCONTROL)
0.1          ; deltain, initial time step size for simulation
.false., 50.0, 1e-3 ; control_head, dhead_allowed, dhead_min_allowed
.false., 15.0, 1e-6 ; control_sat, dsat_allowed, dsat_min_allowed
.true., 15.0, 1e-6 ; control_conc, dconc_allowed, dconc_min_allowed (transient)
*** Group 8:Solver data ***
1.0d-30,1.0d-10,1.0d-30  ; RESIDUAL,RELATIVE,ABSOLUTE (ERRORS)
.false.      ; true if solver information
.true.       ; true if compute the residual
.false.      ; true if 2nd-order factorization
*** Group 9:Newton-Raphson parameters***
*** Group 10:Dirichlet nodes ***
.true.       ; true if dirichlet nodes
.true.       ; true if use coordinates to define 1st-type zones
2,           ; number of zones
0.0, 10.0, 8.0, 8.0, 0.0, 2.0 ; up hill boundary ("North" of 4-11)
1,           ; number of time intervals
.false.      ; function for head
8.0, -1.0, 1.0e10, ; prescribed head, time on, time off
0,0, 10.0, 0.0, 0.0, 0.0, 2.0 ; down hill boundary ("South" of 4-7)
1,           ; number of time intervals
.false.      ; function for head
6.8, -1.0, 1.0e10   ; prescribed head, time on, time off
*** Group 11: Second-type b.c. ***
.false.      ; true if 2nd-type b.c.
*** Group 12: Seepage face data ***
.False.
*** Group 13:Source/sink ***
.false.      ; true if inj/with wells
*** Group 14: Observ. well ***
.false.      ; true if observ wells
*** Group 15: Fracture data ***
.true.       ; true if fractured
3                          ; nfrac_temp - number of fractures
1000.0                     ; fluid density (rho)
113.0                      ; visc
7.32e10                    ; grav.
2                          ; number of different sets of fractures
.true.                     ; the current set refers to fractures
0.0                        ; spec. storage within the fracture
.true.                     ; the current set refers to fractures
0.0                        ; spec. storage within the fracture
5.0, 5.0, 4.0, 8.0, 0.0, 2.0, 1e-4, 3, 1 ; yz fracture
5.5, 5.5, 0.0, 4.0, 0.0, 2.0, 1e-4, 3, 1 ; yz fracture
0.0, 10.0, 4.0, 4.0, 0.0, 2.0, 1e-4, 2, 1 ; xz fracture
*** Group 15b: Output Grids ***
.false.
*** Group 16: Simulation control param for transport ***
.true.       ; MASSBALC
.true.       ; XTERMS (dispersion)
.false.      ; CVOLUME
.false.      ; BIOCHEM
*** Group 17: Transport Output control parameters ***
0, 0         ; KWRITHC, KPMASBC
*** Group 18: Transport parameters ***
0.15         ; Longitudinal dispersivity, AL
0.0, 0.      ; horizontal and vertical dispersivity
1.0          ; tortuosity
1.60         ; Soil bulk density (kg/M^3)
*** Group 19: Transport parameters for the solute ***
1            ; NSPECIES
0            ; IBAT
.false.      ; KD_RAND, not random Kd
5.18e-05     ; DIFFRAC
2.209e-04    ; CLAMDA [1/T]
0            ; NPA
0.0          ; Distribution cofficient
*** Group 20: Initial conditions ***
.false.      ; KRESTARC
.true.       ; DEFAULT_IC
0.0          ; default initial concentration
*** Group 21: Orthomin solver data ***
1.0d-30, 1.0d-10, 1.0d-25 ;residual, relative and absolute convergence
.false.      ; solver info. output, ISOLV_INFOC
.false.      ; no upstream-weighting of velocities
1.0, 1.0, 1.0  ; weighting factor for x, y, & z directions (not used)
*** Group 22: Dirichlet node data ***
.true.       ; 1st type boundary conditions
.true.       ; true if use coordinates
1,           ; number of 1st type zones
1,           ; number of concentration intervals
1.0, 0.0, 40.0  ; conc, ton, toff
5.0, 5.0, 6.0, 6.0, 0.0, 2.0 ; extent in x/y/z grid
*** Group 23: 3rd-type boundary condition ***
.false.      ; no 3rd type boundary condition
*** Group 24: Concentration at Injection Wells ***
.false.      ; there is not an injection well
*** Group 25: Fracture data for transport ***
.true.       ; there are fractures for transport problem
0.2                        ; al (dispersivity in the fractures)
0.0                        ; at
1.0                        ; retardation
0.2                        ; al (dispersivity in the fractures)
0.0                        ; at
1.0                        ; retardation
*** Group 26: Immiscible phase dissolution Data ***
.false.      ; There is no dissolution
```

df13

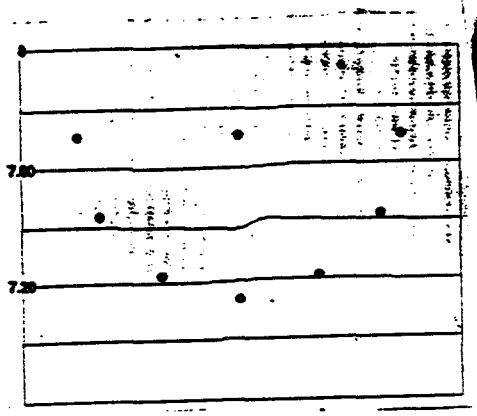

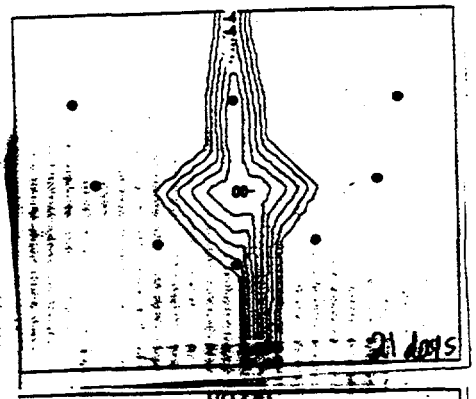

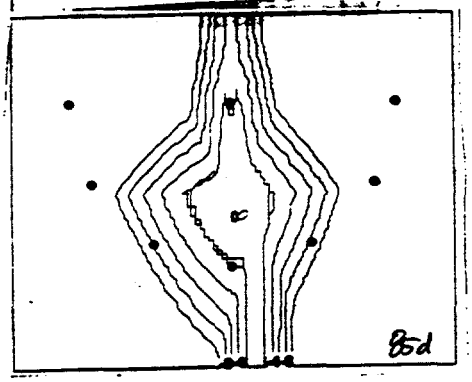

Y_{2m} distance

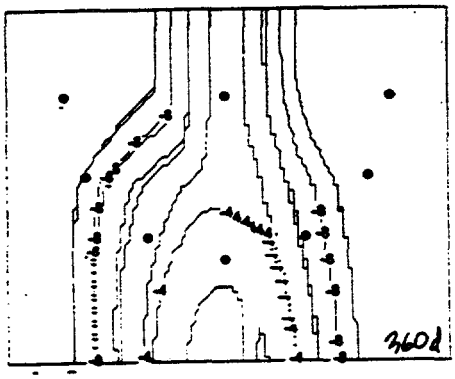

$K_{xy} = 0.02\ m/d$

$\alpha_L = 0.15\ m$ } matrix

$\alpha_T = 0$ }

$d_{L,f} = 0.2\ m$ } fracture

$\alpha_{T,f} = 0$ }

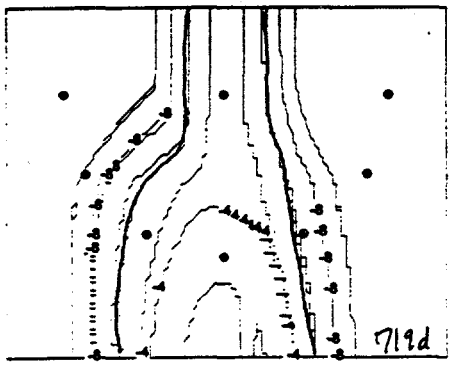

$2b = 100\ \mu m$

```
*** Group 1:Title ***
df14.dat :
*** Group 2:Simulation control param ***
.false.      ; true if random grid generation
.true.       ; true if finite difference for blocks or prisms
.true.       ; true if mass balance
.true.       ; true if saturated
.true.       ; true if hydraulic head defines the problem
.true.       ; true if hydraulic head is outputted
.true.       ; true if transport is performed
.true.       ; true if simulation is performed
.false.      ; true if y-axis is vertical
.true.       ; true if generate grid
*** Group 3:Output control parameters ***
0,1,1,0,0,0,0,
KPMSH,KPHEAD,KPCONC,KPVEL,KPSAT,KRESTAR,KPMASB
.true.       ; true if the above also echoes to unit 66 (ASCII)
*** Group 4:Grid data ***
.true.       ; true if generate grid from coordinates
101  NX
81,  NY
2,  NZ
.false.      ; true if the spacing is variable
10.0, 8.0, 2.0  ;xl,yl,zl (constant spacing)
*** Group 5:Physical parameters ***
.FALSE.      ; true if random k
.TRUE.       ; true if use coordinates to define property zones
1, NZONES
0.0, 10.0, 0.0, 8.0, 0.0, 2.0  ; xfrom,xto,yfrom,yto,zfrom,zto
0.02, 0.02, 1e-18, 0.00, 0.40  ;KX,KY,KZ,SS,por
*** Group 6: initial conditions ***
.false.      ; krestar
.true.       ; true if all init cond are default
8.0,         ; initial Head
*** Group 7:Output times ***
.false.      ; true if steady-state
0.0          ; tinit, time transport is started
4            ; nt_out, number of output times
21,85,360,719   ; output times (days)
0.5, 0.5     ; time weighting for flow then transport
5, 5         ; peclet crit, courant crit (when warnings occur)
.true.       ; automatic time step for transport (TCONTROL)
0.1          ; deltain, initial time step size for simulation
.false., 50.0, 1e-3 ; control_head, dhead_allowed, dhead_min_allowed
.false., 15.0, 1e-6 ; control_sat, dsat_allowed, dsat_min_allowed
.true., 15.0, 1e-6 ; control_conc, dconc_allowed, dconc_min_allowed (transient)
*** Group 8:Solver data ***
1.0d-30,1.0d-10,1.0d-30  ; RESIDUAL,RELATIVE,ABSOLUTE (ERRORS)
.false.      ; true if solver information
.true.       ; true if compute the residual
.false.      ; true if 2nd-order factorization
*** Group 9:Newton-Raphson parameters***
*** Group 10:Dirichlet nodes ***
.true.       ; true if dirichlet nodes
.true.       ; true if use coordinates to define 1st-type zones
2,           ; number of zones
0.0, 10.0, 8.0, 8.0, 0.0, 2.0 ; up hill boundary ("North" of 4-11)
1,           ; number of time intervals
.false.      ; function for head
8.0, -1.0, 1.0e10, ; prescribed head, time on, time off
0.0, 10.0, 0.0, 0.0, 0.0, 2.0 ; down hill boundary ("South" of 4-7)
1,           ; number of time intervals
.false.      ; function for head
6.8, -1.0, 1.0e10   ; prescribed head, time on, time off
*** Group 11: Second-type b.c. ***
.false.      ; true if 2nd-type b.c.
*** Group 12: Seepage face data ***
.False.
*** Group 13:Source/sink ***
.false.      ; true if inj/with wells
*** Group 14: Observ. well ***
.false.      ; true if observ wells
*** Group 15: Fracture data ***
.true.       ; true if fractured
3                          ; nfrac_temp - number of fractures
1000.0                     ; fluid density (rho)
113.0                      ; visc
7.32e10                    ; grav.
2                          ; number of different sets of fractures
.true.                     ; the current set refers to fractures
0.0                        ; spec. storage within the fracture
.true.                     ; the current set refers to fractures
0.0                        ; spec. storage within the fracture
5.0, 5.0, 4.0, 8.0, 0.0, 2.0, 1e-4, 3, 1 ; yz fracture
5.2, 5.2, 0.0, 4.0, 0.0, 2.0, 1e-4, 3, 1 ; yz fracture
0.0, 10.0, 4.0, 4.0, 0.0, 2.0, 1e-4, 2, 1 ; xz fracture
*** Group 15b: Output Grids ***
.false.
*** Group 16: Simulation control param for transport ***
.true.       ; MASSBALC
.true.       ; XTERMS (dispersion)
.false.      ; CVOLUME
.false.      ; BIOCHEM
*** Group 17: Transport Output control parameters ***
0, 0         ; KWRITHC, KPMASBC
*** Group 18: Transport parameters ***
0.15         ; Longitudinal dispersivity, AL
0.0, 0.      ; horizontal and vertical dispersivity
1.0          ; tortuosity
1.60         ; Soil bulk density (kg/M^3)
*** Group 19: Transport parameters for the solute ***
1            ; NSPECIES
0            ; IBAT
.false.      ; KD_RAND, not random Kd
5.18e-05     ; DIFFRAC
2.209e-04    ; CLAMDA [1/T]
0            ; NPA
0.0          ; Distribution cofficient
*** Group 20: Initial conditions ***
.false.      ; KRESTARC
.true.       ; DEFAULT_IC
0.0          ; default initial concentration
*** Group 21: Orthomin solver data ***
1.0d-30, 1.0d-10, 1.0d-25 ;residual, relative and absolute convergence
.false.      ; solver info. output, ISOLV_INFOC
.false.      ; no upstream-weighting of velocities
1.0, 1.0, 1.0  ; weighting factor for x, y, & z directions (not used)
*** Group 22: Dirichlet node data ***
.true.       ; 1st type boundary conditions
.true.       ; true if use coordinates
1,           ; number of 1st type zones
1,           ; number of concentration intervals
1.0, 0.0, 40.0  ; conc, ton, toff
5.0, 5.0, 6.0, 6.0, 0.0, 2.0 ; extent in x/y/z grid
*** Group 23: 3rd-type boundary condition ***
.false.      ; no 3rd type boundary condition
*** Group 24: Concentration at Injection Wells ***
.false.      ; there is not an injection well
*** Group 25: Fracture data for transport ***
.true.       ; there are fractures for transport problem
0.2                        ; al (dispersivity in the fractures)
0.0                        ; at
1.0                        ; retardation
0.2                        ; al (dispersivity in the fractures)
0.0                        ; at
1.0                        ; retardation
*** Group 26: Immiscible phase dissolution Data ***
.false.      ; There is no dissolution
```

dF14.

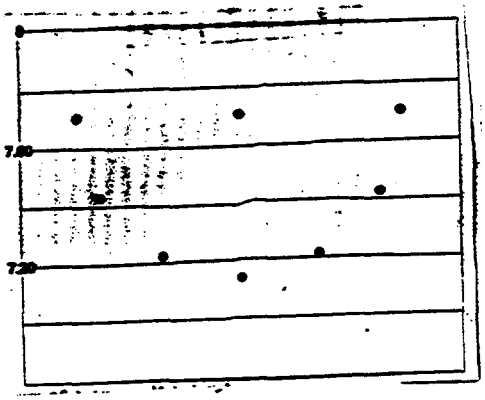

head distribution

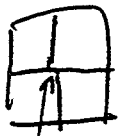

0.2m distance

$K_{x,y} = 0.02 m/d$

$\alpha_L = 0.15m$ } matrix
$\alpha_T = 0$

$\alpha_{L,f} = 0.2m$ } fracture
$\alpha_{T,f} = 0$

$2b = 100\mu m$

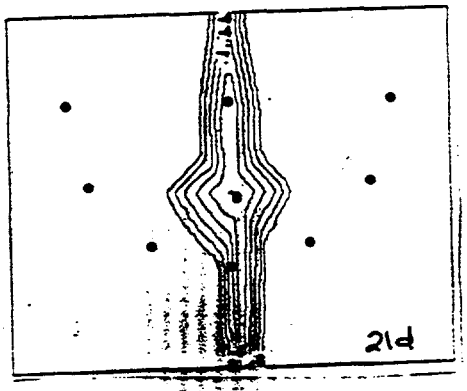

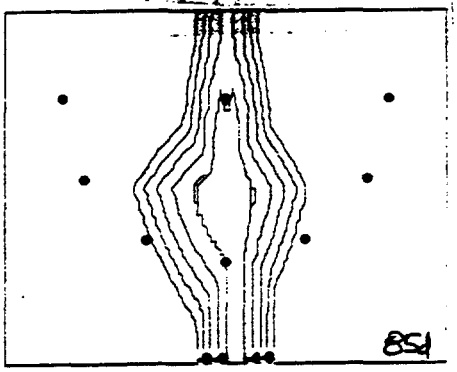

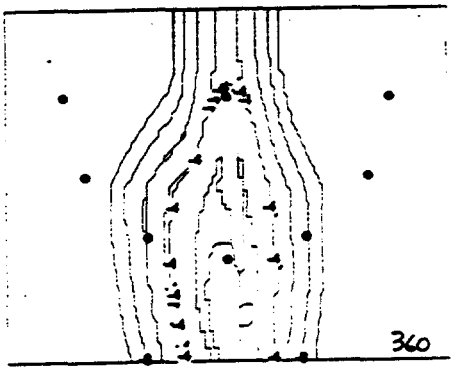

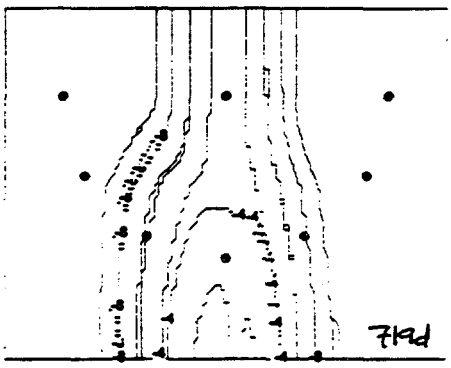

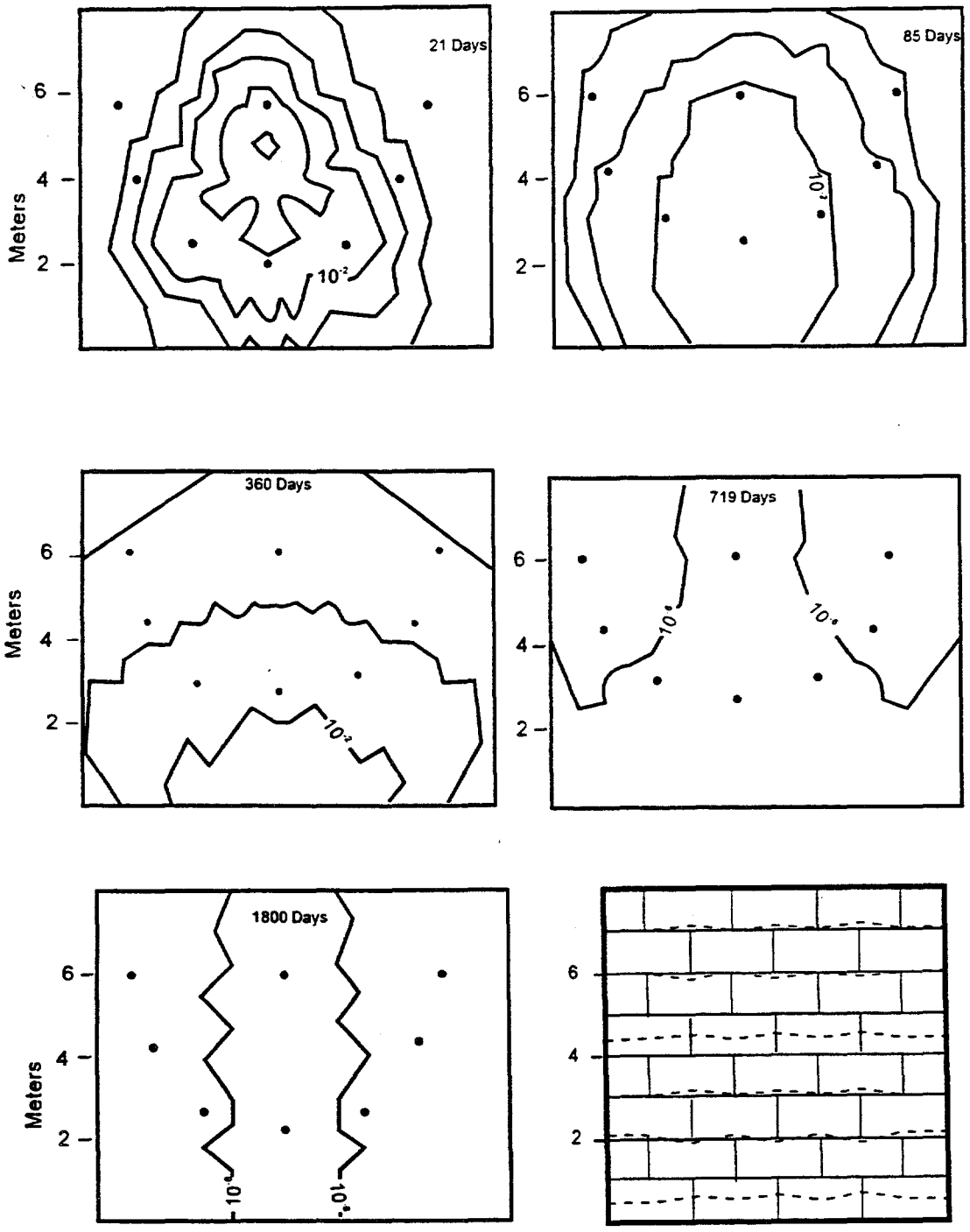

DF-EPM Simulation results using V=0.01 M/d, α_L=0.8m, α_T=0 and $\bar{a}_b$=150μm

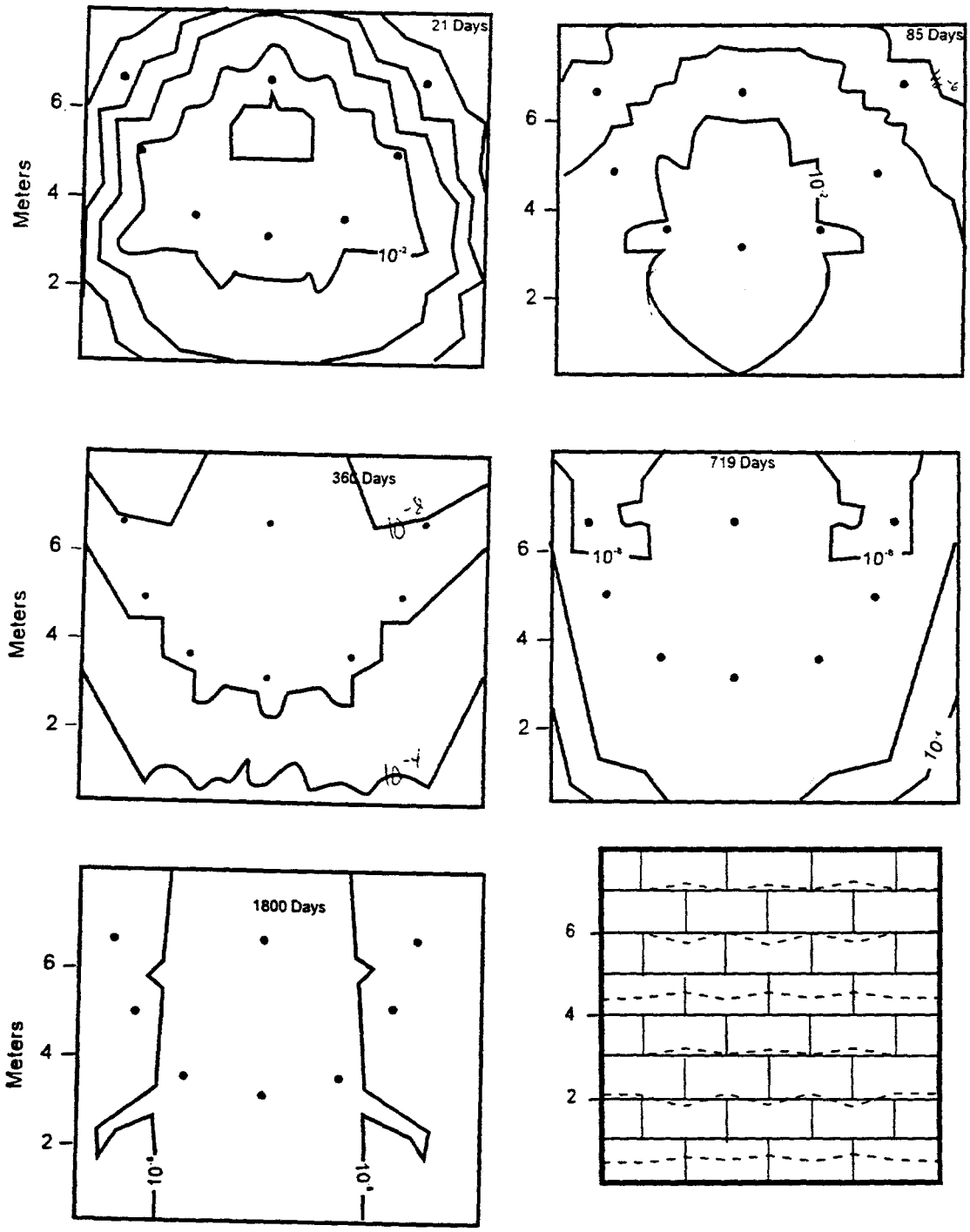

OF-EPM Simulation results using V=0.01 m/d, d_L=0.8, α_T=0, 2b=250 μm

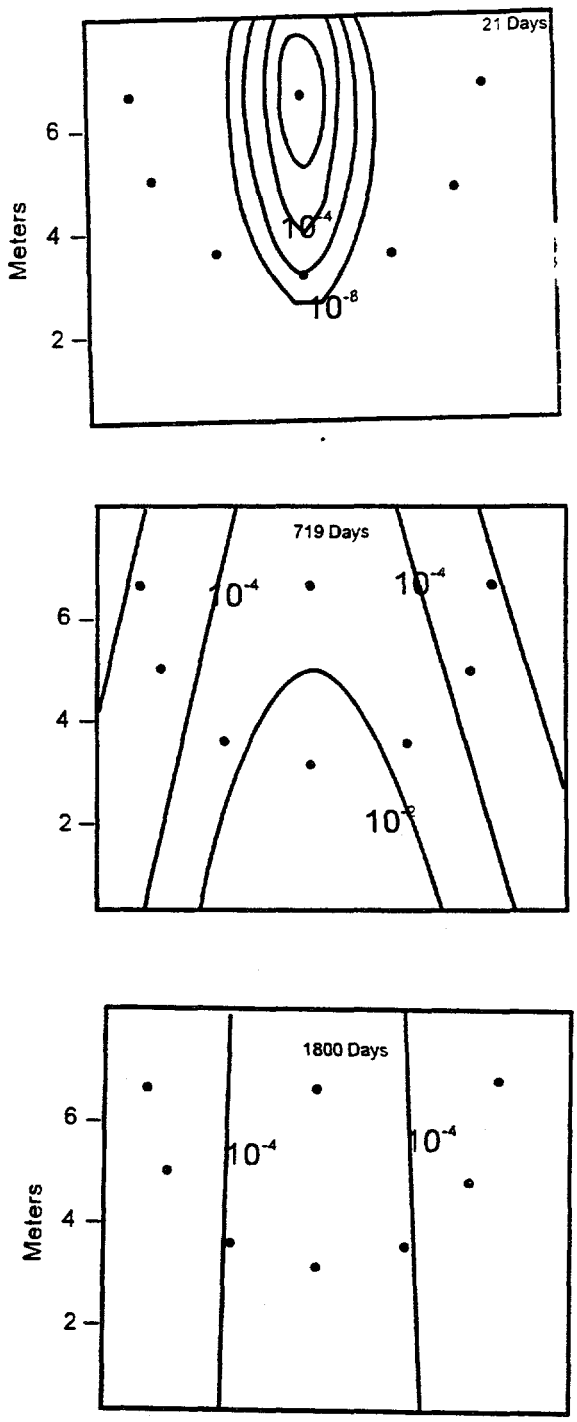

Best-Fit EPM Simulation with $V=0.01^{M}/d$ $\alpha_L=0.8m$ and $\alpha_T=0.08m$ (supplement to Figure 2.5)

VITA

Paige L. Stafford was born and raised in southeastern Wisconsin, and graduated from High School in 1982. Directly after high school, she joined the United States Army where she spent four years with Signal Corps Intelligence. Two of those years were spent in Augsburg, Germany. From 1987-1988, she attended Radford University, in Radford, Virginia, but transferred to the University of Wisconsin, Milwaukee in 1988, where she graduated with a Bachelor's of Science degree in Geology in 1992. In 1993, she entered the Master's program in Geology at the University of Tennessee, Knoxville.

While in the U.S. Army, Paige Stafford worked with communications equipment in both tactival and stategic environments. As an undergraduate, Paige Stafford worked for temporary employment agencies as an executive and legal secretary. She also worked as a research assistant for the Geology Deparment at the University of Wisconsin, Milwaukee. As a graduate student, she worked as a teaching and research assistant for the Department of Geological Sciences at the University of Tennessee, Knoxville. She also worked part-time at Oak Ridge National Laboratory, Oak Ridge, Tennessee, in the Environmental Sciences Division as a research assistant.

INTERNAL DISTRIBUTION

1. F. A. Anderson
2. L. V. Asplund
3. L. D. Bates
4. H. L. Boston
5. R. B. Clapp
6. R. B. Cook
7. T. K. Cothron
8. J. H. Cushman
9. V. H. Dale
10. A. F. Diefendorf
11. R. B. Dreier
12. T. O. Early
13. N. T. Edwards
14. D. E. Fowler
15. C. W. Gehrs
16. C. S. Haase
17. S. G. Hildebrand
18. D. D. Huff
19. G. K. Jacobs
20. W. K. Jago
21. P. Kanciruk
22. R. H. Ketelle
23. H. L. King
24. A. J. Kuhaida
25. A. Laase
26. J. M. Loar
27. G. R. Moline
28. C. A. Motley
29. R. S. Poling
30 J. Powers
31. D. E. Reichle
32. C. T. Rightmire
33. W. E. Sanford
34. F. E. Sharples
35. D. S. Shriner
36 P. L. Stafford
37. S. H. Stow
38. L. E. Toran
39. D. B. Watson
40. S. H. Welch
41. S. L. Winters
42 M. W. Yambert
43. T. F. Zondlo
44. Central Research Library
45-59. ESD Library
60-61. Laboratory Records Dept.
62. Laboratory Records, ORNL-RC
63. ORNL Patent Section
64. ORNL Y-12 Technical Library

EXTERNAL DISTRIBUTION

65. Robert Benfield, Tennessee Department of Environmental Conservation, U.S. Department of Energy Oversite Office, 761 Emory Valley Road, Oak Ridge, TN 37831

66. G. W. Bodenstein, U.S. Department of Energy, Oak Ridge Operations Office, IRC Building, P. O. Box 2001, Oak Ridge, TN 37838-8541

67. M. Broido, Acting Director, Environmental Sciences Division, Department of Energy, 19901 Germantown Road, Germantown, MD 20874

68. F. A. Donath, Director, Institute for Environmental Education, Geological Society of America, 1006 Las Posas, San Clemente, CA 92673

69. E. K. Evans, Jacobs Engineering, 125 Broadway Avenue, Oak Ridge, TN 37831

70. D. W. Freckman, Director, College of Natural Resources, 101 Natural Resources Building, Colorado State University, Fort Collins, CO 80523

71. Paul Hofman, U.S. Department of Energy, Oak Ridge Operations Office, IRC Building, P. O. Box 2001, Oak Ridge, TN 37838-8541

72. Larry D. McKay, University of Tennessee, Department of Geology, 306 G&G Building, Knoxville, TN 37996-1410

73. A. Patrinos, Associate Director, Office of Health and Environmental Research, Department of Energy, G-165, Germantown, MD 20874

74. G. S. Sayler, Professor, 10515 Research Drive, Suite 100, The University of Tennessee, Knoxville, TN 37932-2567

75. D. K. Solomon, University of Utah, Department of Geology and Geophysics, 717 W. C. Browning Building, Salt Lake City, UT 84112-1183

76. David Webster, U. S. Geological Survey, 810 Broadway, Suite 500, Nashville, TN 37203

77. F. J. Wobber, Environmental Sciences Division, Office of Health and Environmental Research, ER-74, Department of Energy, 19901 Germantown Road, Germangown, MD 20874

78. Office of Assistant Manager for Energy Research and Development, U.S. Department of Energy Oak Ridge Operations, P. O. Box 2001, Oak Ridge, TN 37831-8600

79-80. Office of Scientific and Technical Information, P.O. Box 62, Oak Ridge, TN 37831